Technische Universität München

Lehrstuhl für anorganische Chemie mit Schwerpunkt Neue Materialien

Synthesis and Characterization of Lithium- and Sodium-Rich Transition-Metal Germanides and Stannides

Alexander Henze

Dank sage ich

Abbreviations

A	alkali metal
ARP	anisotropic replacement parameter
ASA	atomic sphere approximation
COHP	crystal orbital hamilton population
DFT	density functional theory
DOS	density of states
DTA	differential thermal analysis
E	main group element
EC	ethylene carbonate
EDX	energy dispersive X-ray spectroscopy
E_F	Fermi energy
LIB	lithium-ion battery
LMTO	linear muffin tin orbital
M	metal atom
PC	propylene carbonate
Ppm	parts per million
sof	site occupation factor
T	transition metal
Tr	group 13 element
Tt	group 14 element
TB	tight-binding
Vol.-%	volume percentage
XRD	X-ray diffraction

Abstract

Intermetallic solid state compounds have been investigated for a long time due to their great variety concerning their compositions and crystal structures as well as chemical and physical properties. The search for new intermetallic compound aims at improved properties for certain applications as well as the general understanding of this compound class. The focus of this thesis was set on the reduction of binary compounds of late transition-metal germanides and stannides using the light alkali metals Li and Na. The resulting new polar intermetallic compounds were structurally analyzed using single crystal X-ray diffraction and investigated for their thermal and magnetic behavior. For selected compounds, band structure calculations as well as an analysis of the bond strengths were carried out. With Li as the reducing agent it was possible to identify the most Li rich compounds in the systems Li-Ag-Ge and Li-Cu-Sn being **$Li_{12}AgGe_4$** and **Li_6CuSn_2**. The change of the structure type of $Li_{12}AgGe_4$ from $Li_{13}Ge_4$ to $Li_{13}Si_4$ was traced back to the strong Ag-Ge bond in the [Ge-Ag-Ge] trimer. It was also possible to synthesize Li filled polyanionic networks in the systems Li-Ag-Ge and Li-Ni-Ge, namely in the compounds **Li_2AgGe**, **$Li_{2.53}AgGe_2$**, **$Li_2Ag_{1-x}Ge_{1+x}$** and **$Li_{14}Ni_{8.3}Ge_{8.7}$**. While the first three compounds exhibit distorted diamond-like polyanionic networks of Ag and Ge which are notorious also for their Li ion mobility, the latter compound consists of filled interconnected rhombic dodecahedral clusters. This kind of cluster has never been observed before from solid state synthesis, but has crystallized before from solutions. Replacing Li and Ge by the larger Na and Sn, respectively, led to the first two compounds in the Na-Ag-Sn system **$Na_{29}Ag_{17.8}Sn_{43}$** and **$Na_{13}Ag_3Sn_{24}$**. Both compounds consist of icosahedra which are interconnected by additional cluster units forming polyanionic networks. These kinds of networks are especially known for Ga and In containing compounds. The formation of these structures was traced back to the low amount of electrons provided by Ag as well as the bigger size of Na which is more capable of separating distinct polyanionic units in solid state compounds than Li.

Zusammenfassung

Intermetallische Festkörperverbindungen werden schon seit langem aufgrund ihrer großen Vielfalt an möglichen Zusammensetzungen und Kristallstrukturen, sowie ihren chemischen und physikalischen Eigenschaften untersucht. Die Suche nach neuen intermetallischen Verbindungen zielt auf die Verbesserung dieser Eigenschaften für spezielle Anwendungen wie Batteriematerialien, sowie das generelle Verständnis dieser Verbindungsklasse ab. Der Schwerpunkt dieser Arbeit lag auf der Reduktion von binären Übergangsmetall-Germaniden und -Stanniden durch die leichten Alkalimetalle Li und Na. Die auf diese Weise hergestellten neuen, polar-intermetallischen Verbindungen wurden mittels Einkristalldiffraktometrie aufgeklärt und auf ihr thermisches und magnetisches Verhalten hin untersucht. Für ausgewählte Verbindungen wurden weiterhin die Bandstruktur sowie die Bindungsstärken zwischen den Atomen berechnet. Durch den Einsatz von Lithium als Reduktionsmittel konnten mit $Li_{12}AgGe_4$ und Li_6CuSn_2, die lithiumreichsten Verbindungen in den Systemen Li-Ag-Ge und Li-Cu-Sn identifiziert werden. Die Änderung des Strukturtyps von $Li_{12}AgGe_4$ von $Li_{13}Ge_4$ zu $Li_{13}Si_4$ konnte auf die sehr starke Ag-Ge Bindung in dem Trimer [Ge-Ag-Ge] zurückgeführt werden. Des Weiteren wurden Verbindungen mit Lithium gefüllten polyanionischen Netzwerken hergestellt. Dabei handelte es sich um die Verbindungen Li_2AgGe, $Li_{2.53}AgGe_2$, $Li_2Ag_{1-x}Ge_{1+x}$ und $Li_{14}Ni_{8.3}Ge_{8.7}$. Während die ersten drei Verbindungen aus einem diamant-artigen Netzwerk aus Ag und Ge bestehen, wird das Netzwerk in $Li_{14}Ni_{8.3}Ge_{8.7}$ von verbrückten Rhombendodekaedern gebildet. Diese Art von Clustern wurde zuvor nur auf lösungsmittelchemischem Weg hergestellt, aber noch nie durch eine Festkörpersynthese. Durch das Ersetzen von Li und Ge durch die schwereren Elemente Na und Sn konnten die ersten beiden intermetallischen Verbindungen im System Na-Ag-Sn, $Na_{29}Ag_{17.8}Sn_{43}$ und $Na_{13}Ag_3Sn_{24}$ hergestellt werden. Beide Verbindungen bestehen aus Ikosaedern, die durch weitere Cluster zu einem dreidimensionalen polyanionischen Netzwerk verknüpft werden. Derartige Strukturen sind bisher vor allem von Ga und In enthaltenden Verbindungen bekannt. Die Bildung dieser Strukturen konnte auf die geringe Menge an Elektronen die Ag für diese Verbindungen zur Verfügung stellt und auf die Größe des Na, welches stärker als Li in der Lage ist unterschiedliche polyanionische Strukturen voneinander zu trennen, zurückgeführt werden.

Table of Contents

Note

This work is composed as a paper style thesis. For articles which are already published in peer-reviewed journals the bibliographic data are given, manuscripts prepared for submission are included in chapter 6.

The relevance of this work for science and research as well as the scope and outline are provided as introduction in chapter 1. Chapter 2 and Chapter 3 summarize the results and discussion. While Chapter 2 deals with Li rich transition metal tetrelides which were investigated for their potential use in Li ion batteries, Chapter 3 presents new three-dimensional networks of interconnected clusters. An overall summary of this work is given in Chapter 4. The details on the synthesis and characterization of the compounds as well as computational work are summed up in Chapter 5.

1 Introduction

In view of the fact that two third of all elements listed in the periodic table of elements are metals it does not surprise that intermetallic compounds bare a huge diversity of different structures and properties. The investigations on new intermetallic compounds are unfortunately still related a lot to the principle of "try and error". But the more different compounds are found and characterized, the more we understand about the driving forces leading to the formation of these structures and properties. These include packing effects as well as electronic and energy factors. The goal of course is that one day all of these aspects are understood so well, that new compounds can be predicted and materials with desired properties can be designed as they are needed. For now, we still relate on informed guessing when it comes to the synthesis of new compound and sometimes we get rewarded with compound containing outstanding new structures and properties.

1.1 Zintl concept and polar intermetallics

The terms "intermetallic compounds", "intermetallic phases" and "intermetallics" are three loosely defined expressions describing compounds containing two or more metals. These terms are not only used for compounds containing the early s- d- and f-block elements, but also the early p-block elements including the semimetalls Si and Ge as well as Sn. For the description of intermetallic phases the categorization into classes such as Heusler- and half-Heusler phases, Hume-Rothery phases, Laves phases and Zintl phases has been proven quite useful though the separation of these groups is not sharp. The former groups are used to classify compounds with mainly intermetallic bonding, while Zintl phases and the adjacent polar intermetallics contain a polyanionic substructure which is often dominated by covalent bonds.

The Zintl concept primarily states, that compounds formed by the combination of very electropositive elements, e.g. alkaline, alkaline-earth and rare earth elements and rather electronegative (semi)metals from the p block elements including late transition metals like silver or platinum will perform a formally full charge transfer from the electropositive to the electronegative element. The semimetals or metalloids are a group of elements located between the metals and the nonmetals and occur along a diagonal in

the periodic system from boron to tellurium. The resulting intermetallic compounds can consequently be described as salt-like. Thus, while it is possible to observe 2-center 2-electron bonding and even lone pairs in the polyanionic subpart of a Zintl compound, no covalent bonds between the anionic and the cationic part of it should be considered. The oligomeric or polymeric anionic substructures follow the 8-N rule by which they can be understood quiet well compared to different intermetallic compounds where the occurring multicenter bonding is quiet less understood and predictable. If the polyanionic substructure contains clusters which cannot be described using the 8-N rule, Wade-Mingos rules, introduced to describe the bonding situation in borans, can be applied as an extension to the Zintl concept to describe them.[1-3]

Due to their bonding characteristics, Zintl phases should always be stoichiometric compounds. Ideally, they should be semiconductors with a small band gap. This is not true though for a considerable number of compounds including NaTl, the compound Zintl introduced the concept on in the first place.[4] In most of these cases, a gap or pseudo-gap is close or at the Fermi level in the respective Density of States (DOS). For the latter compounds the term "metallic Zintl phase" has been introduced.[5] The magnetic behavior of Zintl phases should be diamagnetic, as all electrons should be paired. The correlation between crystal and electronic structure was emphasized by Klemm.[6, 7] During his investigations it became evident, that not all intermetallic compounds can be described as Zintl phases, though. A numerous amount of compounds composed of an electropositive and one or more electronegative metals do not follow the Zintl rules and hence have to be described as polar intermetallic phases. In comparison to Zintl phases, polar intermetallic phases are not able to perform a complete electron transfer from the electropositive to the electronegative part of the respective compound. Hence, the substructures build by the more electronegative metal atoms of these compounds cannot be described using only the 8-N rule, but hypervalent multicenter bonding and delocalized bonds have to be considered as well as fractional bonds.[8, 9] This leads to unusual local coordinations of the metal atoms in the polyanionic substructure, e.g. if chains or two dimensional nets are build. Electron poor elements like the triels also tend to form three-dimensional networks of interconnected clusters.[10] Especially Ga and In are famous for this behavior considering compounds like $Na_{22}Ga_{39}$ and $Na_7In_{11.8}$.[11, 12] The properties of polar intermetallic phases differ from perfect Zintl compounds in their metallic behavior as the weaker bonding within the polyanionic substructure does not lead to an opening of the

DOS at the Fermi level. A consequence of this is that structure determining factors as the electron count, size and packing effects become way more important for the stabilization of the structures. Another consequence is the frequent occurring of deviations from the ideal electron count. In general, Zintl phases and polar intermetallic phases are not strictly divided. Instead, the transition between them is fluent. Compounds in this transition area between these concepts are especially interesting as they often provide unexpected structures or bonding situations challenging existing concepts and teach about the true characters of intermetallic compounds.

1.2   *Solid state compounds in Lithium-ion batteries*

The need for energy storing materials is ever increasing in our modern society. The most energy is still produced by burning of fossil fuels. But regarding the impact on the atmosphere and the finiteness of these energy sources, renewable energy sources are on the rise. One of the main disadvantages of two of the main energy sources, namely sun and wind is their lack of steady availability. Energy storing would compensate this disadvantage and therefore lead to lower costs and higher acceptance of this kind of energy producing. Furthermore, more and more portable devices are invented. The solutions to all of these challenges are effective, light and low priced energy storing materials. The state of the art for all kinds of portable devices even up to cars are lithium-ion batteries (LIBs).[13] The use of Li containing materials is advantageous, as Li presents the lowest reduction potential of all elements allowing the highest possible cell potential in LIBs. Furthermore, Li stands out through its very low weight and its ionic radius, which is the smallest of all single charged ions. Finally, the ion mobility for Li ions is higher than for multi-charged elements, which makes Li superior to elements like Mg in view of the ion diffusivity being the limiting factor for battery power performance. The first batteries based on Li were already invented in 1962 but were not rechargeable at the time. The first rechargeable Li containing batteries were invented in the late 70s among others at TU München. But the low amount of loading cycles due to the building of dendrites at the Li anode and the resulting overheating and explosion of some batteries were big issues that had to be addressed.[14] The introduction of graphite as an anode material decreased these safety problems as Li can be reversibly intercalated into the graphite, but the formation of dendrites is inhibited.[15] In combination with layered

transition metal oxides, whose first and most commercially successful example is $LiCoO_2$ as a cathode material[16] and non-aqueous electrolytes like ethylene carbonate (EC) or propylene carbonate (PC), SONY was able to commercialize the Li-ion batteries in the early 1990s. Regarding the three main components of LIBs, anode and cathode materials as well as electrolytes, the former two are interesting for solid state investigations. Solid state electrolytes are investigated as well though, but a different setup of the cell is needed for their application. In recent approaches regarding the cathode material, phases different to the $LiTO_2$ (T = Cr, Co, Ni) were investigated regarding their suitability as cathode materials. Examples of these are the spinels LiT_2O_4 (T = Mn, Co),[17, 18] olivine structured $LiTPO_4$ (T = Mn, Fe, Co, Ni)[19-22] phases and orthosilicates Li_2TSiO_4 (T = Mn, Fe, Co)[23-25]. Also compounds like $LiBSi_2$ are discussed for this purpose.[26]
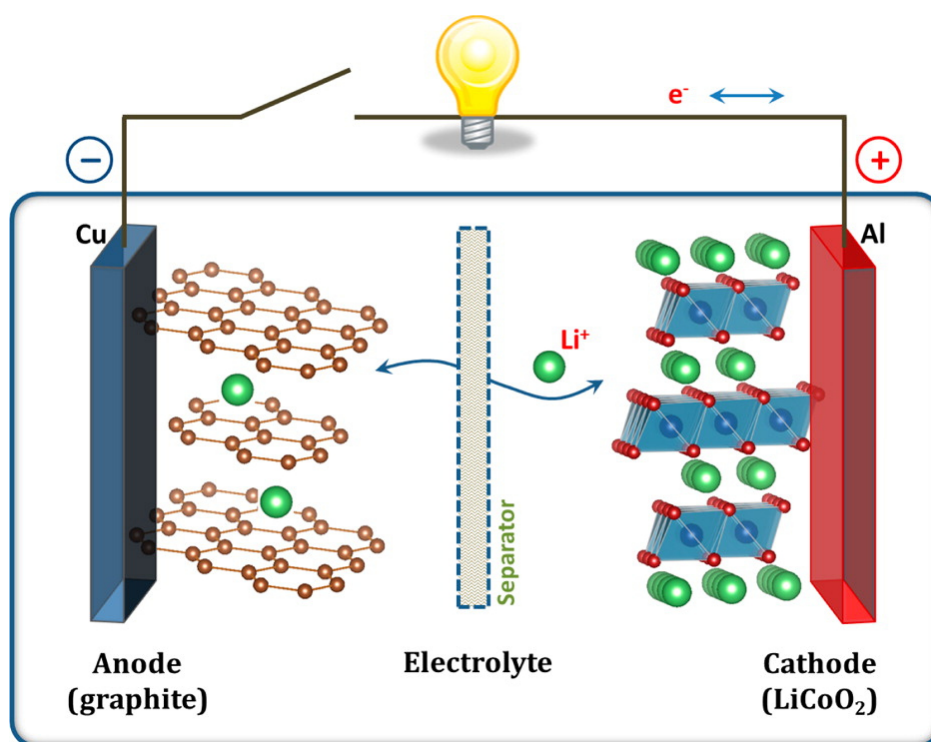
Figure 1 Schematic drawing of a Li-ion battery using graphite as anode, liCoO$_2$ as cathode and a fluid electrolyte. Reprinted with permission from ref. 13. Copyright 2016 American Chemical Society.

On the other hand, graphite is still the most commonly used anode material. This is due to the high 2D mechanical stability, Li transport and electrical conductivity it provides. Graphite also combines low cost, weight and volume change during lithiation/delithiation

with a high availability. The lithiation up to LiC_6 has a theoretical specific capacity of 372 mAhg^{-1}.[27] The two types of commercially important anodes are graphitic carbons and hard carbons. Graphitic carbons consist of large grains of graphite and are almost able to achieve the theoretical charge capacity. They do not match well with PC-based electrolytes though, as these intercalate in the graphite layers and lead to exfoliation and loss of capacity.[28] In comparison, hard carbons consist of rather small grains of graphite with disordered orientation and nanovoids between them. This leads to a reduced exfoliation and volume expansion, but also reduces the volumetric capacity.[29]

As an alternative to graphite based anode materials, lithium titan oxides ($Li_4Ti_5O_{12}$ / LTO) were introduced and commercialized.[30] Suffering from an even lower theoretical capacity of 175 mAhg^{-1} LTOs are advantages with a higher thermal stability as well as high rates and cycle lives. Furthermore, LTO is very safe due to its high potential which prevents Li dendrite formation even at high rates. Through carbon coating LTOs are stable for tens of thousands of cycles making it a good material for low energy but high power high cycle life Li ion batteries.

A way to dramatically increase the theoretical specific capacity of anodes is the use of higher tetrel elements than carbon in intermetallic alloy electrodes. As weight is always an issue with battery materials the lighter tetrelides Si and Ge with theoretical capacities of 4200 mAhg^{-1} and 1564 mAhg^{-1} respectively are investigated intensifly.[31, 32] But also Sn, though comparatively heavy, has drawn some attention with its theoretical specific capacity of 960 mAh/g^{-1}.[33, 34] The biggest problem with these materials is their suffering from high volume changes during the lithiation/delithiation processes up to 240% for Ge and 270% for Si.[35] This leads to contact losses of the electrode material and continuative to a heavy loss of capacity during the first cycles and a low coulombic efficiency.[36] A lot of efforts have been made to overcome the problems with strong volume expansion and contraction on the lithium alloying/dealloying process of pure Si, Ge and Sn as anode materials. These efforts concern for example the reduction of the particle size, which has been shown to be successful for all of the group 14 elements. The idea behind this reduction of particle size is to create a higher interfacial area leading to higher charge/discharge rates. Furthermore the shortening of the path for Li$^+$ ions should increase the power capabilities as well as the accommodation of the strain of lithium insertion/removal increases the cycle life of the anode material. But there are also some difficulties that appear with the usage of nanostructures. These include a low tap density

which results from the low surface to volume ratio and leads to low energy densities. Additionally the high surface reactivity and safety issues due to the high flammability of metallic nanopowders are concerns which have to be regarded.

Among these three elements, Si not only provides the highest theoretical capacity, but also shines with low weight, a very high availability which comes along with low costs. For this reason it is the most investigated of these three elements. To overcome the issues of low cycle life, high volume change, low conductivity and tapping density, different strategies have been tested. These strategies include reduction of the particle size, nanostructuring of micro-sized electrode materials,[37] doping with additional elements[38] and the creation of one-dimensional nanowires.[39] All these strategies have drastically improved the performance of Si as anode material and it is considered one of the most promising materials for the substitution of graphite in LIBs. But for now, still a lot of work has to be done to overcome problems like unsatisfying rate performances, capacity retention and fabrication costs.

Ge has drawn less attention than Si due to its higher costs, resulting from the lower availability its lower theoretical capacity and its higher weight. Nevertheless, it provides some advantages like its higher electronic conductivity and its lithium ion diffusivity which is 400 times higher at room temperature than the one of Si.[40, 41] Still, Ge suffers from a lot of the same problems as Si, especially the high volumetric change on lithiation/delithiaton. Different strategies have been addressed to overcome these issues for Ge including the use of carbon as a buffer layer,[42] the reduction of the particle size to the nanoscale, the adoption of a three-dimensional porous structure,[43] or the formation of amorphous GeO_x with small size.[44] These strategies led to good performances of Ge based anodes. However, the low abundance and therefore high costs of Ge will probably result in Ge anodes being always stuck to special purpose applications.

Sn, though the heaviest of the tetrelides investigated for their appliance as anode materials in LIBs already been used by in commercialized anode materials e.g. in a Co-Sn alloy with small amounts of Ti.[45, 46] Hence, the strategy of forming tin-based intermetallic anodes has already proven that it can be quite successful and further investigations concerning transition metal alloys with elements like Fe, Ni and Cu are made.[47, 48] Especially the Cu-Sn system with the binary compound Cu_6Sn_5 stands out with high capacities.[49, 50] Additionally, the introduction of C as a confining buffer in binary T-Sn

systems has been investigated and was shown to improve the cycling response of the respective lithium cells.[51, 52] Also the integration of Sn in conductive matrices such as carbon has been investigated a lot to accommodate the strain of volume expansion during lithiation and provide a proper electronic conductivity for the overall electrode. Therefore, graphite, carbon nanotubes, graphene and different forms of mesoporous and amorphous carbon are used to create Sn based anode materials. These materials contain Sn@carbon nanoparticles[53] and graphene confined Sn nanosheets[54] among other structures. Also Sn-C composite materials formed from nanoparticles have been introduced.[55]

1.3   *Scope and outline of this work*

The group 14 in the periodic table includes elements that due to their central position in this table and the accompanied average electronegativity and large amount of possible bonds are quite versatile in their chemical behavior. In combination with more electropositive metals they are able to form varying kinds of structures. This ranges from 0-dimensional particles like dumbbells and isolated rings as well as different forms of clusters over one-dimensional chains to two-dimensional planes and three-dimensional networks. This versatility which also comes with scores of different bonding situations makes tetrel element containing compounds interesting candidates in a lot of different areas[56, 57] including magnetic and superconducting as well as thermoelectric materials and many more. A lot of different structures containing tetrel elements are obtainable in combination with the small alkali metals Li and Na. The higher alkali metals are showing similar chemical properties, but their size seems to allow only the stabilization of smaller amounts of different structures. If late transition metals are added too these binary Li-*Tt* systems, it is possible to obtain a multitude of different compounds featuring new and unusual bonding situations that are able to teach a lot about the character of the involved elements. Furthermore, especially the lithiation of binary M-*Tt* systems like Cu-Sn and Ni-Sn is investigated due to their potential as anode materials in Li ion batteries (see chapter 1.2). In view of this thesis, the scores of possible combinations of these elements required the setting of some focus points. Si for sure is the most investigated element of the tetrels due its importance in the semiconductor industry and its potential in new anode materials for LIBs. This should not cover that only recently parts of the binary Li-Si

phase diagram have been reviewed and distinctively revised. Also in promising ternary systems for anode materials like Li-Cu-Si new compounds have been found just recently and there might be even more. The focus of this work is set on investigations in ternary systems containing the higher homologues Ge and Sn though. Even though Ge and Sn are also investigated a lot for their potential in LIBs as presented in chapter 1.2, their ternary *A-M-Tt* systems are often investigated quite sparsely and in some of them not a single ternary compound is known. Inspired by the high Li ion mobility in compounds of the Li-Ag-Sn system like $LiAg_2Sn$ and Li_2AgSn_2, **chapter 2** of this thesis aims at investigations in neighboring systems to find and characterize new and possibly even superior compounds for anode materials while **chapter 3** aims more at a better understanding of the structures these elements are able to build and the attended properties of the compounds. Suitable ternary systems which were investigated for Li rich compounds included Li-Ag-Ge and Li-Cu-Sn, substituting one of the elements of the Li-Ag-Sn system by a lighter one. This comes with the intuition that weight is an important issue when it comes to LIBs, but also had the very small number of known compounds in the respective systems at that time in mind. As especially the Li rich compounds are interesting for their status as target compounds during the lithiation process, a special focus was set on the Li rich parts of these systems. This kept in mind though, that high Li ion mobility were found for compounds with Li in polyanionic networks as in Li_2MSn_2 (*M* = Cu, Ag, Au) which cannot be viewed as specifically Li rich. Previously, only three rather Li poor elements had been found in this ternary system,[58] investigations in the Li rich part of this system were performed. The investigations in the Li rich part of the Li-Ag-Ge system led to the discovery of several new compounds. The structures of these compounds were determined via single crystal X-ray diffraction. Their thermal and magnetic behavior was investigated using differential thermal analysis (DTA) and Squid measurements. Band structures and COHPs were calculated to determine the bonding situations and electronic properties. The results on Li filled 3D networks inspired a closer inspection of the transition between these networks.

The investigations in the Li-Cu-Sn system did not only aim at compounds structurally related to those from the Li-Ag-Sn system, but especially for the target compound of the lithiation of the binary Cu-Sn system which shows the highest capacity of binary *M*-Sn systems. For this reason investigations were carried out in the Li-rich area of the ternary system resulting in the discovery of the Li-richest compound known in this system using

high-temperature synthesis. The structure of the compound was determined via single crystal X-ray diffraction and verified as far as possible using powder diffraction, EDX methods and Fourier Electron Density mapping.

These investigations were also extended to the neighboring Li-Ni-Ge system. In this system only two compounds with very common compositions and structures had been described before. The investigations led to the discovery of a new ternary compound in this system with a unique structure of interconnected clusters which was determined using single-crystal X-ray diffraction. As structures including interconnected clusters and Li are very rare due to the small size of the Li ion which is barely able to separate this kind of polyanionic substructure, we turned to the Na-Ag-Sn system, substituting the light Li of the earlier mentioned Li-Ag-Sn system be the bigger Na. This approach aimed at closer understanding of the chemistry of intermetallic Sn containing compounds regarding the remarkable structures which have been found in the Na-Cu-Sn and the neighboring Na-Zn-Sn systems. In these systems, Na filled channels as in Na_2ZnSn_5[59] are found as well as interconnected clusters in $Na_{29}Zn_{24}Sn_{32}$[60] and isolated clusters as in $Na_{12}Cu_{12}Sn_{21}$.[61] The kind of structure which is build seems to be strongly depended on the *M:Tt* ratio and therefore on the amount of electron deficit introduced to the binary Na-Sn system. The influence by the introduction of the even electron poorer Ag should be even greater and the structures of ternary, Ag containing compounds are supposed to mimic the structures known from Ga and In if the respective *M:Tt* ratio is given. The actual investigations in the Na-Ag-Sn system led to the discovery of the first two known ternary compounds composed of these elements. The structures of these compounds where determined using single crystal X-ray diffraction and contain interconnected clusters and cluster-like three-dimensional networks as expected. Their thermal and magnetic behavior was investigated using DTA and SQUID techniques.

1.4 References

(1)   Wade, K. *Journal of the Chemical Society D: Chemical Communications* **1971**, 792-793.

(2)   Mingos, D. *Nature* **1972,** *236*, 99-102.

(3)   Wade, K. *Inorganic and Nuclear Chemistry Letters* **1972,** *8*, 823-827.

(4)   Grube, G.; Schmidt, A. *Zeitschrift für Elektrochemie und angewandte physikalische Chemie* **1936,** *42*, 201-209.

(5)   Nesper, R. *Prog. Solid St. Chem.* **1990,** *20*, 1-45.

(6)   Klemm, W. *Proc. Chem. Soc. London* **1958**, 329-341.

(7)   Klemm, W.; Busmann, E. *Z. Anorg. Allg. Chem.* **1963,** *319*, 297-311.

(8)   Rundle, R. E. *J. Am. Chem. Soc.* **1947,** *69*, 1327-1331.

(9)   Rundle, R. E. *The Journal of Chemical Physics* **1949,** *17*, 671-675.

(10)   Belin, C.; Tillard-Charbonnel, M. *Prog. Solid St. Chem.* **1993,** *22*, 59-109.

(11)   Ling, R.; Belin, C. *Acta Crystallographica Section B: Structural Crystallography and Crystal Chemistry* **1982,** *38*, 1101-1104.

(12)   Sevov, S. C.; Corbett, J. D. *Inorg. Chem.* **1992,** *31*, 1895-1901.

(13)   Goodenough, J. B.; Park, K.-S. *J. Am. Chem. Soc.* **2013,** *135*, 1167-1176.

(14)   Whittingham, M. S. *Chemical Reviews* **2004,** *104*, 4271-4302.

(15)   Owen, J. R. *Chemical Society Reviews* **1997,** *26*, 259-267.

(16)   Mizushima, K.; Jones, P.; Wiseman, P.; Goodenough, J. *Materials Research Bulletin* **1980,** *15*, 783-789.

(17)   Choi, S.; Manthiram, A. *J. Electrochem. Soc.* **2002,** *149*, A162-A166.

(18)   Lee, M.-J.; Lee, S.; Oh, P.; Kim, Y.; Cho, J. *Nano Letters* **2014,** *14*, 993-999.

(19)   Choi, D.; Wang, D.; Bae, I.-T.; Xiao, J.; Nie, Z.; Wang, W.; Viswanathan, V. V.; Lee, Y. J.; Zhang, J.-G.; Graff, G. L.; Yang, Z.; Liu, J. *Nano Letters* **2010,** *10*, 2799-2805.

(20)   Yamada, A.; Chung, S. C.; Hinokuma , K. *J. Electrochem. Soc.* **2001,** *148*, A224-A229.

(21)   Lloris, J. M.; Pérez Vicente, C.; Tirado, J. L. *Electrochem. Solid-State Lett.* **2002,** *5*, A234-A237.

(22)   Wang, D.; Xiao, J.; Xu, W.; Zhang, J.-G. *Meeting Abstracts* **2010,** *MA2010-03*, 372.

(23)   Świętosławski, M.; Molenda, M.; Furczoń, K.; Dziembaj, R. *Journal of Power Sources* **2013,** *244*, 510-514.

(24)   Nytén, A.; Abouimrane, A.; Armand, M.; Gustafsson, T.; Thomas, J. O. *Electrochemistry Communications* **2005,** *7*, 156-160.

(25)   Gong, Z. L.; Li, Y. X.; Yang, Y. *Journal of Power Sources* **2007,** *174*, 524-527.

(26)   Zeilinger, M.; van Wüllen, L.; Benson, D.; Kranak, V. F.; Konar, S.; Fässler, T. F.; Häussermann, U. *Angew. Chem. Int. Ed.* **2013,** *52*, 5978-5982.

(27)   Nagaura, T.; Tozawa, K. *Prog. Batteries Solar Cells* **1990,** *9*, 209.

(28)   Aurbach, D.; Markovsky, B.; Weissman, I.; Levi, E.; Ein-Eli, Y. *Electrochimica Acta* **1999,** *45*, 67-86.

(29)   Dahn, J. R.; Zheng, T.; Liu, Y.; Xue, J. *Science* **1995,** *270*, 590.

(30)   Aldon, L.; Kubiak, P.; Womes, M.; Jumas, J. C.; Olivier-Fourcade, J.; Tirado, J. L.; Corredor, J. I.; Pérez Vicente, C. *Chem. Mater.* **2004,** *16*, 5721-5725.

(31)   Wen, C. J.; Huggins, R. A. *J. Solid State Chem.* **1981,** *37*, 271-278.

(32)   Goward, G. R.; Taylor, N. J.; Souza, D. C. S.; Nazar, L. F. *J. Alloys Comp.* **2001,** *329*, 82-91.

(33)   Courtney, I. A.; Dahn, J. *J. Electrochem. Soc.* **1997,** *144*, 2045-2052.

(34)   Zhang, W. M.; Hu, J. S.; Guo, Y. G.; Zheng, S. F.; Zhong, L. S.; Song, W. G.; Wan, L. J. *Advanced Materials* **2008,** *20*, 1160-1165.

(35)   Baggetto, L.; Notten, P. H. L. *J. Electrochem. Soc.* **2009,** *156*, A169-A175.

(36)   Wang, J.; Chen-Wiegart, Y.-c. K.; Wang, J. *Angew. Chem. Int. Ed.* **2014,** *53*, 4460-4464.

(37)   Yi, R.; Dai, F.; Gordin, M. L.; Chen, S.; Wang, D. *Advanced Energy Materials* **2013,** *3*, 295-300.

(38)   Rousselot, S.; Gauthier, M.; Mazouzi, D.; Lestriez, B.; Guyomard, D.; Roué, L. *Journal of Power Sources* **2012,** *202*, 262-268.

(39)   Chan, C. K.; Peng, H.; Liu, G.; McIlwrath, K.; Zhang, X. F.; Huggins, R. A.; Cui, Y. *Nat Nano* **2008,** *3*, 31-35.

(40)   Fuller, C. S.; Severiens, J. C. *Phys. Rev.* **1954,** *96*, 21–24.

(41)   Graetz, J.; Ahn, C. C.; Yazami, R.; Fultz, B. *J. Electrochem. Soc.* **2004,** *151*, A698–A702.

(42)   Xue, D.-J.; Xin, S.; Yan, Y.; Jiang, K.-C.; Yin, Y.-X.; Guo, Y.-G.; Wan, L.-J. *J. Am. Chem. Soc.* **2012,** *134*, 2512-2515.

(43)   Song, T.; Jeon, Y.; Samal, M.; Han, H.; Park, H.; Ha, J.; Yi, D. K.; Choi, J.-M.; Chang, H.; Choi, Y.-M.; Paik, U. *Energy Environ. Sci.* **2012,** *5*, 9028-9033.

(44)   Wang, X.-L.; Han, W.-Q.; Chen, H.; Bai, J.; Tyson, T. A.; Yu, X.-Q.; Wang, X.-J.; Yang, X.-Q. *J. Am. Chem. Soc.* **2011,** *133*, 20692-20695.

(45)   Idota, Y.; Kubota, T.; Matsufuji, A.; Maekawa, Y.; Miyasaka, T. *Science* **1997,** *276*, 1395-1397.

(46)   Fan, Q.; Chupas, P. J.; Whittingham, M. S. *Electrochem. Solid-State Lett.* **2007,** *10*, A274-A278.

(47)   Wang, X.-L.; Han, W.-Q.; Chen, J.; Graetz, J. *ACS Applied Materials & Interfaces* **2010,** *2*, 1548-1551.

(48)   Chou, N. H.; Schaak, R. E. *J. Am. Chem. Soc.* **2007,** *129*, 7339-7345.

(49)   Trahey, L.; Vaughey, J. T.; Kung, H. H.; Thackeray, M. M. *J. Electrochem. Soc.* **2009,** *156*, A385-A389.

(50)   Wolfenstine, J.; Campos, S.; Foster, D.; Read, J.; Behl, W. *Journal of power sources* **2002,** *109*, 230-233.

(51)   Mao, O.; Dunlap, R.; Dahn, J. *J. Electrochem. Soc.* **1999,** *146*, 405-413.

(52)   Beaulieu, L.; Dahn, J. *J. Electrochem. Soc.* **2000,** *147*, 3237-3241.

(53)   Yu, Y.; Gu, L.; Wang, C.; Dhanabalan, A.; van Aken, P. A.; Maier, J. *Angew. Chem. Int. Ed.* **2009,** *48*, 6485-6489.

(54)   Luo, B.; Wang, B.; Li, X.; Jia, Y.; Liang, M.; Zhi, L. *Advanced Materials* **2012,** *24*, 3538-3543.

(55)   Derrien, G.; Hassoun, J.; Panero, S.; Scrosati, B. *Advanced Materials* **2007,** *19*, 2336-2340.

(56)   Westbrook, J. H.; Fleischer, R. L., *Intermetallic Compounds, Magnetic, Electrical and Optical Properties and Applications of*. John Wiley & Sons: 2000.

(57)   Sauthoff, G. *Intermetallics* **2000,** *8*, 1101-1109.

(58)   Kevorkov, D. G.; Pavlyuk, V. V.; Bodak, O. I. *Pol. J. Chem.* **1997,** *71*, 712–715.

(59)   Stegmaier, S.; Kim, S.-J.; Henze, A.; Fässler, T. F. *J. Am. Chem. Soc.* **2013,** *135*, 10654-10663.

(60)   Kim, S.-J.; Hoffman, S. D.; Fässler, T. F. *Angew. Chem.* **2007,** *119*, 3205-3209.

(61)   Stegmaier, S.; Fässler, T. F. *J. Am. Chem. Soc.* **2011,** *133*, 19758–19768.

2 Lithium-Rich Transition-Metal Tetrelides for Anodes in Lithium Ion Batteries

2.1 Introduction

As presented in chapter 1.2 the low theoretical specific capacity of graphite which represents the most common anode material, the substitution through intermetallic Li containing compounds is discussed. For this purpose, a lot of binary intermetallic compounds containing Li and main group elements have been tested. Prominent examples include the main group elements Al, In, Si, Ge, Sb. An overview of the crystal chemistry and electrochemical data of these binary compounds were given by Nesper and Huggins.[1, 2] A different approach is made by introducing transition metals into these binary compounds. This leads to the formation of two- and three-dimensional polyanionic networks build by the main group and the transition metal. The Li atoms in these structures often fill cages or channels provided by the polyanionic network. The first compounds in this field were found by H.-U. Schuster and A. Weiss.[3, 4] Since then, a lot of different compounds have been found and researched for their Li ion mobility, especially through Li NMR techniques as these compounds combine high Li packing densities with a high stability and therefore long lifecycles.[5, 6] An extensive overview on ternary compounds of Li-transition metal-tetrelides was given by Pöttgen et al.[7] A lot of these compounds show Li-ion mobility in one or more directions. Between the more than 100 compounds reported, Li_2AgSn_2, $LiAg_2Sn$ and $Li_3Rh_4Si_4$ outstand with the highest Li-ion mobility.[7-9] Investigations in the compounds Li_2MSn_2 (M = Cu, Ag, Au) showed that the Li ion mobility does not relate directly to the size of the Li occupied channels, but that different factors like polarization, the concrete bonding situation and the level of distortion of the channels play an important role.[8] The intention to learn more about this kind of compounds led to investigations in the Li-Ag-Ge and Li-Cu-Sn phase diagrams. Prior to this work, only very few reports were made on ternary compounds originating from these phase diagrams. For Li-Ag-Ge the first reported ternary compound was $Li_8Ag_3Ge_5$ in 1972.[10] A closer investigation in 1997 showed though, that this compound actually may have the composition $Li_3Ag_2Ge_3$ and additionally reported on the two compounds $LiAg_2Ge$ and $Li_3Ag_3Ge_2$.[11] All these structures were solved from powder data though. Structure solutions from single crystal X-ray diffraction have not been reported.

Additionally, the absence of any reports on Li rich compounds in this phase diagram is eye-catching and led to investigations in this area of the Li-Ag-Ge system.
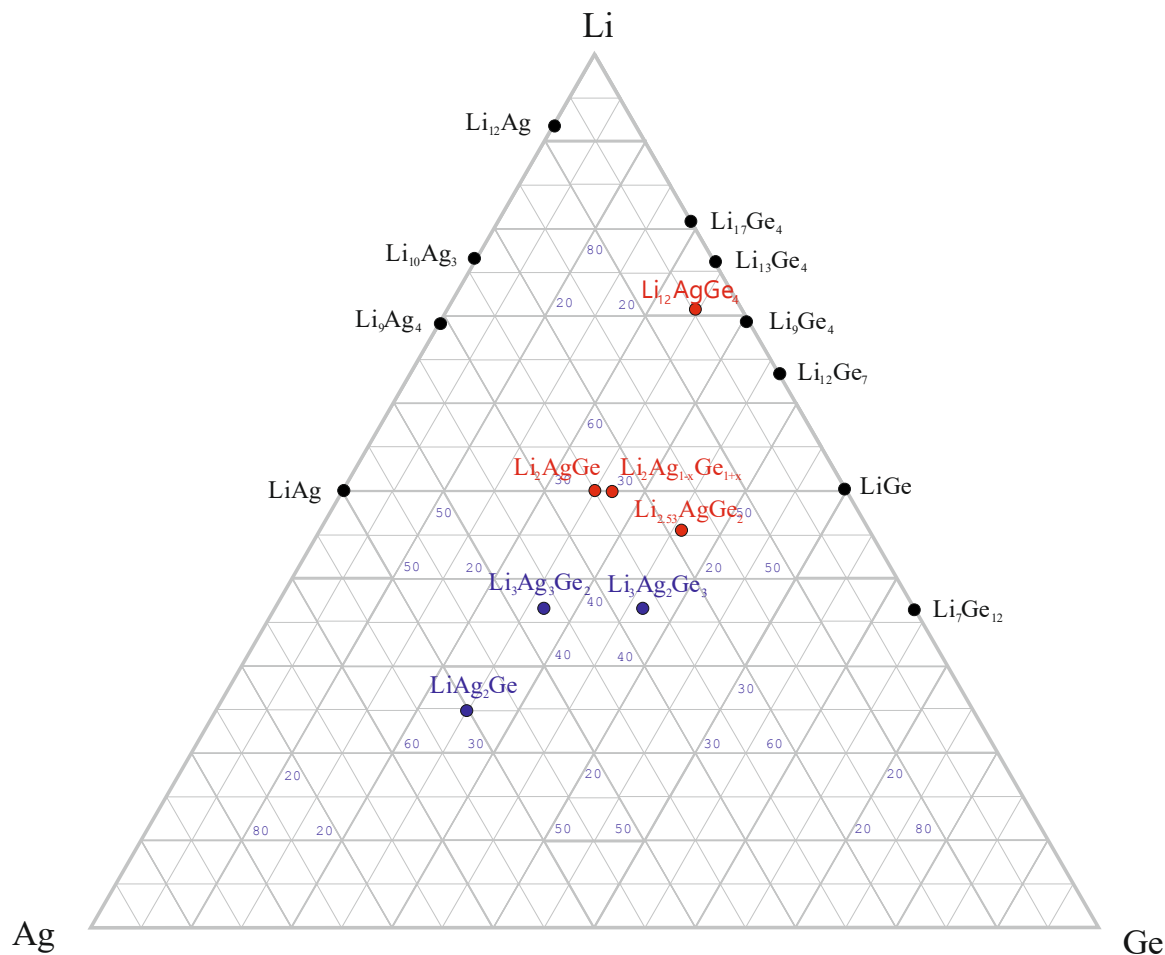
Figure 2. Concentration diagram of the ternary system Li-Ag-Ge. Selected binary compounds, ternary compounds known in front of this thesis and compounds synthesized in this thesis are marked in black, blue and red respectively.

The first ternary compounds in the Li-Cu-Sn system have been reported as early as in the Li-Ag-Ge system. The compounds Li_2CuSn and $LiCu_2Sn$ were first described almost 50 years ago.[3, 4, 12] Due the successful implementation of Sn containing anode materials for Lithium ion batteries and the high capacity of the lithiation of binary Cu-Sn compounds the interest for this phase system has revived recently. During the time of this thesis, reports on the compounds Li_2CuSn_2[8] and $Li_3Cu_6Sn_4$[13] as well as Li_3CuSn and $Li_6Cu_3Sn_2$[14] have been made. But especially for the lithiation of binary Cu-Sn, the Li richest ternary compound in this system is important.

In the following, new Li rich transition metal tetrelides are presented which might help to achieve a better understanding of the structural and electronic requirements for increasingly efficient and powerful anode materials for LIBs.

2.2   Li-rich ternary compounds in the Li-Ag-Ge system

See publication 6.1:   Switching the Structure Type upon Ag Substitution: Synthesis and Crystal as well as Electronic Structures of $Li_{12}AgGe_4$
A. Henze, T.F. Fässler, *Inorg. Chem.* **2016**, *55*, 822-827.

See publication 6.2:   Fully and Partially Li-Stuffed Diamond Polytypes with Ag-Ge Structures: Li_2AgGe and $Li_{2.53}AgGe_2$

A. Henze, V. Hlukky, T.F. Fässler, *Inorg. Chem.* **2015**, *54*, 1152-1158.

See manuscript 6.3:   Synthesis and Structural Characterization of $Li_2Ag_{1-x}Ge_{1+x}$ (x = 0.06)

A. Henze, T.F. Fässler, manuscript in preparation

Within the scope of this work the Li rich part of the Li-Ag-Ge system was investigated. Therefore preformed alloys of Ag and Ge in the expected stoichiometry were reacted with elemental Li at high-temperatures. The structures of all compounds were determined using single crystal X-ray diffraction. These investigations yielded three new ternary compounds with a Li-filled three-dimensional polyanionic network of Ag and Ge, while one compound showed isolated Ge_2 and $AgGe_2$ particles. The three compounds with a polyanionic network of Ag and Ge are Li_2AgGe, $Li_2Ag_{1-x}Ge_{1+x}$ (x = 0.06(11)) and $Li_{2.53}AgGe_2$. The structures of all three compounds derive from the NaTl structure type and exhibit a diamond like polyanionic network with different degrees of distortion. The degree of distortion depends on the amount of homoatomic bonds in the structure. The compound with the most homoatomic bonds in its structure is $Li_{2.53}AgGe_2$. In this compound the Ge atoms form unique one-dimensional chains in form of the number eight. Therefore every Ge atom forms two homoatomic bonds. The Ag atoms in this structure bridge the one dimensional chains of Ge to the distorted diamond-like

polyanionic network without forming any homoatomic bonds. Therefore two homoatomic bonds occur for every three atoms of the polyanionic partial structure in this compound. The resulting degree of distortion of the polyanionic network is so strong, that the interatomic distances between some Li positions in the cationic partial structure get too small, resulting in one completely unoccupied position as well as another position that is only occupied by 32(6) %. In comparison, the structure of Li_2AgGe consists of layers of Ge_2 dumbbells and isolated Ge atoms which are, as in $Li_{2.53}AgGe_2$, connected via Ag atoms to form a diamond-like polyanionic network. In this network also Ag-Ag contacts occur resulting in two homoatomic bonds for every four atoms of the polyanionic partial structure. The resulting degree of distortion is smaller than in $Li_{2.53}AgGe_2$ and every Li position in the cationic partial structure is occupied. Investigations in the part of the ternary concentration diagram between these two compounds resulted in the discovery of the compound $Li_2Ag_{1-x}Ge_{1+x}$ (x = 0.06(11)). This compound was found as main phase in all experiments with a starting composition of Li:Ag:Ge = 2:1−x:1+x (x = 0.1, 0.2 0.5). In opposition to Li_2AgGe and $Li_{2.53}AgGe_2$ the positions of the polyanionic network in this compound are not ordered. Instead, every position in the diamond-like polyanionic network is mixed-occupied by Ag and Ge in the same ratio. If the Ag:Ge ratio in this compound would be 1:1 which is in the limits of the standard deviation an undistorted diamond-like polyanionic network with perfect tetrahedral angles of 109.47° would be expected. In fact, the respective angles in this compound are 108.56° and 109.93° compared with 107.62° and 111.26° in Li_2AgGe. This indicates that there are still some homoatomic contacts in this compound which result from the small excess of Ge in contrast to Ag on the respective positions. An excess of Ag can be rejected due to the used starting compositions. Regarding the electronic structure of these compounds, it should be noted that none of these compounds is electron precise. As DOS calculations for $Li_{2.53}AgGe_2$ confirm, there is some electron density at the Fermi level in this compound which is results in a metallic character of the compound. This is also expected for Li_2AgGe and $Li_2Ag_{1-x}Ge_{1+x}$ regarding their lustrous metallic appearance.

Comparing these three compounds to the three compounds $LiAg_2Ge$, $Li_3Ag_2Ge_3$ and $Li_3Ag_3Ge_2$ known previous to this work it occurs that the structures of $LiAg_2Ge$ and $Li_3Ag_2Ge_3$ also derive from the Heusler structure, while $Li_3Ag_3Ge_2$ crystallizes in the Cu_3Au structure type. Due to the low amount of Li in $LiAg_2Ge$ and $Li_3Ag_2Ge_3$ more than

half of the tetrahedral voids are occupied by Ag or Ge and no diamond-like polyanionic substructure occurs.

a)   b)   c)
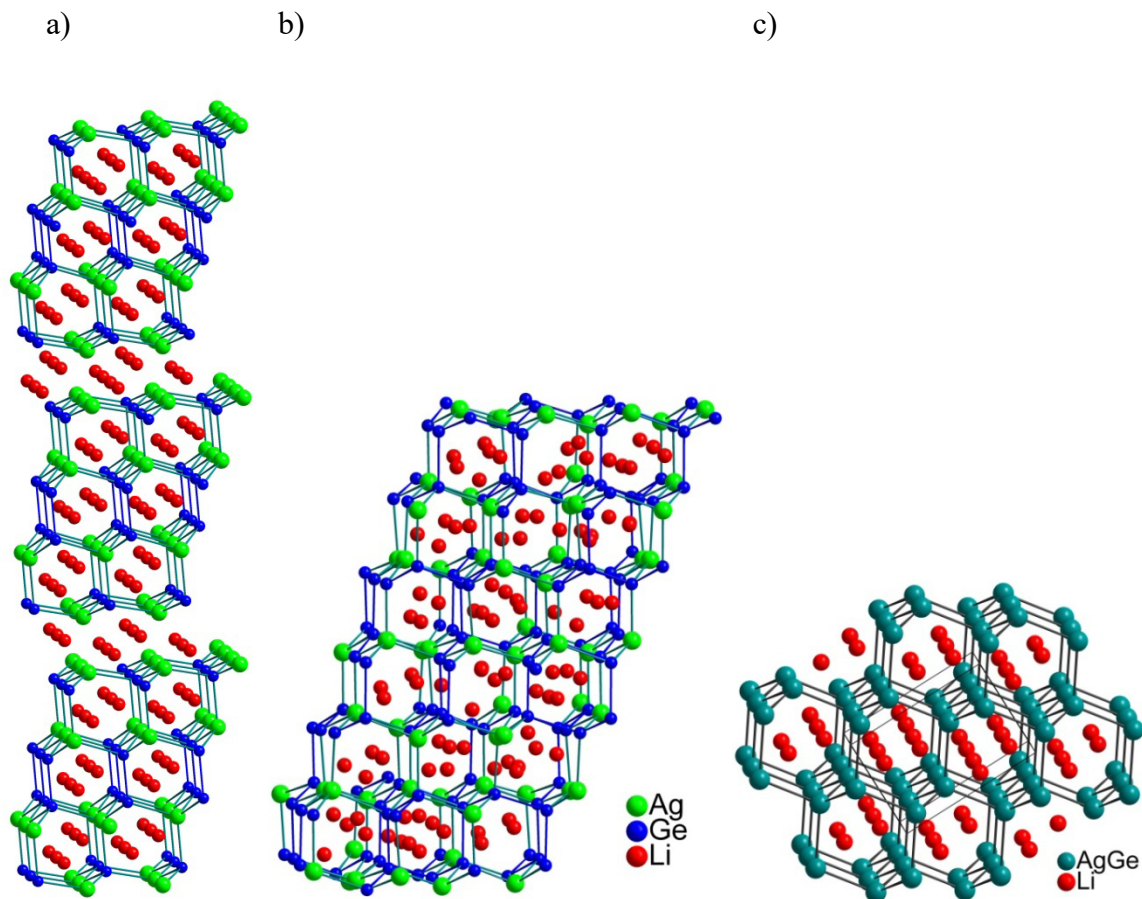
Figure 3. Li-filled distorted polyanionic networks of a) Li_2AgGe b) $Li_{2.53}AgGe_2$ and c) $Li_2Ag_{0.94}Ge_{1.06}$

The Li richest compound that was found in the Li-Ag-Ge system was $Li_{12}AgGe_4$. The structure of this compound includes Ge_2 dumbbells and a unique $[Ge-Ag-Ge]^{7-}$ trimer. These structural units remind on the Ge_2 dumbbells and isolated Ge atoms in Li_2AgGe though the "Ge-Ag-Ge" units in Li_2AgGe are not linear. Though $Li_{12}AgGe_4$ is looking like a substitution product of $Li_{13}Ge_4$ it crystallizes in the structure type of $Li_{13}Si_4$ which is different to $Li_{13}Ge_4$. This is rather surprising, as $Li_{13}Ge_4$ should represent the energetically favored structure type. This was shown by substitution experiments including Mg in the structure.[15] Searching for an explanation for this unusual behavior, an analysis of the density of states (DOS) and a closer look on the bonding situation using crystal orbital Hamilton population (COHP) calculations was conducted. The results

17

showed an optimization of the very strong Ag-Ge bonds in the $[\text{Ge-Ag-Ge}]^{7-}$ trimer, while the Ge-Ge bond in the Ge_2 dumbbells and Li-Ge bonds are not optimized energetically. As the formation of the $[\text{Ge-Ag-Ge}]^{7-}$ trimer through substitution of a Li with a Ag position can only be achieved within the $Li_{13}Si_4$ structure type and not the $Li_{13}Ge_4$ structure type, the formation of this trimer seems to be the reason for this switch.
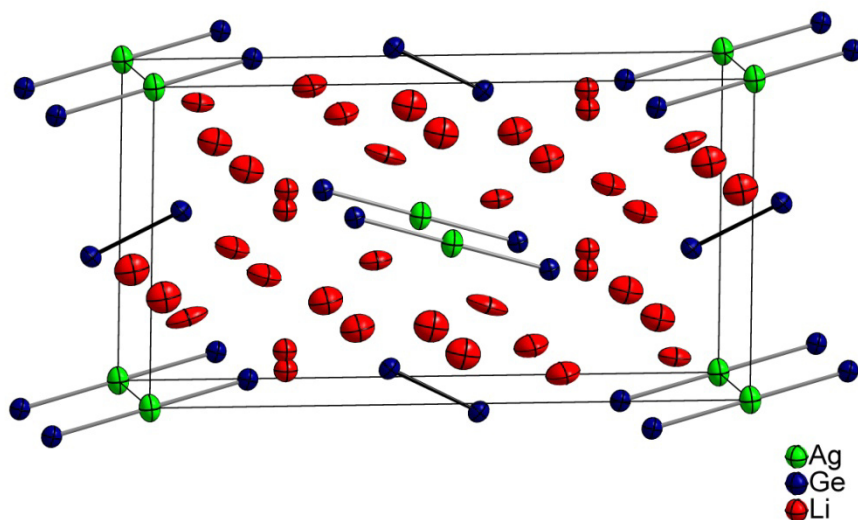
Figure 4. Structure of $Li_{12}AgGe_4$.

2.3   *Synthesis and Structure of Li_6CuSn_2*

See manuscript 6.4   The Copper Stannide with the Highest Lithium Content: Synthesis and Structural Characterization of Li_6CuSn_2

A. Henze, T.F. Fässler, manuscript in preparation

The rising interest in Sn containing intermetallic compounds as anode materials in LIBs led to investigations in the Li-Cu-Sn system. High-temperature synthesis using a premelted Cu-Sn alloy and elemental Li yielded the new compound Li_6CuSn_2 which now represents the Li-richest compound in this phase system. The structure of the compound was investigated using single-crystal X-ray diffraction. The polyanionic part of the structure is formed by Cu and Sn. These elements form nearly planar two-dimensional

18

layers of six-membered rings with only heteroatomic contacts between the elements. There are holes in these layers though, as only 50% of the Cu positions are occupied statistically. An ordered model of this structure leads to a layered arrangement of Cu-Sn chains where every Cu position is surrounded by three Sn atoms, while the Sn atoms posses only one or two neighboring Cu atoms. Between these polyanionic layers, Li is intercalated in form of two two-dimensional layers also consisting of nearly planar six-membered rings. As the polyanionic layers, the Li containing layers contain holes as one of the two independent Li positions is only occupied by 50% just as the Cu position is. Therefore in the ordered model of this compound the Li positions arrange in chains as well. Variations in the synthesis of the compound might lead to an ordered variant of the compound with only full occupied atomic positions. The long ellipsoids in c direction of the half-occupied atoms might be a hint for an incommensurability of the compound. A better solution might hence be achieved by a modulation of the structure.
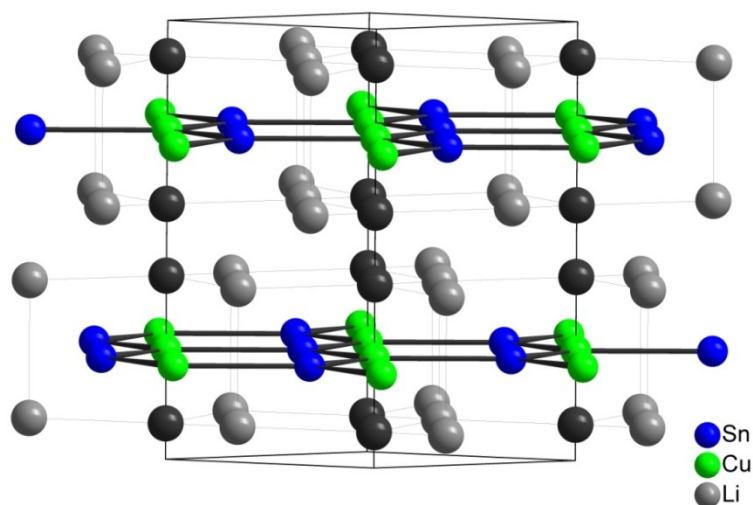
Figure 5. Structure of Li_6CuSn_2. Cu and Li2 positions in dark grey are occupied by 50%, Sn and Li1 positions in light grey are fully occupied.

2.4   References

(1)   Nesper, R. *Prog. Solid St. Chem.* **1990,** *20*, 1-45.

(2)   Huggins, R. A. *Handbook of Battery Materials* **1999**, 359-381.

(3)   Schuster, H.-U.; Thiedemann, D.; Schönemann, H. *Z. Anorg. Allg. Chem.* **1969,** *370*, 160-170.

(4)   Pauly, H.; Weiss, A.; Witte, H. *Z. Metallkd.* **1968,** *59*, 47-58.

(5)   Machill, S.; Rahner, D. *Journal of Power Sources* **1995,** *54*, 428-432.

(6)   Besenhard, J.; Yang, J.; Winter, M. *Journal of Power Sources* **1997,** *68*, 87-90.

(7)   Pöttgen, R.; Dinges, T.; Eckert, H.; Sreeray, P.; Wiemhöfer, H.-D. *Z. Phys. Chem.* **2010,** *224*, 1475-1507.

(8)   Winter, F.; Dupke, S.; Eckert, H.; Rodewald, U. C.; Pöttgen, R. *Z. Anorg. Allg. Chem.* **2013,** *639*, 2790-2795.

(9)   Sreeraj, P.; Wiemhöfer, H.-D.; Hoffmann, R.-D.; Walter, J.; Kirfel, A.; Pöttgen, R. *Solid State Sci.* **2006,** *8*, 843-848.

(10)   Schuster, H.-U.; Kahlert, H. *Z. Naturforsch. B* **1972,** *27*, 79-80.

(11)   Kevorkov, D. G.; Pavlyuk, V. V.; Bodak, O. I. *Pol. J. Chem.* **1997,** *71*, 712–715.

(12)   Kripyakevich, P. I.; Oleksiv, G. I. *Dopovidi Akademii Nauk Ukrains'koi RSR, A* **1970**, 63-65.

(13)   Fürtauer, S.; Effenberger, H. S.; Flandorfer, H. *Z. Kristallogr.* **2015,** *230*, 97-105.

(14)   Fürtauer, S.; Effenberger, H. S.; Flandorfer, H. *Z. Kristallogr.* **2016,** *231*, 79-87.

(15)   Nesper, R. Habilitation, University of Stuttgart, 1988.

3 Interconnected Intermetallic Clusters of Germanium and Tin

3.1 Introduction

The chemistry of intermetallic clusters has always been interesting for chemists as they mark a meeting point between solid state, solution based and gas phase chemistry.[1] The most common clusters are $[E_4]^{4-}$ and $[E_9]^{4-}$ for group 14 elements as well as icosahedra for the triels.[2] But a variety of different homo- and heteroatomic clusters is known from tetrahedra as the smallest possible cluster to clusters build out of more than 100 atoms.[3] To describe heterometallic clusters, the term *intermetalloid* has been introduced. This term derives from the term *metalloid* cluster, which describes large ligand stabilized homometallic clusters of transition and group 13 metals in which the number of direct metal-metal contacts exceeds the number of metal-ligand bonds.[4] Deriving from this concept the term *intermetalloid* cluster was introduced for ligand-free heterometallic clusters of group 14 elements with encapsulated transition metals.[5] But it is also used to describe non-filled and ligand stabilized clusters.[6, 7] Although this concept was introduced for group 14 elements, it applies also for group 13 elements. These elements rarely form clusters in the solid state with some exceptions like AGa$_3$ (A = alkali metal).[8] Instead, due to their low electron count these elements tend to form structures composed of interconnected clusters. The introduction of late transition elements into binary A-Tr (Tr = triel element) systems leads to the formation of heterometallic interconnected cluster which are closely related to those known as intermetalloid.[9, 10] This behavior can be mimicked by the tetrel elements through introduction of electron poor transition metals, which then also leads to interconnected clusters.[11] The outstanding reports on intermetalloid and interconnected intermetallic cluster in the ternary system Na-Cu-Sn[12, 13] and Na-Zn-Sn[11] led to investigations in the neighboring Na-Ag-Sn system. In this system, no ternary compounds had ever been reported. Due to the fact that Ag is only a one electron donor, the existence of compounds with interconnected cluster seemed probable.
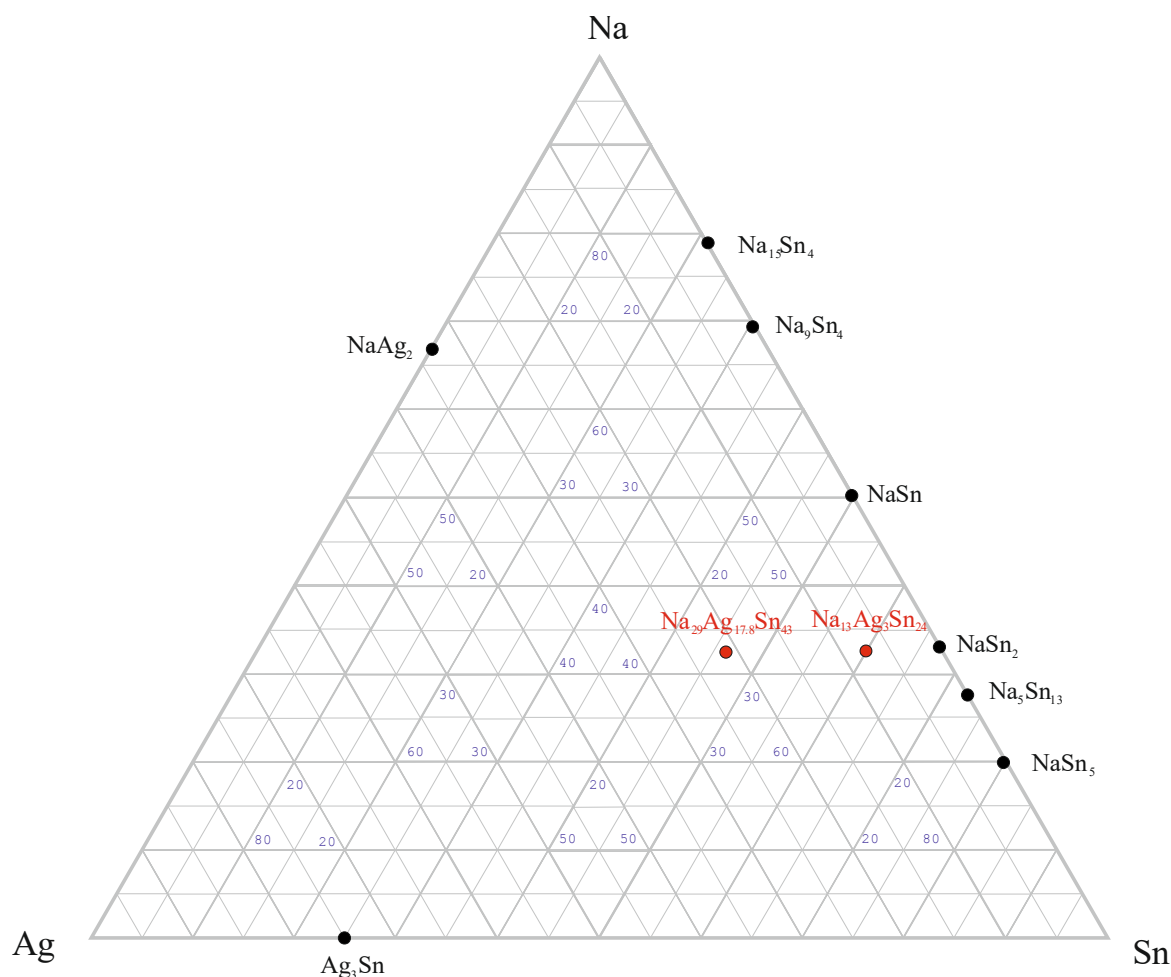
Figure 6. Concentration diagram of the ternary system Na-Ag-Sn. Binary compounds are marked in black and ternary compounds synthesized in this thesis are marked in red.

In contrast to the Na-Ag-Sn system no compound with interconnected clusters were to be expected in the ternary system Li-Ni-Ge, in which prior to this work only the typical Heusler phase $LiNi_2Ge$ and $LiNi_6Ge_6$ which crystallizes in the quite common $LiFe_6Ge_6$ structure type had been reported.[14, 15] Investigations in this system primarily is inspired by other Li containing compounds and their importance for Li ion batteries. Nevertheless Ni and Ge form an extensive amount of different structures in combination with earth-alkali[16-18] and rare-earth elements[19, 20] and Ni is part of a lot of rhombic dodecahedral clusters known from solution based chemistry.[21, 22] In the following, ternary new compounds in phase systems Na-Ag-Sn and Li-Ni-Ge with structures build by interconnected clusters are presented.

3.2 Interconnected Rhombic Dodecahedra in $Li_{14}Ni_{8.3}Ge_{8.7}$

See manuscript 6.5: Synthesis and Structural Characterization of $Li_{14}Ni_{8+x}Ge_{9-x}$ (x = 0.3) featuring the First Rhombic Dodecahedral Cluster in a Solid State Compound

A. Henze, T.F. Fässler, manuscript in preparation

Investigations in the ternary system of Li-Ni-Ge led to the discovery of the new compound $Li_{14}Ni_{8.3}Ge_{8.7}$. This compound crystallizes in its own structure type in the space group $Fm\bar{3}m$ and derives from the Heusler structure. In this structure, rhombic dodecahedral (Ni_8Ge_6) clusters form a face-centered cubic (fcc) packing. The central atomic position in these clusters is occupied by Ni and Ge with an occupation ratio of 30:70 without any signs of ordering. The clusters are interconnected by Ge atoms occupying all of the tetrahedral voids, thus forming a three-dimensional network with large channels in *ac* and *bc* direction. These channels are occupied by Li atoms which adopt interstitial sites as well as the octahedral voids of the fcc packing in form of Li_8 cubes. No electron density could be found inside of these Li_8 cubes. The filled (Ni_8Ge_6) cluster represents a rhombic dodecahedron and is the first such cluster synthesized by a solid state reaction. As the Ge atoms in the tetehedral voids are formally charged 4− the (Ni_8Ge_6) cluster should be formally charged 6− to charge balance the compound. This charge fits well to related clusters like $[Ni@Ni_8(GeEt)_6](CO)_8$. Therefore $[Ni@Ni_8Ge_6]^{6-}(Ge^{4-})_{8/4}$ also represents the first charged rhombic dodecahedral cluster, as this is not known from solution based reactions. The Ge as a main group element in the center of this cluster represents a rather rare exception as only one other cluster is known so far with a main group element centering a rhombic dodecahedron. Theoretical calculations show the stability of such clusters though.

a)
b)

Ge
GeNi
Ni
Li
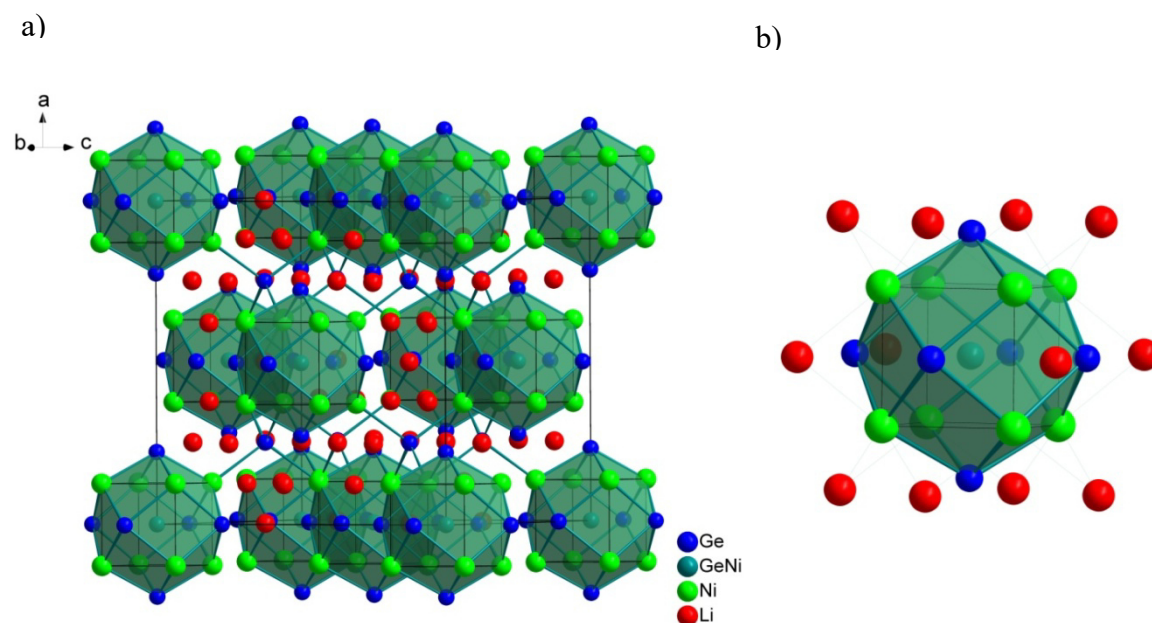
Figure 7. a) Structure of $Li_{14}Ni_{8.3}Ge_{8.7}$. b) filled Ni_8Ge_6 cluster with Li coordination sphere.

3.3 Interconnected Clusters and Cluster-like Networks in $Na_{29}Ag_{17.8}Sn_{43}$ and $Na_{13}Ag_{2.7}Sn_{24}$

See manuscript 6.6:   Synthesis and Structural Characterization of $Na_{29}Ag_{17.8}Sn_{43}$ and $Na_{13}Ag_{2.7}Sn_{24}$

A. Henze, T.F. Fässler, manuscript in preparation

Investigations in the ternary system Na-Ag-Sn resulted in the discovery of the two new compounds $Na_{29}Ag_{17.8}Sn_{43}$ and $Na_{13}Ag_{2.7}Sn_{24}$ representing the first known compounds in this ternary system. The structure of both compounds was investigated using single-crystal X-ray diffraction. The compound $Na_{29}Ag_{17.8}Sn_{43}$ crystallizes in its own structure type in the space group P_6/mmm. Its structure is closely related to compounds like $Na_8K_{23}Cd_{12}In_{48}$ and $Na_{29}Zn_{24}Sn_{32}$.[11, 23] It consists of interconnected icosahedra, triangles and a unique Na centered Ag_7Sn_{13} cluster. This cluster is closely related to M_{18} clusters found in $Na_8K_{23}Cd_{12}Ga_{48}$ and $Na_{30.5}Ag_{2.6}Ga_{57.4}$.[24] A close analysis of the anisotropic replacement parameters led to the introduction of a split position on the central ring of six

24

Sn atoms. Due to this split, the identification of three Sn-Sn bonds was possible which were not considered in the related M_{18} cluster. Looking at the anisotropic replacement parameters in these clusters, these three bonds between the main group atoms should be present too.

The compound $Na_{13}AgSn_{24}$ crystallizes in its own structure type which represents a coloring variant of the Bergman structure. Two Na centered Friauf polyhedra sharing one six-ring plane connect the Sn icosahedron in the center of the unit cell with the ones on the corners. The space in between those double-Friauf polyhedra is occupied by Na atoms and Ag_2 dumbbells. As the compound was synthesized in a crystallographic phase pure manner, the magnetic properties of the compound were investigated using a SQUID. The compound is diamagnetic.

a)

b)

Figure 8. a) Structure of $Na_{29}Ag_{17.8}Sn_{43}$ b) three types of clusters in $Na_{29}Ag_{17.8}Sn_{43}$.

a)   b)
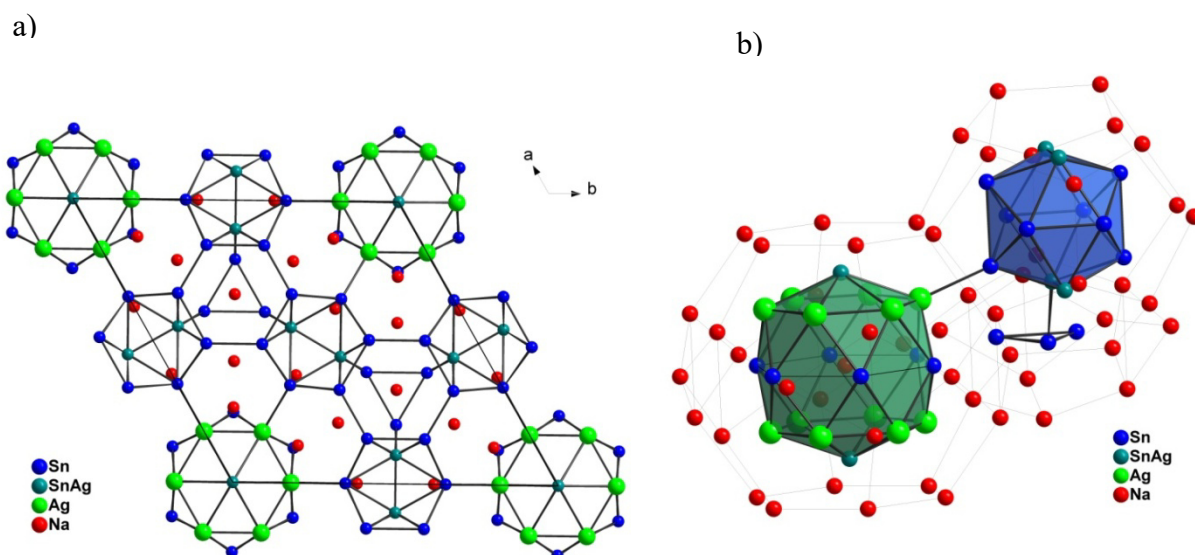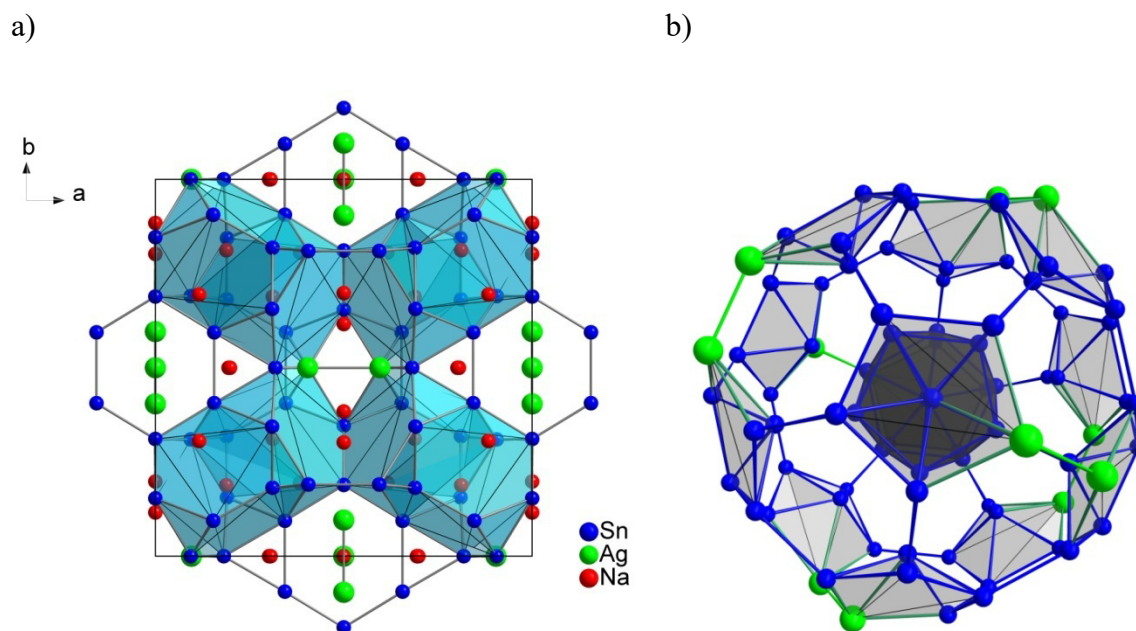
Figure 9. a) Structure of Na$_{13}$Ag$_{2.7}$Sn$_{24}$. b) Buckyball-like surrounding of the central icosahedron.

3.4   References

(1)   Oro, L. A.; Braunstein, P.; Raithby, P. R., *Metal clusters in chemistry*. Wiley-vch Weinheim, Germany: 1999; Vol. 3.

(2)   Belin, C.; Tillard-Charbonnel, M. *Prog. Solid St. Chem.* **1993,** *22*, 59-109.

(3)   Tran, N. T.; Powell, D. R.; Dahl, L. F. *Angew. Chem. Int. Ed.* **2000,** *39*, 4121-4125.

(4)   Schnepf, A.; Schnöckel, H. *Angew. Chem. Int. Ed.* **2001,** *40*, 711-715.

(5)   Fässler, T. F.; Hoffmann, S. D. *Angew. Chem. Int. Ed.* **2004,** *43*, 6242-6247.

(6)   Scharfe, S.; Fässler, T. F. *Philosophical Transactions of the Royal Society of London A: Mathematical, Physical and Engineering Sciences* **2010,** *368*, 1265-1284.

(7)   Fässler, T. F., *Zintl Phases: Principles and Recent Developments*. Springer Science & Business Media: 2011; Vol. 139.

(8)   Belin, C.; Ling, R. *COMPTES RENDUS DE L ACADEMIE DES SCIENCES SERIE II* **1982,** *294*, 1083-1086.

(9)   Cordier, G.; Müller, V. *Z. Naturforsch. B* **1995,** *50*, 23-30.

(10)   Tillard-Charbonnel, M.; Chouaibi, N.; Belin, C.; Lapasset, J. *J. Solid State Chem.* **1992,** *100*, 220-228.

(11)   Kim, S.-J.; Hoffman, S. D.; Fässler, T. F. *Angew. Chem.* **2007,** *119*, 3205-3209.

(12)   Stegmaier, S.; Fässler, T. F. *J. Am. Chem. Soc.* **2011,** *133*, 19758–19768.

(13)   Stegmaier, S.; Fässler, T. F. *Angew. Chem.* **2012,** *124*, 2701 –2704.

(14)   Schuster, H. U.; Mewis, A. *Z. Naturforsch, B* **1969,** *24*, 1190.

(15)   Buchholz, W.; Schuster, H. U. *Z. Anorg. Allg. Chem.* **1981,** *482*, 40-48.

(16)   Siggelkow, L.; Hlukhyy, V.; Wahl, B.; Fässler, T. F. *Eur. J. Inorg. Chem.* **2011,** *2011*, 4012-4024.

(17)   Hlukhyy, V.; Eck, S.; Fässler, T. F. *Inorg. Chem.* **2006,** *45*, 7408-7416.

(18)   Hlukhyy, V.; Siggelkow, L.; Fässler, T. F. *Inorg. Chem.* **2013,** *52*, 6905-6915.

(19)   Bodak, O.; Bruskov, V.; Pecharskij, V. **1982**.

(20)   Salvador, J.; Gour, J.; Bilc, D.; Mahanti, S.; Kanatzidis, M. *Inorg. Chem.* **2004,** *43*, 1403-1410.

(21)   Zebrowski, J. P.; Hayashi, R. K.; Bjarnason, A.; Dahl, L. F. *J. Am. Chem. Soc.* **1992,** *114*, 3121-3123.

(22)   Fenske, D.; Basoglu, R.; Hachgenei, J.; Rogel, F. *Angew. Chem. Int. Ed.* **1984,** *23*, 160–162.

(23)   Flot, D. M.; Tillard-Charbonnel, M. M.; Belin, C. H. E. *J. Am. Chem. Soc.* **1996,** *118*, 5229-5235.

(24)   Henning, R. W.; Corbett, J. D. *Z. Anorg. Allg. Chem.* **2002,** *628*, 2715-2723.

4   Summary and Conclusion

The field of intermetallic solid state chemistry though being investigated for a long time, still has a lot to offer. Regarding the number of possible to already found intermetallic compounds, it seems clear that still a lot of smart solutions for striking problems of our modern world are up to be found by solid state chemists.

In view of the many possibilities offered, the focus of this thesis was set on the chemistry of group 14 elements Ge and Sn in ternary intermetallic compounds. These elements were in any case reacted with one of the two alkali metals Li and Na. The reaction of the rather electronegative group 14 elements with the electropositive alkali metals leads to the reduction of the tetrel elements and the formation of polyanionic substructures. This includes clusters, as well as two dimensional layers or three dimensional networks. The introduction of a third element from the late transition metals offers the possibility of broader variations in these structures. This enables possibilities from designing properties of already known structures to producing structures that can only be stabilized by the influence of the transition metals.

In view of the very strong interest in Li containing compounds due to their possible use in Li ion batteries, ternary systems containing Li, transition metals and group 14 elements where analyzed and a few where identified for further investigations due to a low amount of known phases and their potential regarding neighboring systems. One of these systems identified for closer investigations was Li-Ag-Ge. Although three compounds where already known in this system, the existence of another four compounds with the compositions Li_2AgGe, $Li_{2.53}AgGe_2$ and $Li_2Ag_{1-x}Ge_{1+x}$ (x = 0.06) as well as $Li_{12}AgGe_4$ were proven in this thesis. The structure of these compounds was analyzed using single crystal X-ray diffraction. Thus it was possible to show that the first three compounds are composed of a NaTl like structure with Ag and Ge building a diamond-like polyanionic substructure with different degrees of distortion. This polyanionic networks are all filled with Li. Investigations on the thermal and magnetic behavior of the compounds showed stability up to high temperatures and diamagnetic behavior. Calculations on the band structure of $Li_{2.53}AgGe_2$ showed a pseudo band gap near the Fermi level, resulting in overall metallic behavior of the compound. A similar behavior can be assumed for the other two compounds based on their appearance.

In contrast to these structures, the Li rich phase $Li_{12}AgGe_4$ does not form a three dimensional polyanionic substructure, but consists of $[Ge_2]^{5-}$ dumbbells and a unique $[Ge-Ag-Ge]^{7-}$ trimer. The compound surprisingly does not crystallize in the $Li_{13}Ge_4$, but in the $Li_{13}Si_4$ structure type, even though this structure type should be energetically less stable as shown through substitution experiments with Mg. Investigations in the bonding situations including COHP calculations revealed that the Ag-Ge bond is particularly short and strongly favored on an energetic level. The possible formation of the $[Ge-Ag-Ge]^{7-}$ trimer thus seems to be the driving force to this choice of structure type. While Ge_2 dumbbells similar to those in $Li_{12}AgGe_4$ are also found in binary Ge containing compound, the trimer has never been described before and represents one of the smallest possible intermetalloid clusters.

Two different ternary systems containing Li that were selected for closer investigations were the Li-Ni-Ge and the Li-Cu-Sn system. It was possible to identify one rather Li rich compound that had not been described before in each system. In the Li-Cu-Sn system, the compound Li_6CuSn_2 was synthesized and characterized. The structure of this compound can be described as nearly planar two-dimensional layers of Cu and Sn with intercalated layers of Li atoms. The layers exhibit some holes though, as the Cu and one of the two Li positions are only 50% occupied each. Therefore the structure consists of strings of Cu and Sn in a layered order.

In the Li-Ni-Ge system the compound $Li_{15}Ni_{8.3}Ge_{8.7}$ was synthesized which is build of Ni_8Ge_6 clusters filled with Ni or Ge with a ratio of 30:70. These clusters are bridged over Ge atoms thus forming a three-dimensional polyanionic network. The large channels in this network are filled with Li atoms. The compound is electronically balance and can be viewed as a Zintl compound. In view of the extraordinary clusters in the Na-Cu-Sn and Na-Zn-Sn systems, the neighboring Na-Ag-Sn system was investigated. It was possible to find and analyze the first two compounds in this ternary system, which are $Na_{29}Ag_{17.8}Sn_{43}$ and $Na_{13}Ag_{2.7}Sn_{24}$. Both compounds feature interconnected clusters related to those known from triel containing compounds, especially with Ga and In. It was possible to trace this back to the low amount of electrons provided by Ag. The structural analysis of $Na_{29}Ag_{17.8}Sn_{43}$ showed that the unique $Sn_{13}Ag_7$ cluster found in this compound is related to already known M_{18} clusters. The structure of $Na_{13}Ag_{2.7}Sn_{24}$ which derives from the Bergman structure is build of distorted Sn_{12} icosahedra interconnected by Friauf polyhedra and contains isolated Ag_2 dumbbells.

5 Methods

5.1 General experimental procedures

Before the experimental work was started, it was already supposed that besides the used alkali metals also a lot of the product might not be stable against air and moisture. Regarding this, all work was executed using an argon-filled glovebox (MBraun 20 G) and other inert gas techniques. The used Argon was welding Argon of the Westfalen AG with a purity of 99.996 Vol.-% which was dried over P_2O_5, molecular sieve and a heated (T = 750 °C) titanium sponge before using. The amount of water and oxygen in the glovebox used to be less than 0.1 ppm.

5.2 Synthesis

5.2.1 Starting Materials

All used elements are listed in Table 1. All elements were stored in an argon-filed glovebox to prevent any oxidation from air and moisture. Transition metals and group 14 elements were used as provided by the producer. The Li-rods were covered by a layer of Li-oxides which was removed by cutting before the subjacent lustrous metallic Li was weighed in. Na-oxides on the Na rods were removed by cutting as well.

Table 1:   Specifications of starting materials

Element	Shape	Supplier	Purity /%
Li	Rods	Rockwood Lithium	99
Li	Rods	Sigma Aldrich	99.9
Na	Rods	Merck	99
Ni	Wire	Johnson-Matthey	99.9
Cu	Wire	Sigma Aldrich	99.9
Ag	Wire	Sigma Aldrich	99.9
Ge	Chunks	Chempur	99.999
Sn	Granules	Chempur	99.999

5.2.2   Reaction container and sample preparation

Tantalum and niobium ampoules were used as reaction containers during this work. They were prepared by cutting approximately 5 cm long pieces of a respective tube (2000 mm length, 10 mm external diameter, 0.5 mm wall thickness). These pieces were closed by crimping them on one side and sealed with an arc-melter (water-cooled arc furnace, MAM-1, JOHANNA OTTO GmbH) afterwards. Prior to sample loading, these ampoules with one sealed side were cleaned by washing (under ultrasonification) with diluted nitric acid, deionized water and acetone for 10 minutes each. Afterwards they were dried and stored in an oven at 120 °C. The cleaned and dried ampoules were then transferred to an argon filled glovebox and loaded with the starting materials. Afterwards the second end of the ampoules was sealed inside of the glovebox and the ampoule was transferred to a furnace.

5.3   *Experimental Characterization*

5.3.1   Powder X-ray Diffraction

In an argon-filled glove box, the respective sample was grounded to a homogeneous powder in an agate mortar and filled into a glass capillary. The capillaries were sealed using a hot tungsten filament and capillary wax. For data collection a Stoe Stadi P powder diffractometer with Cu-K$_\alpha$ radiation (λ = 1.54056 Å, Ge(111) monochromator) and equipped with a position-sensitive detector (DECTRIS MYTHEN DCS 1K) was used. The samples were measured in Debye-Scherer geometry at room temperature.

The Stoe WINXPOW program[1] package was used for phase analysis. For the phase identification, the powder patterns of the measured samples were compared with powder patterns of known phases using the search/match module, the ICSD (FINDIT)[2] and the PEARSON'S CRYSTAL DATA crystallographic data base[3].

5.3.2   Single crystal X-ray Diffraction

For single crystal X-ray diffraction experiments, single crystals of the respective compound were selected in an argon-filled glove box equipped with a microscope. For low-temperature measurements the crystals were mounted on the top of a glass fiber

which was fixed in a sample holder pin using perfluoropolyalkylether and transferred to the diffractometer using suitable containers. For room temperature measurements the single crystals were mounted on a glass fiber which was put into a glass capillary and the capillary was sealed by a hot tungsten wire. The capillaries were than mounted in a sample holder pin. For data collection an Oxford Xcalibur3 diffractometer system (Sapphire3 CCD detector) and a Bruker AXS X-ray diffractometer system (APEX II, κ-CCD detector) were used. Both diffractometers use Mo K_α radiation (λ = 0.71073 Å, graphite monochromator). The Xcalibur3 diffractometer uses a sealed tube X-ray source, while the Bruker AXS diffractometer uses a rotating anode (Nonius FR591). Both diffractometers were equipped with an OXFORD INSTRUMENTS Cryojet cooling system (nitrogen jet) allowing low temperature measurement.

The data processing for measurements was carried out using the respective diffractometer software. In case of the Xcalibur3 diffractometer the software used was the Oxford CrysAlis RED software[4].

5.3.3 Differential Thermal Analysis

Differential Thermal Analysis investigations were performed using a Netzsch DSC 404 Pegasus apparatus equipped with a DTA carrier system. Nb crucibles were used as reaction containers. The crucibles were cleaned according to the Nb and Ta crucibles described in Chapter 5.2. Afterwards they were transferred into an Ar filled glove box and loaded with 40 – 70 mg of the respective sample. The open end was than crimped and sealed by arc-welding inside of the glove box. An empty, sealed crucible was used as a reference. All measurements were performed under an Argon flow of 60-70 mL·min^{-1}. The heating/cooling rate was set to 5 K·min^{-1} or 10 K·min^{-1}. After the measurement, the samples were regained in an Argon-filled glove box by opening of the Nb-containers. For data processing, the program Proteus thermal analysis was used.[5]

5.3.4 Energy dispersive X-ray Spectroscopy

For qualitative and semi-quantitative analysis of the composition of selected single crystals was performed by energy dispersive X.ray spectroscopy. Therefore a Joel-5900LV scanning electron microscope system operating at 20kV was used and equipped with an Oxford Instruments Inco energy dispersive X-ray microanalysis system was used.

After determining the unit cell of the respective single crystal by single crystal X-ray diffraction, the single crystal was transferred into an argon-filled glove box and mounted on a graphite platelet which was fixed on a cylindrical aluminum sample holder.

5.3.5 Magnetic Measurements

The determination of the magnetic properties of selected compounds was realized using a MPMS XL5 Squid magnetometer (Quantum Design). The respective sample was prepared by filling 30 – 50 mg into a gelatin capsule which was fixed in the middle of a plastic straw. All data were corrected for the sample holder and ion-core diamagnetism using Pascal's constants.[6]

5.4 Electronic structure calculations

DFT electronic structure calculations were carried out using the Tight-Binding (TB) version of the Linear Muffin Tin Orbital (LMTO) method in the Atomic Sphere Approximation (ASA).[7] The exchange-correlation potential was used according to von Barth and Hedin.[8] The k-space integration was performed by the tetrahedron method.[9] The radii of the atomic sphere as well as the radii of the interstitial empty spheres were determined according to Jepsen and Anderson.[10] The basis sets employed in the calculations are stated in the respective publications and manuscripts.

5.5 References

(1)   Stoe *WinXPOW*, 2.08; Stoe & Cie GmbH: Darmstadt, 2003.

(2)   *FindIt, Inorganic Crystal Structure Database (ICSD)*, Version 14-1; Fachinformationszentrum Karlsruhe (FIZ): Karlsruhe, Germany, 2014.

(3)   Villars, P.; Cenzual, K. *Pearson's Crystal Data: Crystal Structure Base for Inorganic Compounds*, Version 1 (Realease 2007/08); ASM International: Materilas Park, Ohio, USA, 2003.

(4)   Stoe *CrysAlis RED*, 1.171.33.34; Oxford Diffraction Ltd.: 2009.

(5)   *Netzsch Proteus Thermal Analysis*, 4.8.2; Netzsch-Gerätebau GmbH: Selb, Germany, 2006.

(6)   Bain, G. A.; Berry, J. F. *J. Chem. Educ.* **2008,** *85*, 532–536.

(7)   van Schilfgaarde, M.; Paxton, T. A.; Jepsen, O.; Andersen, O. K.; Krier, G. *The Stuttgart Tight-Binding LMTO-ASA program*, 4.7; Max Planck Institut für Festkörperforschung, 1997.

(8)   von Barth, U.; Hedin, L. *J. Phys. C: Solid State Phys.* **1972,** *5*, 1629–1642.

(9)   Blöchl, P. E.; Jepsen, O.; Andersen, O. K. *Phys. Rev. B.* **1994,** *49*, 16223–16233.

(10)   Jepsen, O.; Andersen, O. K. *Z. Phys. B.* **1995,** *97*, 35–47.

6 Publications and Manuscripts

6.1 Switching the Structure Type upon Ag Substitution: Synthesis and Crystal as well as Electronic Structures of $Li_{12}AgGe_4$

A. Henze, T.F. Fässler,

Inorg. Chem. **2016**, *55*, 822-827.

Inorganic Chemistry

Switching the Structure Type upon Ag Substitution: Synthesis and Crystal as well as Electronic Structures of Li$_{12}$AgGe$_4$

Alexander Henze and Thomas F. Fässler*

Department Chemie, Technische Universität München, Lichtenbergstrasse 4, Garching, D-85747 Germany

Ⓢ Supporting Information

ABSTRACT: Li-rich compounds of metals and semimetals are interesting candidates for anode materials for rechargeable batteries. The investigation of the Li-rich part of the Li−Ag−Ge phase diagram led to the discovery of the new compound Li$_{12}$AgGe$_4$, which represents the Li-richest phase in the ternary phase system. The phase-pure compound is synthesized by high-temperature reaction of Li with stoichiometric amounts of premelted reguli of Ag and Ge. The structure was determined by single-crystal X-ray diffraction. Li$_{12}$AgGe$_4$ crystallizes in the Li$_{13}$Si$_4$ structure type in the space group *Pbam* (no. 55) with lattice parameters of a = 8.0420(2) Å, b = 15.1061(4) Å, and c = 4.4867(1) Å and exhibits the unique Zintl anion [AgGe$_2$]$^{7-}$—iso(valence) electronic to the CO$_2$ molecule—and Ge$_2$ dumbbells. Li$_{12}$AgGe$_4$ adopts the atom packing of the lighter homologue Li$_{13}$Si$_4$ and not that of Li$_{13}$Ge$_4$ by the selective substitution of one out of seven Li positions by Ag. The calculation of the electronic structure indicates metallic property and the presence of strong covalent bonds between Ag and Ge in the linear triatomic Ge−Ag−Ge unit as well as π character between the Ge atoms of the dumbbells. The Ag−Ge bond order of the linear AgGe$_2$ unit reaches its maximum at E_F of Li$_{12}$AgGe$_4$ with full occupancy of all atomic positions (in contrast to the related Li$_{12}$Ag$_{1-x}$Si$_4$), indicating that the formation of covalent Ag−Ge bonds is the driving force for the formation of the structure type.
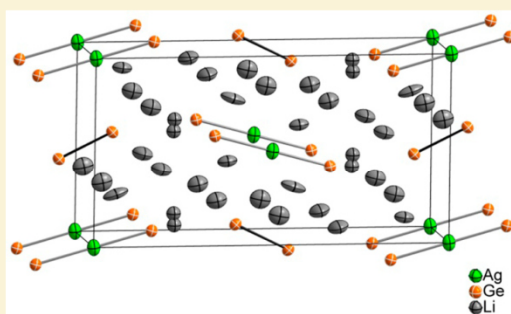
INTRODUCTION

The need for power storage in portable devices has led to strong interest in new Li-ion conducting materials. In particular, binary and ternary Li and group 14 element (*Tt*) containing compounds have gained high interest for providing compounds that can replace graphite as anode materials in Li-ion batteries. Si-containing compounds have been investigated intensively,[1,2] as they combine a very high specific theoretical capacity of 3579 and 4200 mA h g^{-1} (Li$_{15}$Si$_4$[3] and Li$_{17}$Si$_4$,[4] respectively), with a high natural abundance of the element and therefore relatively low costs. However, also Ge-containing compounds have raised some interest due to a 400 times higher Li diffusivity in bulk Ge compared to that in Si at room temperature.[5−7] The integration of transition metals (*M*) in these binary systems offers a wider range for promising compounds with interesting structures like three-dimensional networks with Li-containing channels[8−10] but sometimes also leads to the formation of unexpected new Zintl anions.[11] The existence of molecular Zintl anions in Li-rich binary Li tetrelides is known for (Si$_2$) and (Ge$_2$) dumbbells, e.g., in Li$_{14}$Si$_6$ and Li$_9$Ge$_4$, respectively,[12,13] and [Si$_5$]$^{6-}$ rings and [Si$_4$]$^{10-}$ stars in Li$_{12}$Si$_7$.[14] The introduction of a third element in these binary phase systems broadens in the case of electropositive metals the variety on the size and shape of homoatomic Zintl anions.[15,16] In the case of transition metals that are in principle capable to simply substitute the electropositive metal, also strong interactions up to covalent

bonds with the tetrel element are possible, thus becoming part of the anionic substructure.[11] In view of the remarkable properties of germanium compounds, we reinvestigated the ternary Li−Ag−Ge system. In addition to the known compounds LiAg$_2$Ge, Li$_3$Ag$_3$Ge$_2$, and Li$_3$Ag$_2$Ge$_3$[17] we recently reported on the new ternary compounds Li$_2$AgGe and Li$_{2.53}$AgGe$_2$[18] with Li-containing networks. The former has been the Li-richest reported compound in this system. Further investigations in the Li-richer part of the system now led to the new compound Li$_{12}$AgGe$_4$ with considerably higher Li content and which contains Ge−Ge dumbbells beside the unique [Ge−Ag−Ge]$^{7-}$.

EXPERIMENTAL SECTION

Synthesis. The starting materials for the synthesis of Li$_{12}$AgGe$_4$ were Li rods (99.9%, Sigma-Aldrich), Ag wire (99.9%, Sigma-Aldrich), and Ge pieces (99.999%, ChemPur). All materials were handled in a glovebox (MBraun 20 G, argon purity 99.996%) to exclude any contact with air and moisture. The title compound Li$_{12}$AgGe$_4$ was first synthesized by premelting Ag and Ge (ratio 1:2) in an arc furnace (Mini Arc Melting System, MAM-1, Johanna Otto GmbH) to obtain a regulus of the binary compound with the expected stoichiometry. Subsequently, this regulus was put into a niobium ampule together with Li, so that the final ratio of Li:Ag:Ge was 17:3:6. The ampule was

Article

sealed and transferred into a silica tube. The silica tube was evacuated and put into a vertical resistance tube furnace. After heating to 800 °C and slow cooling to room temperature with 0.1 K min^{-1} the sample was transferred into a glovebox. For a phase-pure synthesis the binary reguli was premelted using 112 mg (1.04 mmol) of Ag and 302 mg (4.15 mmol) of Ge. A 87 mg (12.46 mmol) amount of Li was added to this regulus in a niobium ampule. The sample was heated to 750 °C and tempered for 24 h. Afterward, it was cooled to 670 °C with a rate of 0.1 K min^{-1} and tempered for 48 h. Subsequently, it was cooled to room temperature with a rate of 0.1 K min^{-1}. The product was obtained as a brittle, lustrous silver powder, which is sensitive to air and moisture.

Powder and Single-Crystal X-ray Diffraction and Structural Refinement. For powder diffraction analysis the material was finely ground and sealed in a glass capillary. The sample was measured at room temperature using a Stoe Stadi P powder diffractometer with Cu Kα radiation (λ = 1.54056 Å, Ge(111) monochromator) and a position-sensitive detector (Mython 1K). The Stoe WINXPOW program[19] package was used for phase analysis.

For the single-crystal diffraction study a single crystal was mounted on the top of a glass capillary using perfluoropolyalkylether. The data were collected by an Oxford Xcalibur3 diffractometer system (Sapphire3 CCD detector; Mo Kα radiation, λ = 0.71073 Å, graphite monochromator, sealed tube X-ray source). The Oxford CrysAlis RED software[20] was used for data processing, and the Stoe X-RED/X-SHAPE software[21,22] was used for an empirical absorption correction. X-Prep[23] was used for space group determination and data merging (identical indices only). The programs XS[24] and XL[25] were used for the structure solution (Direct Methods) and refinement. Selected crystallographic data are given in Tables 1, 2, and 3. All atoms are ordered except for one Li position, which has been refined using a split model (Li6a/Li6b).

Table 1. Crystal Data and Structure Refinement

formula	Li$_{12}$AgGe$_4$
fw (g mol^{-1})	481.51
space group	*Pbam* (no. 55)
Z	2
unit cell params (Å)	a = 8.0420(2), b = 15.1061(4), c = 4.4867(1)
P_{calcd} (g cm^{-3})	2.934
abs coeff (mm^{-1})	12.59
F(000) (e)	422.0
cryst shape/color	block/silver
temp. (K)	130
Θ range	3.70−32.74
index range	−12 ≤ h ≤ 11
	−22 ≤ k ≤ 14
	−6 ≤ l ≤ 6
no. of reflns collected	9860
no. of unique reflns	1066
data/param	901/55
GOF on F^2	1.133
R_1, wR_2 (I > 2 $\sigma(I)$)	0.0293, 0.0692
R_1, wR_2 (all data)	0.0355. 0.0713
largest diff. peak and hole (e Å^{-3})	1.52 and −1.53

EDX Measurements. EDX analysis was carried out on a Jeol 5900LV scanning electron microscope equipped with an Oxford Instruments energy-dispersive X-ray microanalysis system. The investigated crystals were tested for the correct unit cell by single-crystal XRD. The quantitative analysis showed only the presence of the elements Ag and Ge with no other elements heavier than Na detectable.

Magnetic Measurements. Magnetic measurements were performed using a Quantum Design MPMS 5 XL SQUID magnetometer.

Table 2. Atomic Coordinates and Equivalent Isotropic Displacement Parameters for Li$_{12}$AgGe$_4$

atom	Wyckoff	x	y	z	$U_{iso}{}^{s}/U_{eq}$ (Å^2)
Ag1	2a	0	0	0	0.016(1)
Ge1	4g	0.08487(5)	0.16264(3)	0	0.011(1)
Ge2	4h	0.06898(5)	0.42522(3)	1/2	0.010(1)
Li1	4g	0.1555(11)	0.5208(6)	0	0.020(3)
Li2	4g	0.7398(11)	0.1558(6)	0	0.016(3)
Li3	4g	0.9094(10)	0.3126(7)	0	0.026(3)
Li4	4h	0.737(1)	0.4134(6)	1/2	0.035(3)
Li5	4h	0.4067(8)	0.3999(6)	1/2	0.023(3)
Li6a	4h	0.069(4)	0.2524(9)	1/2	0.013(5)^s
Li6b	4h	0.130(5)	0.2505(11)	1/2	0.013(6)^s

^{s}isotropically refined, occupation ratio Li6a:Li6b = 0.58:0.42.

Table 3. Interatomic Distances for Li$_{12}$AgGe$_4$

atoms	atoms	distances (Å)
Ag1	Ge1	2.5499 (5)
	Li1	2.788 (9)
	Li2	3.149 (9)
	Li4	3.221 (6)
	Li5	2.808 (5)
Ge1	Li1	2.992 (9)
	Li2	2.777 (9)
	Li3	2.637 (8)
	Li4	2.802 (5)
	Li5	2.825 (5)
	Li6a	2.624 (7)
	Li6b	2.63 (1)
Ge2	Ge2	2.5170 (6)
	Li1	2.757 (5)
	Li2	2.901 (6)
	Li3	3.094 (7)
	Li4	2.894 (9)
	Li5	2.743 (7)
	Li6a	2.61 (1)
	Li6b	2.69 (2)
Li1	Li1	2.58 (2)
	Li2	2.75 (2)
	Li3	2.57 (2)
	Li4	2.602 (6)
	Li5	3.528 (9)
Li2	Li3	2.70 (2)
	Li5	2.746 (7)
	Li6a	2.97 (2)
	Li6b	2.80 (2)
Li3	Li4	3.045 (9)
	Li6a	2.74 (2)
	Li6b	3.01 (3)
Li4	Li5	2.66 (1)
	Li6a	2.85 (3)
	Li6b	2.62 (3)
Li5	Li5	3.38 (2)
	Li6a	2.65 (3)
	Li6b	2.90 (3)

A 36.8 mg amount of a phase-pure sample of Li$_{12}$AgGe$_4$ was measured at an applied field of 10 000 Oe over a temperature range of 2−300 K. All data were corrected for the sample holder and for ion-core diamagnetism using Pascal's constants.[26] The molar susceptibility X_m is negative in the range between −1.0 and and −1.2 × 10^{-3} emu mol^{-1} and temperature independent for temperatures above 50 K, as

expected for diamagnetic compounds. The increasing values for X_m at lower temperatures indicate the presence of paramagnetic impurities, which may result from impurities in the starting materials and/or impurities in the synthesis too small to be detected by powder diffraction. The graph is shown in Figure S-2 in the Supporting Information.

Electronic Structure Calculations. DFT electronic structure calculations were carried out with the tight-binding (TB) version of the linear muffin tin orbital (LMTO) method in the atomic sphere approximation (ASA).[27] The exchange-correlation potential was parametrized according to von Barth and Hedin.[28] The k-space integration was performed by the tetrahedron method.[29] Radii of the atomic spheres and interstitial empty spheres were determined according to Jepsen and Anderson.[30] The basis set of short-range atom-centered TB-LMTOs contained s-p valence functions for Li, s-f valence functions for Ag, and s-d valence functions for Ge. The Li 2p, Ag 4f, and Ge 3d orbitals were included using a downfolding technique; 105 irreducible k points were used.

■ RESULTS

The reaction of a premelted alloy of the nominal composition Ag:Ge = 1:4 with Li at 800 °C resulted in the formation of $Li_{12}AgGe_4$ as a phase-pure material. Recently, we found that the synthesis of ternary intermetallic compounds of alkali metals could be accomplished by reacting preformed mixtures of the binary phases of a late transition metal such as Co or Cu and a tetrel element, rather than by simply reacting the three elements under consideration. It turned out that molten reguli of Co–Sn or Cu–Sn react with alkali metals to form intermetallic compounds that contain intermetalloid clusters[31] such as $Co@Sn_9$[32] and $Sn@Cu_{12}@Sn_{20}$,[33,34] which are separated in the neat solid by alkali metals. The here presented ternary phase contains a binary $AgGe_2$ unit that can be seen as the smallest possible cluster consisting of two elements. The electronic structure of these clusters follows the description of molecular anions by the formal transfer of the valence electrons of the alkali metal to the atoms of the intermetalloid cluster. However, the description of the chemical bond in these cluster units cannot easily be achieved by following the 8-N or Wade rules, whereas the application of a delocalized molecular orbital model for the cluster leads to a reasonable result, and in analogy to Zintl phases, all valence electrons are localized in chemical bonds or lone pairs of the intermetalloid clusters.

Structure Description. $Li_{12}AgGe_4$ consists of (Ge_2) dumbbells and linear $(AgGe_2)$ units that are surrounded by Li atoms (Figure 1). All atomic positions are fully occupied and ordered, except for one Li position, which is split into two neighboring positions. The (Ge_2) dumbbells as well as the $(AgGe_2)$ rod are ecliptically stacked at a distance of 4.480(1) Å (lattice parameter a) between the parallel units. The Ge–Ge distance in the (Ge_2) dumbbells is 2.510(1) Å and thus in the range of the dumbbells in Li_2AgGe (2.54 Å[18]) but shorter than in the dumbbells in $Li_{13}Ge_4$ (2.62 Å[35,36]) and longer than that in Li_3NaGe_2 (2.39 Å), [37] which contains two double-bonded Ge atoms. The dumbbells are surrounded by a cage of 18 Li atoms with Ge–Li distances in the range from 2.610(14) to 3.094(7) Å (Figure 2a). Linear Tt-M-Tt units (Tt = tetel element, M = Cu, Ag) are known for the silicides Li_7CuSi_2[11] and $Li_{12}Ag_{1-x}Si_4$ but have not yet been observed for Tt = Ge, and for the heavier homologue tin the related linear Sn–Zn–Sn unit is present in Na_6ZnSn_2.[38] The Ag atom in $Li_{12}AgGe_4$ is located at the crystallographic inversion center, and thus, the Ge–Ag–Ge bond angle is 180°. The Ag–Ge distance in the $(AgGe_2)$ unit is 2.546(1) Å and thus much shorter than the
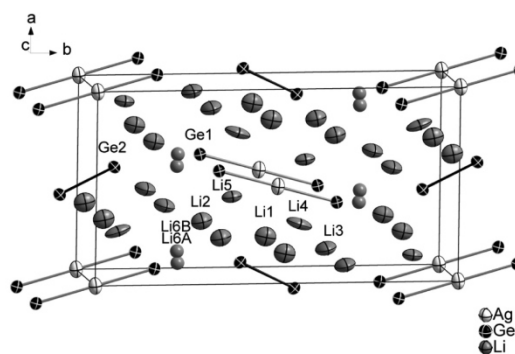

Figure 1. Crystal structure of $Li_{12}AgGe_4$. Li, Ag, and Ge are shown as ellipsoids with 90% probability level in gray, white, and black, respectively, except for Li6A and Li6B which are presented as gray spheres. Note the split position on this Li site.
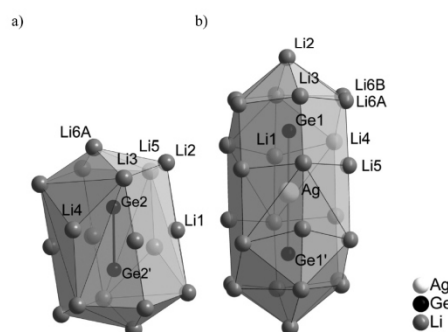

Figure 2. Li coordination polyhedra for the Ge-dumbbell (a) and the $AgGe_2$ unit (b). Li, Ag, and Ge are shown as spheres in gray, white, and black, respectively.

Ag–Ge contacts in Li_2AgGe or $LiAg_2Ge$[17] with 2.74 Å or in $Li_{2.52}AgGe_2$ with a shortest Ag–Ge distance of 2.65 Å. It is very close to the distance of 2.54 Å in the clathrate-I $Ba_4Ag_3Ge_{20}$[39] with Ag and Ge atoms both having a tetrahedral coordination and falls also in the range of Ag–Ge bonds in molecular examples.[40] The $AgGe_2$ unit in $Li_{12}AgGe_4$ is surrounded by a cage of 22 Li atoms with Li–Ge distances ranging from 2.62 Å for Li6a–Ge1 to 2.99 Å for Li1–Ge1. All Li–Ge distances fit well in the range of those found in LiGe (2.64–3.24 Å).[41] The Li–Ag distances range from 2.788(9) to 3.221(6) Å from Li1–Ag1 to Li4–Ag1, respectively, which is in the range of those in LiAg.[42] Apart from the covalently bonded $AgGe_2$ units, the coordination environment of the Ge and Ag atoms resemble Frank–Kasper-type polyhedra. The Ge atoms are surrounded by a distorted double-capped hexagonal antiprism (14-atom polyhedron) with the Ag atom representing one of the caps, and vice versa the Ag atoms are in the center of another 14-vertices Frank–Kaspar polyhedron with the Ge atoms representing the caps (Figure 2b). The formation of these intergrown Frank–Kaspar polyhedra around the $[AgGe_2]$ trimer indicates a close packing in this part of the structure, which is, however, not present in the surrounding of the (Ge_2) dumbbells. $Li_{12}AgGe_4$ crystallizes in the space group Pbam and is isotypic to $Li_{12}Ag_{1-x}Si_4$.[43] It represents a coloring variant of the binary $Li_{13}Si_4$[44] and $Li_{12}Ag_{1-x}Si_4$, and it even displays the
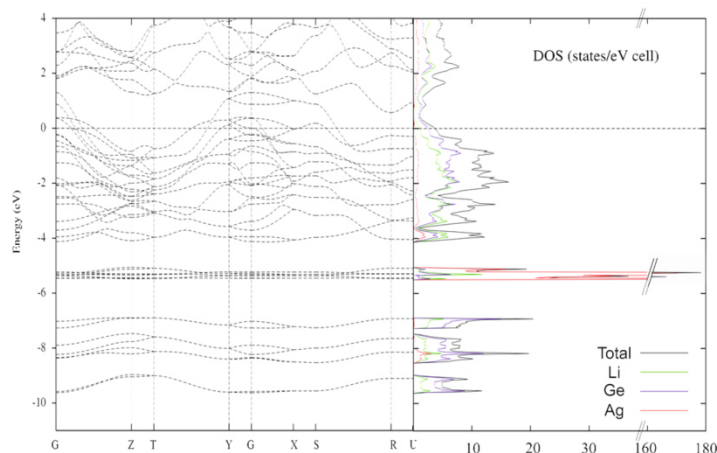
Figure 3. Bands structure (left) and total as well as partial density of states (DOS). Contributions to the DOS of Ag, Ge, and Li are marked in red, purple, and green, respectively.

same split positions of the Li atoms which seems to be typical for this structure type.

Electronic Structure. $Li_{12}Ag_{1-x}Si_4$ and Li_7CuSi_2 both have linear 16-valence-electron Si–M–Si rods and according to the $(8 - N)$ rule can be described as Zintl phases containing the $[Si-M-Si]^{7-}$ Zintl anion, which is iso(valence) electronic to the CO_2 molecule. Assuming similarly a liner coordinated Ag atom in $[Ge-Ag-Ge]^{7-}$ in $Li_{12}AgGe_4$—or alternatively Ag^+ and two Ge^{4-}—a formal charge of -5 must be attributed to the Ge_2 dimer. Consequently, its chemical bonding has to be considered between a single, $[Ge-Ge]^{6-}$, and a double bond, $[Ge=Ge]^{4-}$. We recently presented the first example with a true Ge=Ge double bond in Li_3NaGe_2 with rather short Ge–Ge distances of 2.390 Å. The longer Ge–Ge distance in $Li_{12}AgGe_4$ of 2.510(1) Å supports the occupation of antibonding π^* states of the $[Ge=Ge]$ dimer resulting also in metallic properties. Notice that also the above-mentioned Li_3NaGe_2 is metallic even though it formally possesses the electron count of an electron-precise Zintl phase $(Li^+)_3(Na^+)$-$([Ge=Ge]^{4-})$.[38]

The calculated total and partial density of states (DOS) and band structure of $Li_{12}AgGe_4$ are shown in Figure 3. They are consistent with the DOS and band structure of $Li_{12}Ag_{1-x}Si_4$ with the difference that in the case of $Li_{12}Ag_{1-x}Si_4$ E_F is situated very close to a minimum in the DOS, whereas for $Li_{12}AgGe_4$ more states are present at E_F. This can be explained by the more polarizable character of Ge compared to Si, which leads to more pronounced Ge lone pair states at E_F. Resulting from this $Li_{12}AgGe_4$ is a metal. According to magnetic measurements (Supporting Information, Figure S-2) the diamagnetic contributions are more pronounced than the Pauli paramagnetic ones.

Ge and Li show significant atomic orbital contributions at the Fermi level, especially from the 4p orbitals of Ge1 and from the Li 2s and 2p orbitals. The Ag 3d states are located at -5 eV and strongly hybridize with the 4p states of Ge1 supporting the perception of an $[AgGe_2]^{7-}$ anion with covalent Ag–Ge bonds and significant stabilization by the surrounding Li atoms. For a quantitative view on the bonding situation, the crystal orbital Hamilton populations (COHPs) were calculated (Figure 4 and Figure S3). The integrated overlap population (iCOHP)
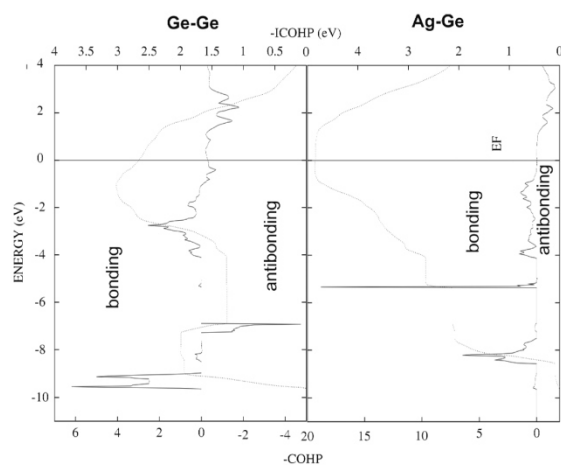

Figure 4. Crystal orbital Hamilton populations (COHPs) and integrated (iCOHP) curves for Ag–Ge (left) and Ge–Ge bonds (right). iCOHP values at E_F are 4.84 eV for the Ag–Ge and 2.66 eV for the Ge–Ge bond.

reaches a maximum at the Fermi level for the Ag–Ge bond, indicating a very strong covalent bond, which corresponds very well with the very short Ag–Ge distance. Similarly, the COHP for Li–Ge bonds shows that there are considerable contributions and that a maximum is reached for band filling up to E_F (Supporting Information). Consequently, no defects on the Ag position are expected for this structure since the majority of bonding contributions are at an optimum. A similar electronic situation with 16 valence electrons has been described for $[Sn-Zn-Sn]^{6-}$ for which a partial double-bond character has been established.[38] In contrast to the strong Ag–Ge bond in $Li_{12}AgGe_4$, the COHP curve for the Ge–Ge bond of the dumbbells shows that below E_F also antibonding states are occupied. This matches the picture of the occupation of π^* states and a weakening of the Ge–Ge double bond, which is most probably the reason for the metallic behavior of the compound.

DISCUSSION

$Li_{13}Si_4$[2] and $Li_{13}Ge_4$[35,36] crystallize in different structure types which significantly differ in their atom packing. Although $Li_{12}AgGe_4$ seems, based on the composition, to be a simple atom-by-atom substitution product of Li by Ag in $Li_{13}Ge_4$ (space group $Cmmm$), it crystallizes in the structure type of $Li_{13}Si_4$ (space group $Pbam$). This is also the case for $Li_{12-x}Ag_{1-x}Si_4$ ($x = 0.15$) but not for $Li_{12.95}Mg_{0.05}Si_4$[35] which again crystallizes in the $Li_{13}Ge_4$ structure type. Thus, a partial substitution of Li by Ag has a considerable influence on the resulting structure type. A significant difference between the two structure types is the formation of a linear Si–Li–Si unit in $Li_{13}Si_4$. During our experiments we found that exactly one Li position is substituted by Ag atoms, and the linear atom arrangement in the Zintl anion Ge–Ag–Ge can only be realized in the $Li_{13}Si_4$ structure type. There is no equivalent Li position allowing for a linear atom arrangement in the $Li_{13}Ge_4$ structure type. Thus, the enhanced stability of the linear $[AgGe_2]^{7-}$ unit seems to be a driving force for the formation of the $Li_{13}Si_4$-type structure. The very short Ag–Ge distance of 2.546(1) Å hints for directed covalent bonds and, in analogy to the iso(valence) electronic CO_2 molecule, even allows double-bond contributions. The (Ge_2) dumbbells with a distance of 2.510(1) Å appear longer than a truly double-bonded system, indicating the population of π^* bands of a $[Ge{=}Ge]^{4-}$ unit. The Fermi level E_F appears at the electron count that maximizes the Ag–Ge bond strength but allows for antibonding Ge–Ge contributions and consequently leads to metallic behavior.

CONCLUSION

Our investigations in the Li–Ag–Ge phase diagram led to the discovery of $Li_{12}AgGe_4$, which now represents the Li-richest compound in this phase diagram. It contains a unique linear 16-valence electron $[AgGe_2]^{7-}$ unit and isolated $[Ge_2]^{5-}$ dumbbells. The latter units correspond to a half-filled degenerate π^* orbital which leads to a delocalized metallic band in the neat solid.

ASSOCIATED CONTENT

ⓈSupporting Information

The Supporting Information is available free of charge on the ACS Publications website at DOI: 10.1021/acs.inorgchem.5b02299.

　　Powder diffractograms, tables of anisotropic displacement parameters, results of the magnetic susceptibility measurement, and Li-Ge COHP plot (PDF)
　　X-ray crystallographic files (CIF)

AUTHOR INFORMATION

Corresponding Author
*E-mail: Thomas.Faessler@lrz.tum.de.

Notes
The authors declare no competing financial interest.

ACKNOWLEDGMENTS

REFERENCES

(1) Hatchard, T. D.; Dahn, J. R. *J. Electrochem. Soc.* **2004**, *151*, A838–A842.
(2) Zeilinger, M.; Fässler, T. F. *Acta Crystallogr., Sect. E: Struct. Rep. Online* **2013**, *69*, i81–i82.
(3) Obrovac, M. N.; Christensen, L. *Electrochem. Solid-State Lett.* **2004**, *7*, A93–A96.
(4) Zeilinger, M.; Kurylyshyn, I. M.; Häussermann, U.; Fässler, T. F. *Chem. Mater.* **2013**, *25*, 4623–4632.
(5) Graetz, J.; Ahn, C. C.; Yazami, R.; Fultz, B. *J. Electrochem. Soc.* **2004**, *151*, A698–A702.
(6) Fuller, C. S.; Severiens, J. C. *Phys. Rev.* **1954**, *96*, 21–24.
(7) Zeilinger, M.; Fässler, T. F. *Dalton Trans.* **2014**, *43*, 14959–14970.
(8) Stegmaier, S.; Fässler, T. F. *Inorg. Chem.* **2013**, *52*, 2809–2816.
(9) Wu, Z.; Mosel, B. D.; Eckert, H.; Hoffmann, R. D.; Pöttgen, R. *Chem. - Eur. J.* **2004**, *10*, 1558–1564.
(10) Lacroix-Orio, L.; Tillard, M.; Belin, C. *Solid State Sci.* **2008**, *10*, 5–11.
(11) Slabon, A.; Budnyk, S.; Cuervo-Reyes, E.; Wörle, M.; Mensing, C.; Nesper, R. *Angew. Chem., Int. Ed.* **2012**, *51*, 11594–11596.
(12) Schnering, H.-G. V.; Nesper, R.; Curda, J.; Tebbe, K.-F. *Z. Metallkd.* **1980**, *71*, 357–363.
(13) Hopf, V.; Schäfer, H.; Weiss, A. *Z. Naturforsch., B: J. Chem. Sci.* **1970**, *25*, 653.
(14) Nesper, R.; von Schnering, H. G.; Curda, J. *Chem. Ber.* **1986**, *119*, 3576–3590.
(15) Scherf, L. M.; Zeilinger, M.; Fässler, T. F. *Inorg. Chem.* **2014**, *53*, 2096–2101.
(16) von Schnering, H. G.; Schwarz, M.; Nesper, R. *Angew. Chem., Int. Ed. Engl.* **1986**, *25*, 566–567.
(17) Kevorkov, D. G.; Pavlyuk, V. V.; Bodak, O. I. *Polym. J. Chem.* **1997**, *71*, 712–715.
(18) Henze, A.; Hlukhyy, V.; Fässler, T. F. *Inorg. Chem.* **2015**, *54*, 1152–1158.
(19) Stoe. *WinXPOW*, 2.08; Stoe & Cie GmbH: Darmstadt, 2003.
(20) Stoe. *CrysAlis RED*, 1.171.33.34; Oxford Diffraction Ltd., 2009.
(21) Stoe. *X-RED32*, 1.48; STOE & Cie GmbH: Darmstadt, 2008.
(22) Stoe. *X-Shape*, 2.11; Stoe & Cie GmbH: Darmstadt, 2008.
(23) Sheldrick, G. M. *XPREP-97*, University of Göttingen: Göttingen, Germany, 1997.
(24) Sheldrick, G. M. *SHELXS-97*, University of Göttingen: Göttingen, Germany, 1997.
(25) Sheldrick, G. M. *SHELXL-97*, University of Göttingen: Göttingen, Germany, 1997.
(26) Bain, G. A.; Berry, J. F. *J. Chem. Educ.* **2008**, *85*, 532–536.
(27) van Schilfgaarde, M.; Paxton, T. A.; Jepsen, O.; Andersen, O. K.; Krier, G. *The Stuttgart Tight-Binding LMTO-ASA program*, 4.7; Max Planck Institut für Festkörperforschung, 1997.
(28) von Barth, U.; Hedin, L. *J. Phys. C: Solid State Phys.* **1972**, *5*, 1629–1642.
(29) Blöchl, P. E.; Jepsen, O.; Andersen, O. K. *Phys. Rev. B: Condens. Matter Mater. Phys.* **1994**, *49*, 16223–16233.
(30) Jepsen, O.; Andersen, O. K. *Z. Phys. B: Condens. Matter* **1995**, *97*, 35–47.
(31) Fässler, T. F.; Hoffmann, S. D. *Angew. Chem., Int. Ed.* **2004**, *43*, 6242–6247.
(32) Hlukhyy, V.; He, H.; Jantke, L.-A.; Fässler, T. F. *Chem. - Eur. J.* **2012**, *18*, 12000–12007.
(33) Stegmaier, S.; Fässler, T. F. *J. Am. Chem. Soc.* **2011**, *133*, 19758–19768.
(34) Stegmaier, S.; Fässler, T. F. *Angew. Chem., Int. Ed.* **2012**, *51*, 2647–2650.
(35) Nesper, R. *Habilitation*; University of Stuttgart: Stuttgart, Germany, 1988.
(36) Nesper, R. *Prog. Solid State Chem.* **1990**, *20*, 1–45.
(37) Scherf, L. M.; Karttunen, A. J.; Pecher, O.; Magusin, P. C. M. M.; Grey, C. P.; Fässler, T. F. *Angew. Chem. Int. Ed.* [Online early

access]. DOI: 10.1002/anie.201508044. Published on-line: Dec 2, 2015.

(38) Kim, S.-J.; Kraus, F.; Fässler, T. F. *J. Am. Chem. Soc.* **2009**, *131*, 1469−1478.

(39) Cordier, G.; Woll, P. *J. Less-Common Met.* **1991**, *169*, 291−302.

(40) Li, J.; Schenk, C.; Winter, F.; Scherer, H.; Trapp, N.; Higelin, A.; Keller, S.; Pöttgen, R.; Krossing, I.; Jones, C. *Angew. Chem., Int. Ed.* **2012**, *51*, 9557−9561.

(41) Menges, E.; Hopf, V.; Schäfer, H.; Weiss, A. *Z. Naturforsch., B: J. Chem. Sci.* **1969**, *24*, 1351−1352.

(42) Zintl, E.; Brauer, G. *Z. Phys. Chem. B* **1933**, *20*, 245−271.

(43) Slabon, A.; Budnyk, S.; Cuervo-Reyes, E.; Wörle, M.; Verel, R.; Nesper, R. *Chem. - Eur. J.* **2013**, *19*, 16528−16531.

(44) Frank, U.; Müller, W.; Schäfer, H. *Z. Naturforsch., B: J. Chem. Sci.* **1975**, *30*, 10−13.

43

<p style="text-align:center">**Supporting Information**</p>

<p style="text-align:center">for</p>

<p style="text-align:center">**Switching the Structure Type upon Ag Substitution: Synthesis and Crystal as well as Electronic Structures of Li$_{12}$AgGe$_4$**</p>

<p style="text-align:center">Alexander Henze, Thomas F. Fässler[*]</p>

E-mail: Thomas.Faessler@lrz.tum.de

Contents

Table S-1. Anisotropic displacement parameters for Li$_{12}$AgGe$_4$.

Figure S-1. Powder diffractogram of a phase-pure sample of Li$_{12}$AgGe$_4$.

Figure S-2. Molar Susceptibility X$_m$ of Li$_{12}$AgGe$_4$.

Table S-1. Anisotropic displacement parameters for Li$_{12}$AgGe$_4$

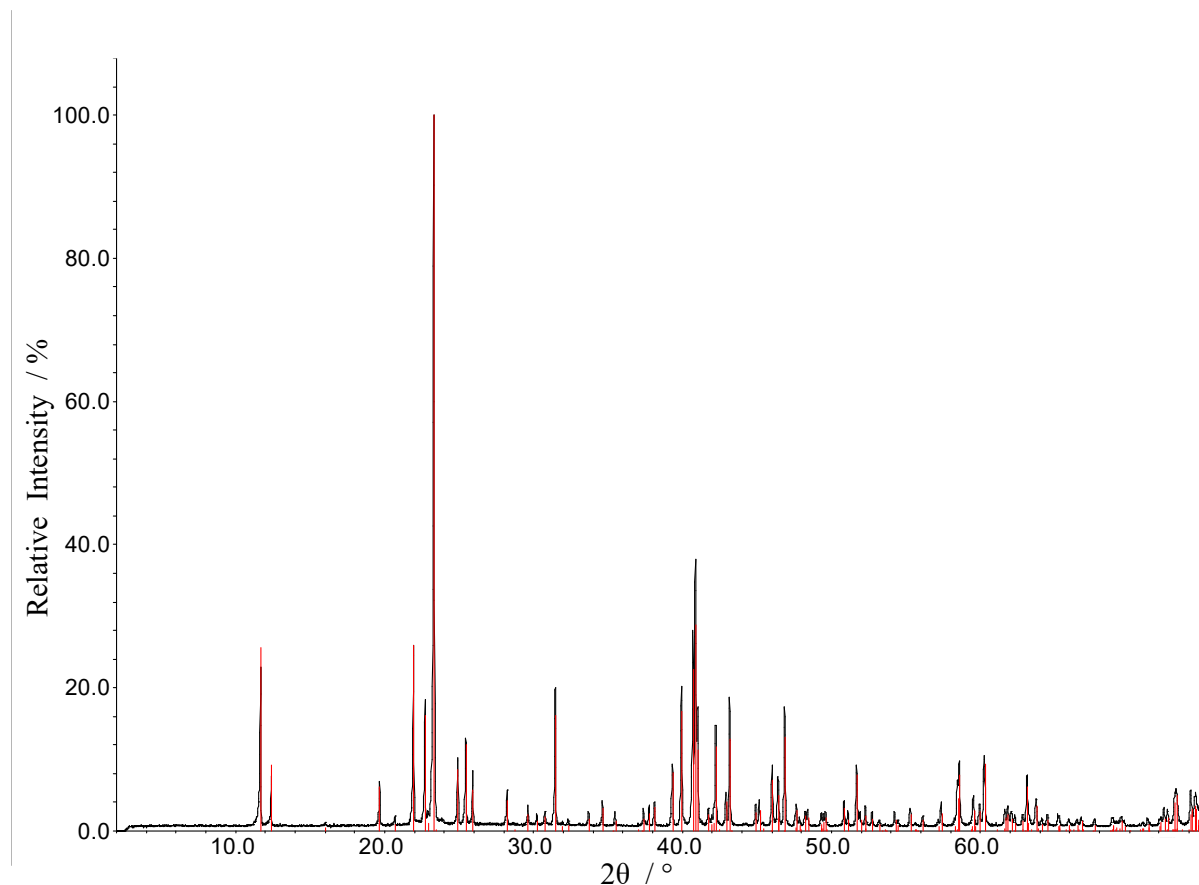| **Li$_{12}$AgGe$_4$**						
Atom	U_{11}	U_{22}	U_{33}	U_{12}	U_{13}	U_{23}
Ag1	0.0180(2)	0.0108(2)	0.0142(2)	−0.0008(2)	0	0
Ge1	0.0110(2)	0.0097(2)	0.0083(2)	0.0004(1)	0	0
Ge2	0.0104(2)	0.0101(2)	0.0095(2)	0.0014(1)	0	0
Li1	0.024(4)	0.029(4)	0.015(3)	−0.001(3)	0	0
Li2	0.019(4)	0.028(4)	0.021(4)	−0.002(3)	0	0
Li3	0.013(4)	0.028(5)	0.058(7)	0.004(3)	0	0
Li4	0.011(3)	0.041(5)	0.020(4)	−0.011(3)	0	0
Li5	0.009(3)	0.025(4)	0.014(3)	0.002(3)	0	0

Figure S-1. Experimental X-ray powder diffractogram of a phase pure sample of $Li_{12}AgGe_4$ (black) with the theoretical pattern of $Li_{12}AgGe_4$ (red).
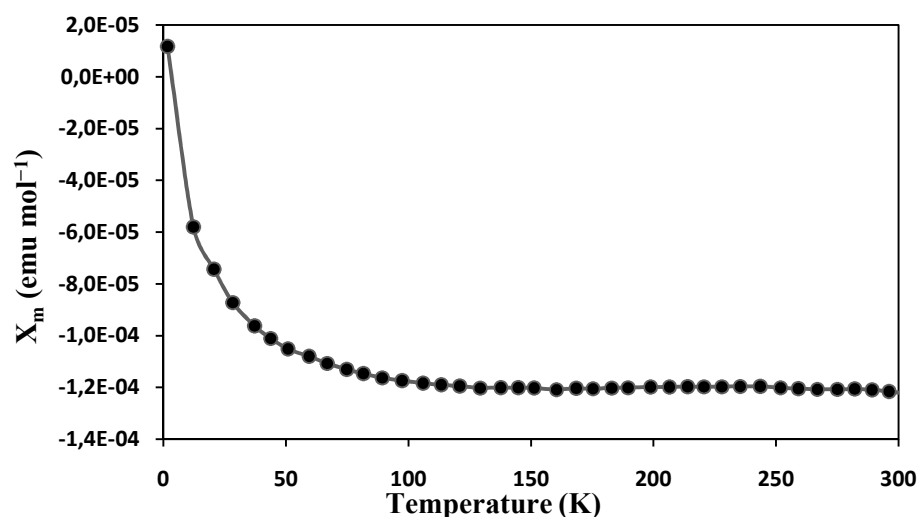
Figure S-2. Molar Susceptibility X_m at applied field of 5000 Oe over a temperature range from 2 – 300 K. The data were corrected for the mass of the sample holder and the ion-core diamagnetism using Pascal's constants. Non-diamagnetic behavior below 50 K results from ferro-magnetic impurities in the sample.

6.2 Fully and Partially Li-Stuffed Diamond Polytypes with Ag-Ge Structures: Li$_2$AgGe and Li$_{2.53}$AgGe$_2$

A. Henze, V. Hlukky, T.F. Fässler,

Inorganic Chemistry

# Fully and Partially Li-Stuffed Diamond Polytypes with Ag−Ge Structures: Li₂AgGe and Li₂.₅₃AgGe₂

Alexander Henze, Viktor Hlukhyy, and Thomas F. Fässler*

Department of Chemistry, Technische Universität München, Lichtenbergstraße 4, 85748 Garching, Germany

Ⓢ *Supporting Information*

ABSTRACT: In view of the search for and understanding of new materials for energy storage, the Li−Ag−Ge phase diagram has been investigated. High-temperature syntheses of Li with reguli of premelted Ag and Ge led to the two new compounds Li_2AgGe and $Li_{2.80-x}AgGe_2$ ($x = 0.27$). The compounds were characterized by single-crystal X-ray diffraction. Both compounds show diamond-polytype-like polyanionic substructures with tetrahedrally coordinated Ag and Ge atoms. The Li ions are located in the channels provided by the network. The compound Li_2AgGe crystallizes in the space group $R\bar{3}m$ (No. 166) with lattice parameters of $a = 4.4424(6)$ Å and $c = 42.7104(6)$ Å. All atomic positions are fully occupied and ordered. $Li_{2.80-x}AgGe_2$ crystallizes in the space group $I4_1/a$ (No. 88) with lattice parameters of $a = 9.7606(2)$ Å and $c = 18.4399(8)$ Å. The Ge substructure consists of unique $^1_\infty[Ge_{10}]$ chains that are interconnected by Ag atoms to build a three-dimensional network. In the channels of this diamond-like network, not all of the possible positions are occupied by Li ions. Li atoms in the neighborhood of the vacancies show considerably enlarged displacement vectors. The occurrence of the vacancy is traced back to short Li−Li distances in the case of the occupation of the vacancy with Li. Both compounds are not electron-precise Zintl phases. The density of states, band structure, and crystal orbital Hamilton population analyses of $Li_{2.80-x}AgGe_2$ reveal metallic properties, whereas a full occupation of all Li sites leads to an electron-precise Zintl compound within a rigid-band model. Li_2AgGe reveals metallic character in the ab plane and is a semiconductor with a small band gap along the c direction.
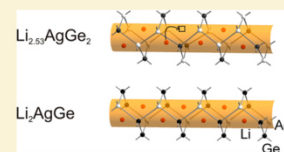
■ INTRODUCTION

The need for energy storage has played a decisive role in many fields of research in the past decade. In the attempt to produce more and more efficient and powerful batteries, Li as the anode material has been replaced by Li-inserting compounds. In this context, compounds containing group 14 elements (Tt) play an important role. Graphite-based electrodes are the state-of-the-art, but Si- and Ge-containing compounds are discussed as alternatives because of the high specific capacity of Si-containing compounds[1,2] and the high lithium diffusivity in Ge-containing compounds.[3,4] Even the element Sn with its much higher mass and thus lower capacity by weight has been considered and investigated for this purpose.[5−7] The addition of a transition metal (T) to binary Li−Tt phases can lead to the formation of two- or three-dimensional polyanionic networks. These networks can act as a stable framework for the Li ions, which are capable of moving in the channels provided by the network. Because there has been much effort to examine ternary Li−T−Si compounds, we also focused on the investigation of Ge-containing phases and report here on our investigations of the phase diagram Li−Ag−Ge. This system has been studied before by the group of Bodak et al., who found the compounds $LiAg_2Ge$, $Li_3Ag_3Ge_2$, and $Li_3Ag_2Ge_3$.[8] Prior to this work, the existence of a Li-rich compound with the composition $Li_8Ag_3Ge_5$ was reported.[9] This compound was investigated by powder X-ray diffraction (XRD) methods, but the atomic parameters have not been reported. According to ref 8, $Li_8Ag_3Ge_5$ corresponds to the structure of $Li_3Ag_2Ge_3$ having, however, a different composition because of several mixed-

occupied sites. All known compounds in this system can be described as polar intermetallics without Ge−Ge bonds or polyanionic Ge substructures. This is also found for all known compounds in the systems Li−Cu−Ge and Li−Au−Ge. Li_2CuGe and Li_2AuGe crystallize in cubic space groups as a typical Heusler phase and a less-ordered lithiated sphalerite-type phase, respectively.[10] Ternary compounds containing Ag, Ge, and an alkali metal heavier than Li are not known.

In this paper, we present the results of our investigations in the Li−Ag−Ge phase diagram with the two new compounds Li_2AgGe and $Li_{2.80-x}AgGe_2$ ($x = 0.27$). Both compounds feature a three-dimensional diamond-like polyanionic Ag−Ge network with intercalated Li ions. All positions in both networks are fully ordered.

■ EXPERIMENTAL SECTION

Synthesis. All materials were handled in an Ar-filled glovebox (MBraun 20 G, argon purity 99.996%). The starting materials were Li rods (99.9%, Sigma-Aldrich), Ag wire (99.9%, Sigma-Aldrich), and Ge pieces (99.999%, ChemPur). Ag and Ge were premelted in an arc furnace (Mini Arc Melting System, MAM-1, Johanna Otto GmbH) to obtain a regulus with the expected binary stoichiometry. For the synthesis of Li_2AgGe, 278 mg (2.57 mmol) of Ag and 187 mg (2.57 mmol) of Ge were used, and for the synthesis of $Li_{2.53}AgGe_2$, 199 mg (1.84 mmol) Ag and 268 mg (3.69 mmol) Ge were used; 36 mg (5.14

47

Inorganic Chemistry

Table 1. Crystal Data and Structure Refinement for Li$_2$AgGe and Li$_{2.53}$AgGe$_2$

formula	Li$_2$AgGe	Li$_{2.53}$AgGe$_2$
fw (g mol^{-1})	194.36	271.14
space group	$R\bar{3}m$ (No. 166)	$I4_1/a$ (No. 88)
Z	12	20
unit cell parameters		
a (Å)	4.4417(1)	9.7606(2)
c (Å)	42.7104(6)	18.4399(8)
volume (Å^3)	729.73(4)	1756.76(9)
D_{calcd} (g cm^{-3})	5.31	5.13
abs coeff (mm^{-1})	20.0	22.2
F(000)	1020	2376
crystal shape/color	block/metallic light pink	block/silver
temperature (K)	150	120
θ range (deg)	2.86–39.17	2.95–32.49
range in hkl	7, 6, 75	14, 14, 27
reflns collected	11488	34366
data/param	613/26	1587/61
GOF on F^2	1.225	1.427
R_1, wR_2 [$I > 2\sigma(I)$]	0.0210, 0.0451	0.0403, 0.0802
R_1, wR_2 (all data)	0.0254. 0.0458	0.0504, 0.0818
largest diff peak and hole (e Å^{-3})	2.28 and −1.41	1.07 and −1.02

mmol) for Li$_2$AgGe and 33 mg of Li (4.79 mmol) for Li$_{2.8-x}$AgGe$_2$ were added to the corresponding binary reguli in a Nb ampule. The ampules were sealed by arc-welding and transferred into a silica tube. The silica tube was evacuated and put into a vertical-resistance tube furnace. The samples were heated to 800 °C and tempered for 24 h. Afterward they were slowly cooled to room temperature with a rate of 0.1 °C min^{-1}. After the ampules were opened, the products were obtained as silver-metallic (Li$_{2.80-x}$AgGe$_2$) and metallic light-pink (Li$_2$AgGe) powders, which were sensitive to air and moisture.

Powder and Single-Crystal XRD and Structural Refinement. For powder XRD analyses, the samples were finely ground to a powder, sealed in glass capillaries, and measured at room temperature

using a STOE Stadi P powder diffractometer with Cu Kα_1 radiation [λ = 1.54056 Å, Ge(111) monochromator] and a position-sensitive detector (Mythen 1K). The STOE WINXPOW program package was used for phase analyses.[11] The powder XRD pattern of the sample Li$_2$AgGe (Figure S-1 in the Supporting Information, SI) showed only the presence of the respective phase. No additional reflections are visible. The powder XRD pattern of the sample Li$_{2.80-x}$AgGe$_2$ (Figure S-2 in the SI) showed the presence of elemental Ge and Ag besides the respective main phase.

For the structure determination, single crystals were mounted on the tip of a glass capillary using perfluoropolyalkyl ether. The data collection was carried out on an Oxford Xcalibur3 diffractometer system (Sapphire3 CCD detector; Mo Kα radiation, λ = 0.71073 Å, graphite monochromator, sealed-tube X-ray source) with crystal cooling in a 150 and 120 K cold N stream for Li$_2$AgGe and Li$_{2.8-x}$AgGe$_2$, respectively. For data processing, the Oxford CrysAlis RED software[12] was used. An empirical absorption correction was performed using the STOE X-RED/X-SHAPE software.[13,14] X-Prep[15] was used for space group determination and data merging (identical indices only). For structure solution (direct methods) and refinement, the programs SHELXS[16] and SHELXL[17] were used. Selected crystallographic data are given in Tables 1 and 2. Interatomic distances and anisotropic displacement parameters are given in the SI (Tables S-1 and S-2).

For Li$_2$AgGe, all positions are fully occupied and ordered. No Ag/Ge mixed occupancies were observed in the Li$_2$AgGe and Li$_{2.8-x}$AgGe$_2$ compounds as well. One Li position in Li$_{2.8-x}$AgGe$_2$ is not fully occupied, and the occupancy factor refines to approximately $^1/_3$. Consequently, no anisotropic models were applied for defective Li1 and neighboring Li4 because of physically unreasonable displacement parameters.

Energy-Dispersive X-ray (EDX) Measurements. EDX analysis was carried out on single crystals of the title compounds Li$_2$AgGe and Li$_{2.53}$AgGe$_2$ using a JEOL 5900LV scanning electron microscope equipped with an Oxford Instruments Inc. EDX microanalysis system. The unit cells of the measured crystals were previously determined by single-crystal XRD to confirm their affiliation to the corresponding phase. Quantitative analysis for both compounds showed the presence of the elements Ag and Ge with no other elements heavier than Na detectable.

Table 2. Atomic Coordinates and Equivalent Isotropic Displacement Parameters for Li$_2$AgGe and Li$_{2.53}$AgGe$_2$

	Li$_2$AgGe				
atom	Wyckoff site	x	y	z	U_{eq}/Å^2
Ge1	6c	$^2/_3$	$^1/_3$	0.61648	0.006(1)
Ge2	6c	0	0	0.52957	0.005(1)
Ag1	6c	$^1/_3$	$^2/_3$	0.63195	0.009(1)
Ag2	6c	$^2/_3$	$^1/_3$	0.55294	0.008(1)
Li1	6c	0	0	0.59294	0.011(2)
Li2	6c	$^1/_3$	$^2/_3$	0.57046	0.015(2)
Li3	6c	$^2/_3$	$^1/_3$	0.49187	0.016(2)
Li4	6c	$^2/_3$	$^1/_3$	0.67840	0.015(2)
	Li$_{2.53}$AgGe$_2$				
atom	Wyckoff site	x	y	z	(U_{iso}/U_{eq})/Å^2
Ge1	8e	0	$^1/_4$	0.45338(4)	0.010(1)
Ge2	16f	0.10022(6)	0.06345(7)	0.36977(4)	0.011(1)
Ge3	16f	0.09598(6)	0.05069(6)	0.04169(4)	0.012(1)
Ag1	4a	0	$^1/_4$	$^1/_8$	0.012(1)
Ag2	16f	0.11604(5)	0.55813(4)	0.28830(3)	0.013(1)
Li1^b	8e	0	$^1/_4$	0.288(2)	0.009(12)^a
Li2	16f	0.0823(10)	0.0769(12)	0.5561(6)	0.017(2)
Li3	16f	0.0886(10)	0.0545(11)	0.2148(7)	0.016(2)
Li4	16f	0.3047(11)	0.1506(11)	0.1318(6)	0.016(2)^a

^{a}Isotropically refined. ^{b}The occupancy parameter of Li1 is 32(6)%.

Differential Thermal Analysis (DTA). Investigations of the thermal behavior of Li$_2$AgGe were carried out in order to check whether the crystal structure changes to a cubic space group at higher temperatures, which is typical of compounds with the composition of Li$_2$TTt.[18] The DTA experiment was carried out using a Netzsch DSC 404 Pegasus apparatus. In an Ar-filled glovebox, a cylindrical Nb crucible was loaded with 65 mg of crystallographically phase-pure Li$_2$AgGe. The ampule was closed by crimping and then sealed by arc-welding inside the glovebox. Then it was transferred to a Netzsch DSC 404 Pegasus apparatus. A sealed Nb crucible without the sample was used as a reference. During the experiment, the sample was heated in an Ar flow with a heating/cooling rate of 10 K min^{-1}. The sample was recovered in an Ar-filled glovebox. For data processing, the program *Proteus Thermal Analysis*[19] was used. Both recorded cycles are almost identical. In the course of heating, one exothermic effect is visible. This effect at an onset temperature of 679.9 °C (peaks at 692.8 and 693.9 °C, respectively) is strong and indicates the congruent melting point of the compound. In the course of cooling, only one endothermic effect is visible at 673.3 and 674.0 °C, respectively, which indicates the crystallization point of the compound. No signs of any changes in the crystal structure at higher temperatures are visible (see the SI, Figure S-3).

Electronic Structure Calculations. The electronic structures were calculated by employing the linear muffin-tin orbital (LMTO) method in the atomic sphere approximation in the tight-binding (TB) program.[20] The exchange-correlation term was calculated within the local density approximation and parametrized according to von Barth and Hedin.[21] The radii of the muffin-tin and empty spheres were determined according to Jepsen and Andersen.[22] The Brillouin zone integrations were performed with a 16 × 16 × 16 special *k*-point grid. The basis set of short-ranged[23] atom-centered TB-LMTOs contained s—p valence functions for Li, s—f valence functions for Ag, and s—d valence functions for Ge. Li 2p, Ag 4f, and Ge 3d orbitals were included using a downfolding technique. In order to handle the defects, we applied a rigid band model: The band-structure calculations for the composition Li$_{2.8}$AgGe$_2$ were carried out with fully occupied Li positions (Li$_{28}$Ag$_{10}$Ge$_{20}$, 218 valence electrons), and the values were calculated with respect to the electron count of the crystallographically determined composition Li$_{2.53(1)}$AgGe$_2$ (Li$_{25.3}$Ag$_{10}$Ge$_{20}$, 215.3 valence electrons) as well as of the electron-precise Zintl phase "Li$_3$AgGe$_2$" (Li$_{30}$Ag$_{10}$Ge$_{20}$, 220 valence electrons). Analysis of the chemical bonding is based on theoretical partial and total density of states (DOS) curves and plots of the crystal orbital Hamilton populations (COHPs).[24]

■ RESULTS

The title compounds were synthesized in high-temperature reactions with Li and a binary Ag/Ge alloy. Both compounds feature diamond-like polyanionic substructures of four-connected Ag and Ge atoms, which are stuffed with Li atoms.

Structure of Li$_2$AgGe. The compound Li$_2$AgGe crystallizes as an ordered variant of the Li$_{13}$Ag$_5$Si$_6$ structure type[25] in the space group $R\bar{3}m$ (No. 166). This is rather unusual because compounds with the typical composition of Heusler phases Li$_2$TTt tend to adopt cubic symmetry, with Li$_2$ZnSi and Li$_2$MnSn crystallizing in hexagonal and tetragonal symmetry, respectively, as exceptions.[26,27] The structure of Li$_2$AgGe contains a 12c diamond-polytype-like polyanionic network, which, in contrast to that of Li$_{13}$Ag$_5$Si$_6$, is fully ordered on all atomic positions. The network consists of puckered layers of six-membered rings that are formed alternately by Ge and Ag atoms. The layers extend in the *ab* direction and are stacked in the *c* direction, with the sequence ABCDA′B′C′D′A″B″C″D″ forming the very long *c* axis (Figure 1a). The stacking type of these layers leads to heteroatomic contacts, as in sphalerite, but also to homoatomic Ag—Ag and Ge—Ge contacts between the layers. The Ag—Ge distances in these layers are 2.751(1) and
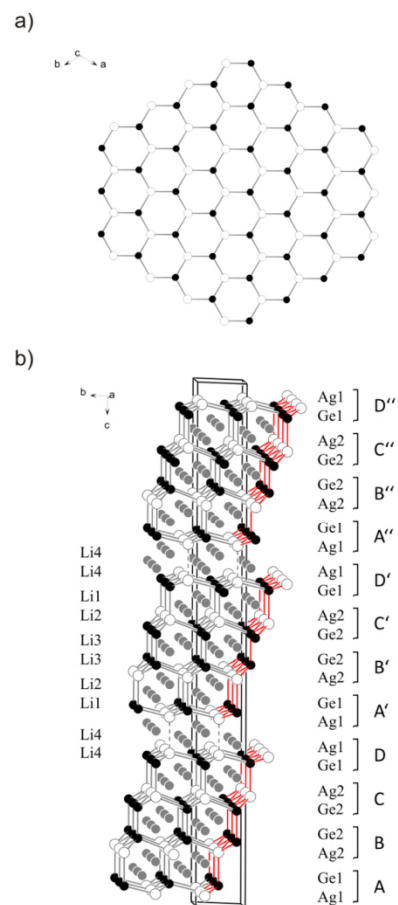

Figure 1. (a) Top view on one representative layer of Li$_2$AgGe. (b) Stacking sequence of the layers along the *c* direction. Li, Ag, and Ge are represented in gray, white, and black spheres, respectively.
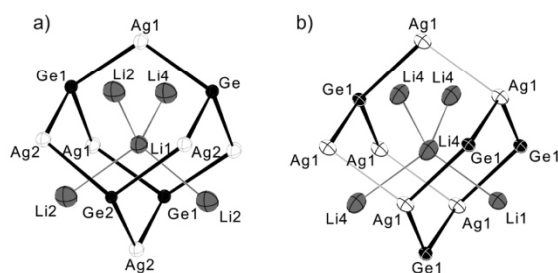

Figure 2. Coordination environment of the (a) Li1 and (b) Li4 atoms. The Li, Ag, and Ge atoms are shown as ellipsoids at the 90% probability level in gray, white, and black, respectively. Ag—Ge contacts are represented as thick black lines, Ag—Ag contacts as thin light-gray lines, and Li—Li contacts as thin dark-gray lines.

2.752(1) Å. The heteroatomic contacts between the layers are slightly shorter at 2.739(1) Å, which is equivalent to the Ag—Ge bond length observed in cubic LiAg$_2$Ge[8] and slightly longer than the sum of the covalent radii of Ag and Ge (2.65 Å).[28] The Ge—Ge contacts between the layers are 2.537(1) Å and thus slightly longer than in α-Ge (2.445 Å)[29] but shorter than in the

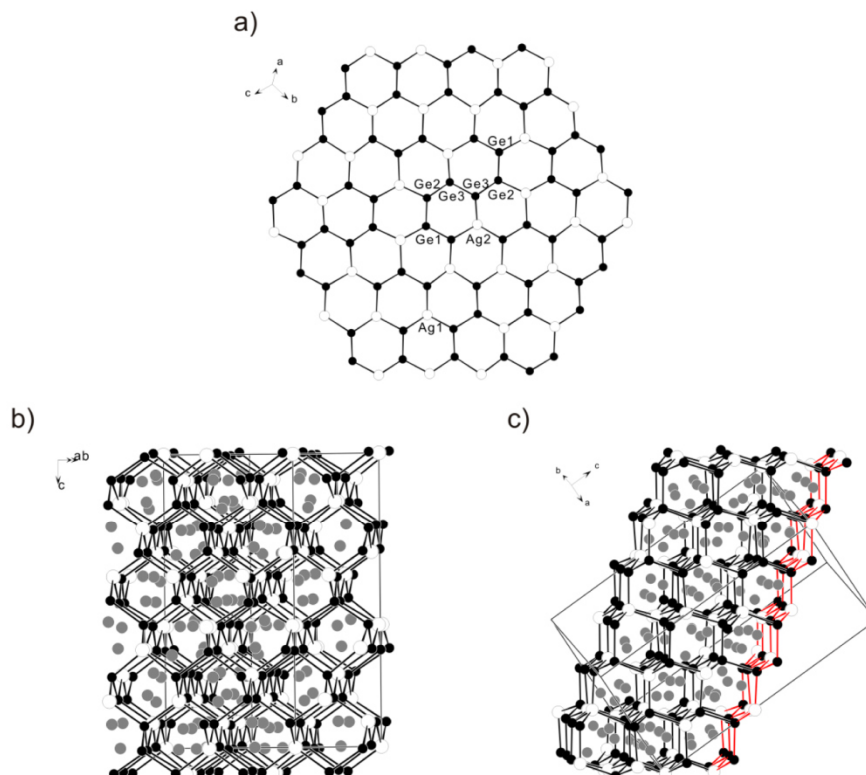**Figure 3.** Crystal structure of $Li_{2.53}AgGe_2$: (a) layer of puckered six-membered rings of Ag and Ge atoms emphasizing the substructure of eight connected Ge atoms in one layer; (b) expanded unit cell; (c) stacking sequence of the layers. A layer as shown in part (a) is emphasized with red bonds. Li, Ag, and Ge are drawn as gray, white, and black spheres, respectively.
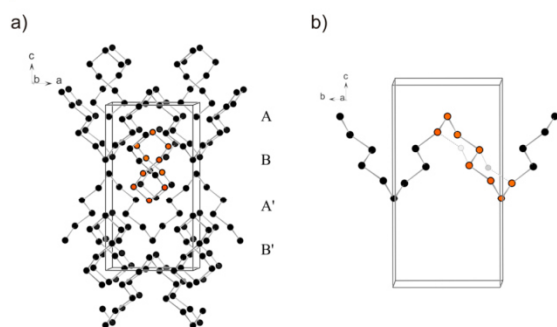

Figure 4. (a) Expanded unit cell of the substructure of $^1_\infty[Ge_{10}]$ chains propagating in the a and b directions. (b) Part of the chain highlighted in part (a) with red atoms with a view along the a direction showing also the coordination to Ag atoms to complete six-membered rings. Ge and Ag are drawn as black and white spheres, respectively; one $[Ge_{10}]$ unit is shown with orange spheres.

dumbbells in $Li_{13}Ge_4$ (2.62 Å).[30] In contrast to the simple cubic sphalerite structure type, also Ag–Ag bonds are formed between the layers. The corresponding distance of 2.965(1) Å is longer than that of the Ag–Ag contacts in the elemental structure (2.889 Å)[31] but shorter than the Ag–Ag contacts in $Li_{13}Ag_5Si_6$.

The structure can also be described as consisting of layers of Ge^{4-} anions that envelop layers of Ge_2^{6-} dumbbells, with all free positions in the tetrahedral coordination sphere being occupied by Ag atoms. In this description, it becomes obvious that $(Ge)^{4-}$ and $(Ge)^{3-}$ occur in a ratio of 1:1, which shows that the compound Li_2AgGe is not a Zintl phase, assuming Li and Ag each donate one electron to Ge, being charged Li^+ and Ag^+, respectively. Thus, the compound is better characterized as a polar intermetallic compound. Electronic structure calculations reveal metallic character in the ab plane and a semiconductor with a small band gap along the c direction (see the SI, Figure S-8). The substructure of the Li cations forms a distorted diamond-like network, which occupies the positions in the hexagonal tunnels provided by the polyanionic substructure. The structure of Li_2AgGe consists of interpenetrating diamond-type nets, and thus a distorted Heusler-type structure results, which is typical of compounds of the composition X_2YZ (X, Y = alkali metal, alkali earth metal, transition metal; Z = element of groups 13−15). The Li−Li distances range from 2.648 to 2.753 Å, which is much shorter than that in body-centered-cubic Li with 3.05 Å.[32] This is due to the highly ionic character of the Li atoms, and no bonds should be considered. The Li−Li distances lie in the range of that of other polar intermetallic compounds like $Li_3Ag_2Ge_3$ with a distance of 2.678 Å.[8] The coordination sphere of each Li position consists of two distorted tetrahedra of Li and Ge, respectively, as well as of an octahedron of Ag atoms (see the SI, Figure S-4).
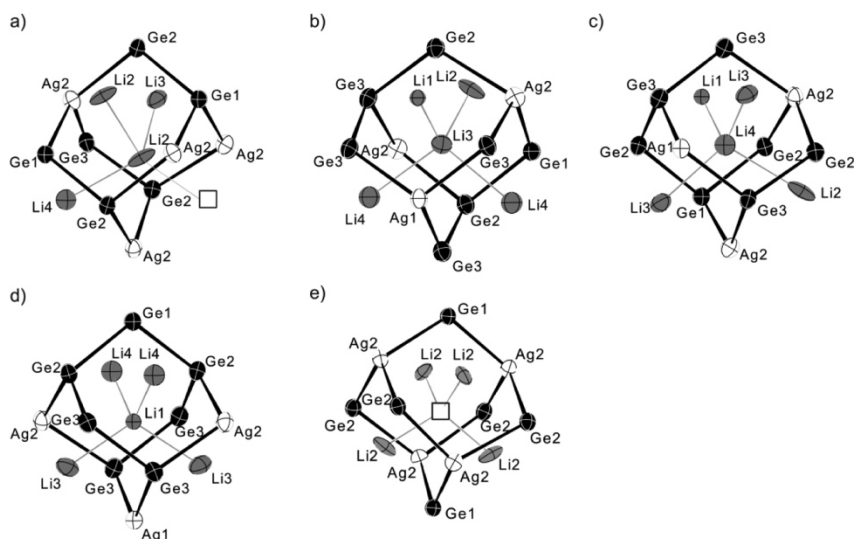
Figure 5. Coordination polyhedra of (a–c) fully occupied Li atoms, (d) the partially occupied position Li1, and (e) the vacancy. Li, Ag, and Ge are shown as ellipsoids at the 90% probability level in gray, white, and black, respectively. Ag–Ge and Ge–Ge contacts are drawn as black lines and Li–Li contacts as thin gray lines.
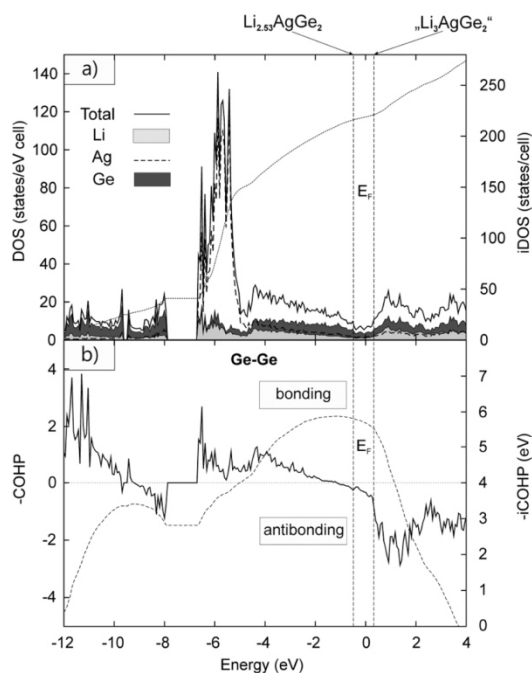

Figure 6. (a) Total, partial, and integrated DOSs. (b) Combined COHP and integrated COHP curves for the four shorter Ge–Ge bonds within the –Ge–Ge– chain calculated for the "$Li_{2.8}AgGe_2$" structure model with fully occupied Li positions. The dashed lines correspond to the Fermi level of the experimentally determined composition $Li_{2.53(1)}AgGe_2$ ($Li_{25.3}Ag_{10}Ge_{20}$, 215.3 valence electrons) and the electron-precise Zintl compound "Li_3AgGe_2" ($Li_{30}Ag_{10}Ge_{20}$, 220 valence electrons).

Structure of $Li_{2.80-x}AgGe_2$ ($x = 0.27$). The compound $Li_{2.53}AgGe_2$ crystallizes in its own structure type in the space

group $I4_1/a$ (No. 88). All atomic positions are completely occupied and fully ordered, except for Li1, which is only partially occupied (Figure 2). As in Li_2AgGe, a diamond-like polyanionic substructure with tetrahedrally coordinated Ag and Ge atoms that form puckered layers occurs (Figure 3a). The layers consist of six-membered rings, with one, two, or three positions being occupied by Ag atoms. All other positions are occupied by Ge atoms with a Ag:Ge ratio of 1:2. The layers are stacked along the [111] direction with Ag–Ge and Ge–Ge bonds between the layers. There are no neighboring Ag positions within or between the layers (Figure 3b,c). The Ag–Ge distances range from 2.650(1) to 2.850(1) Å similar to those of the above-mentioned compounds Li_2AgGe and $LiAg_2Ge$. The Ge atoms form spiral chains of two-bonded Ge atoms with Ge–Ge distances between 2.579(1) and 2.618(1) Å, which are longer than those in α-Ge (2.445 Å)[29] but are in the range of the Ge–Ge distances observed in the $^1_\infty[Ge_2]$ zigzag chains in CaGe (2.592 Å).[33] The distances are significantly shorter than the sum of the van der Waals radii (4.22 Å).[34] Along these $^1_\infty[Ge_{10}]$ chains, a coiled structure becomes evident, which in the projection is shaped like the number "eight". According to the tetragonal symmetry, the chains propagate along the a and b directions (Figure 4a).

The Ag atoms occupy the two free positions in the tetrahedral coordination sphere of each Ge atom connecting the Ge chains into a three-dimensional network. The polyanionic network adopts a 6c diamond-polytype-like structure although stronger distorted as in Li_2AgGe. All Li atoms are intercalated between the Ag–Ge layers occupying 16f and 8e positions (Figure 3). The Li–Li distances range from 2.492(23) to 3.019(15) Å. The Li atoms form a second interpenetrating diamond-type network with one Li position (Li1) partially occupied and one position not occupied (Figure 5). Interestingly, Li2 (in the neighborhood of the vacancy) shows large anisotropic displacement parameters. The defect on the 4b position correlates with rather short distances of 2.261(11) Å to the neighboring Li2 atoms (Figure 5e) and

Article

indicates that occupation of the vacancy is not favorable. The same applies for the not fully occupied Li1 position with nearest Li atoms Li3 and Li4 at 2.492(23) and 2.600(24) Å, respectively. In comparison, the shortest Li−Li distance of fully occupied Li positions is 2.770(15) Å between Li2 and Li3.

Regarding the formal charge of 2− of the Ge atoms in the $^1_\infty[Ge]$ chains and 1+ for each Li and Ag atoms, $Li_{2.53}AgGe_2$ is not an electron-precise Zintl phase. The ratio of the positive and negative formal charges is 1:1.14 and thus rather close to that of Li_2AgGe (1:1.17). If all partially and nonoccupied positions would be occupied with Li atoms, thus forming a diamond-type Li network, the compound with the hypothetical composition Li_3AgGe_2 would be an electron-precise Zintl compound.

In order to analyze the electronic structure of $Li_{2.8−x}AgGe_2$, the band structure and total and partial DOSs (see the SI, Figures S-5, and Figure 6a) were calculated. The low-lying bands between −12.0 and −7.9 eV are predominantly Ge 4s states, whereas the Ag 3d states are located between −6.7 eV up to the Fermi level and hybridize strongly with the Ge 4p and Li 2s,p orbitals. No band gap is observed at the Fermi level of the crystallographically determined composition $Li_{2.53}AgGe_2$ with defective Li positions, indicating metallic behavior. However, a pseudogap is situated close to the Fermi level of the corresponding electron-precise composition "Li_3AgGe_2". Interestingly, there occurs a rather flat DOS at low values between the Fermi levels of the experimentally determined and electron-precise composition. For a more quantitative bond analysis, we calculated the COHPs, which provide a quantitative measure of the strength of the bonding. In the presented COHP curves, positive values are bonding, and negative values are antibonding (see the SI, Figures S-6 and S-7, and Figure 6b). The COHP and integrated COHP curves are maximized for the shortest Ag−Ge bonds just above the Fermi level with the maximum reached for an electron number corresponding to the electron-precise composition "Li_3AgGe_2" (see the SI, Figure S-6), whereas the Ge−Ge bonds within the Ge chains are nearly optimized at a composition corresponding to the experimentally observed composition $Li_{2.53}AgGe_2$ (see the SI, Figure S-7, and Figure 6). The addition of further electrons in order to approach the electron count for a Zintl compound leads to the filling of antibonding Ge−Ge states.

CONCLUSION

Our investigation of the system Li−Ag−Ge led to the discovery of the two new polar intermetallic compounds, Li_2AgGe and $Li_{2.80−x}AgGe_2$ (x = 0.27). These compounds are the first representatives in the systems A−T−Ge with a polyanionic substructure that provides tunnels for the alkali metal. The compounds also bear other interesting structural properties such as the very long c axis in Li_2AgGe, which is untypical for Li_2TTt compounds, or the unique $^1_\infty[Ge_{10}]$ chains and voids in the Li partial structure in $Li_{2.80−x}AgGe_2$ (x = 0.27). Most interestingly, $Li_{2.80−x}AgGe_2$ (x = 0.27) contains not fully occupied Li positions and vacancies, which is a prerequisite for Li mobility within a tetravalent framework. Currently, we are working on a pure-phase synthesis of the compound in order to be able to measure the Li-ion conductivity.

ASSOCIATED CONTENT

S Supporting Information

X-ray crystallographic files in CIF format, tables of interatomic distances and anisotropic displacement parameters for the title compounds, and figures of powder diffractograms and a DTA thermogram, total, partial, and integrated DOS for $Li_{2.53}AgGe_2$, and COHP and integrated COHP for the shorter Ag−Ge and Ge−Ge bonds of $Li_{2.53}AgGe_2$. This material is available free of charge via the Internet at http://pubs.acs.org.

AUTHOR INFORMATION

Corresponding Author
*E-mail: Thomas.Faessler@lrz.tum.de.
Notes
The authors declare no competing financial interest.

ACKNOWLEDGMENTS

DEDICATION

In memoriam of Prof. John Corbett.

REFERENCES

(1) Obrovac, M. N.; Christensen, L. *Electrochem. Solid-State Lett.* **2004**, *7*, A93−A96.
(2) (a) Zeilinger, M.; Benson, D.; Häussermann, U.; Fässler, T. F. *Chem. Mater.* **2013**, *25*, 1960−1967. (b) Zeilinger, M.; Kurylyshyn, I. M.; Häussermann, U.; Fässler, T. F. *Chem. Mater.* **2013**, *25*, 4623−4632. (c) Zeilinger, M.; Baran, V.; van Wüllen, L.; Häussermann, U.; Fässler, T. F. *Chem. Mater.* **2013**, *25*, 4113−4121.
(3) (a) Fuller, C. S.; Severiens, J. C. *Phys. Rev.* **1954**, *96*, 21−24. (b) Graetz, J.; Ahn, C. C.; Yazami, R.; Fultz, B. *J. Electrochem. Soc.* **2004**, *151*, A698−A702.
(4) Zeilinger, M.; Fässler, T. F. *Dalton Trans.* **2014**, *43*, 14959−14970.
(5) Stegmaier, S.; Fässler, T. F. *Inorg. Chem.* **2013**, *52*, 2809−2816.
(6) Wu, Z.; Mosel, B. D.; Eckert, H.; Hoffmann, R.-D.; Pöttgen, R. *Chem.—Eur. J.* **2004**, *10*, 1558−1564.
(7) Thackeray, M. M.; Kepler, K. D.; Vaughey, J. T. Patent WO 00/03443, Application No. PCT/US99/12868.
(8) Kevorkov, D. G.; Pavlyuk, V. V.; Bodak, O. I. *Pol. J. Chem.* **1997**, *71*, 712−715.
(9) Schuster, H.-U.; Kahlert, H. *Z. Naturforsch.* **1972**, *27b*, 79−80.
(10) Pauly, H.; Weiss, A.; Witte, H. *Z. Metallkd.* **1968**, *59*, 47−58.
(11) *WinXPOW*, version 2.08; Stoe & Cie GmbH: Darmstadt, Germany, 2003.
(12) *CrysAlis RED*, version 1.171.33.34; Oxford Diffraction Ltd.: Oxford, U.K., 2009.
(13) *X-RED32*, version 1.48; Stoe & Cie GmbH: Darmstadt, Germany, 2008.
(14) *X-SHAPE*, version 2.11; Stoe & Cie GmbH: Darmstadt, Germany, 2008.
(15) Sheldrick, G. M. *XPREP-97*; University of Goettingen: Goettingen, Germany, 1997.
(16) Sheldrick, G. M. *SCHELXS-97*; University of Goettingen: Goettingen, Germany, 1997.
(17) Sheldrick, G. M. *SCHELXL-97, Program for Crystal Structure Refinement*; University of Goettingen: Goettingen, Germany, 1997.
(18) Schuster, H. U.; Thiedemann, D.; Schoenemann, H. *Z. Anorg. Allg. Chem.* **1969**, *370*, 160−170.
(19) *Netzsch Proteus Thermal Analysis*, version 4.8.2; Netzsch-Gerätebau GmbH: Selb, Germany, 2006.

(20) Schilfgarde, M. v.; Paxton, T. A.; Jepsen, O.; Andersen, O. K.; Krier, G. *The Stuttgard Tight-Binding LMTO-ASA program*, version 4.7; Max Planck Institut für Festkörperförschung: Stuttgart, Germany, 1997.

(21) von Barth, U. V.; Hedin, L. *J. Phys. C* **1972**, *5*, 1629−1642.

(22) Jepsen, O.; Andersen, O. K. *Z. Phys. B* **1995**, *97*, 35.

(23) Andersen, O. K.; Jepsen, O. *Phys. Rev. Lett.* **1984**, *53*, 2571−2574.

(24) Dronskowski, R.; Blochl, P. E. *J. Phys. Chem.* **1993**, *97*, 8617−8624.

(25) Lacroix-Orio, L.; Tillard, M.; Belin, C. *Solid State Sci.* **2008**, *10*, 5−11.

(26) Schuster, H. U.; Schoenemann, H. *Z. Naturforsch.* **1969**, *24*, 1188−1188.

(27) Schuster, H. U.; Kistrup, C. J. *Z. Naturforsch.* **1972**, *20*, 80.

(28) Pauling, L.; Kamb, B. *Proc. Natl. Acad. Sci. U.S.A.* **1986**, *83*, 3569−3571.

(29) Pauling, L. *The Nature of the Chemical Bond*; Cornell University Press: Ithaca, NY, 1960.

(30) Nesper, R. *Habilitation*; University of Stuttgart: Stuttgart, Germany, 1988.

(31) Swanson, H. E.; Tatge, E. *Phys. Rev.* **1955**, *99*, 1737−1743.

(32) Donohue, J. *The Structures of the Elements*; Wiley: New York, 1974.

(33) Eckerlin, B.; Meyer, H. J.; Woelfel, E. *Z. Anorg. Allg. Chem.* **1955**, *281*, 322−328.

(34) Mantina, M.; Chamberlin, A. C.; Valero, R.; Cramer, C. J.; Truhlar, D. G. *J. Phys. Chem. A* **2009**, *113*, 5806−5812.

53

Supporting Information

for

Fully and Partially Li-Stuffed Diamond Polytypes with Ag-Ge Structures: Li$_2$AgGe and Li$_{2.53}$AgGe$_2$

Alexander Henze, Viktor Hlukhyy, Thomas F. Fässler[*]

Department Chemie, Technische Universität München,

Lichtenbergstr. 4, D-85747 Garching, Germany

E-mail: Thomas.Faessler@lrz.tum.de

Contents

Crystal structures

Powder and Single Crystal X-ray diffraction and structural refinement.

Differential Thermal Analysis

Table S-1.   Interatomic distances for Li_2AgGe and $Li_{2.8-x}AgGe_2$ (x = 0.27)

Li_2AgGe		
atoms		**Distance (Å)**
Ge1	Ag1	2.6482 (1)
	Ag2	2.7139 (5)
	Li1	2.754 (3)
	Li2	3.231 (5)
	Li4	2.645 (8)
Ge2	Ge2	2.5262 (8)
	Ag2	2.7517 (2)
	Li1	2.707 (8)
	Li2	3.103 (5)
	Li3	2.723 (3)
Ag1	Ag1	2.9654 (6)
	Li1	3.058 (4)
	Li2	2.626 (9)
	Li4	2.746 (3)
Ag2	Li1	3.081 (5)
	Li2	2.671 (2)
	Li3	2.608 (10)
Li1	Li2	2.738 (4)
	Li4	2.648 (12)
Li2	Li3	2.662 (13)
Li3	Li3	2.657 (5)
Li4	Li4	2.753 (6)
$Li_{2,53}AgGe_2$		
atoms		**Distance (Å)**
Ge1	Ge2	2.579 (1)
	Ag2	2.691 (1)
	Li1	3.040 (50)
	Li2	2.661 (12)
	Li3	3.102 (10)
	Li4	2.654 (10)

Li$_{2,53}$AgGe$_2$		
atoms		**Distance (Å)**
Ge2	Ge3	2.585 (2)
	Ag2	2.669 (1)
	Li1	2.560 (30)
	Li2	2.631 (10)
	Li3	2.822 (12)
	Li4	2.942 (10)
Ge3	Ge3	2.618 (1)
	Ag1	2.650 (1)
	Ag2	2.669 (2)
	Li1	2.610 (30)
	Li3	2.690 (11)
	Li4	2.586 (11)
Ag1	Li1	3.010 (50)
	Li3	2.671 (12)
	Li4	3.131 (10)
Ag2	Li2	2.753 (11)
	Li3	2.652 (10)
	Li4	2.630 (11)
Li1	Li3	2.492 (23)
	Li4	2.600 (24)
Li2	Li2	3.019 (15)
	Li3	2.866 (15)
	Li4	2.846 (16)
Li3	Li4	2.770 (15)

Table S-2. Anisotropic displacement parameters for Li$_2$AgGe and Li$_{2.8-x}$AgGe$_2$ (x = 0.27)

Li$_2$AgGe						
Atom	U_{11}	U_{22}	U_{33}	U_{12}	U_{13}	U_{23}
Ge1	0.0046(2)	0.0046(2)	0.0055(2)	0.0023(1)	0	0
Ge2	0.0053(2)	0.0053(2)	0.0068(2)	0.0027(1)	0	0

Ag1	0.0072(2)	0.0072(2)	0.0117(2)	0.0036(1)	0	0

Li₂AgGe

Atom	U_{11}	U_{22}	U_{33}	U_{12}	U_{13}	U_{23}
Ag2	0.0076(2)	0.0076(2)	0.0082(2)	0.0038(1)	0	0
Li1	0.010(3)	0.010(3)	0.012(3)	0.005(2)	0	0
Li2	0.017(3)	0.017(3)	0.010(3)	0.009(2)	0	0
Li3	0.014(3)	0.014(3)	0.021(4)	0.007(2)	0	0
Li4	0.018(3)	0.018(3)	0.010(3)	0.009(2)	0	0

Li₂.₅₃AgGe₂

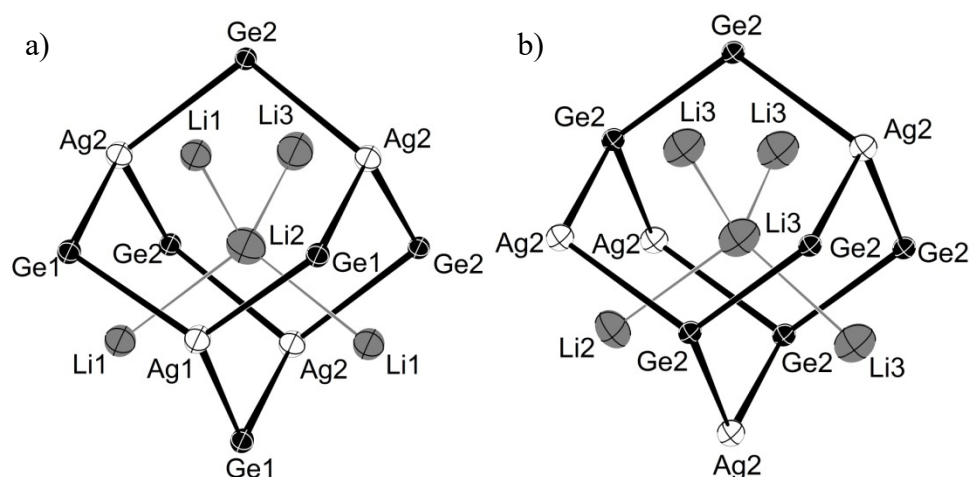| Atom						
Ge1	0.0090(4)	0.0099(4)	0.0117(4)	-0.0004(3)	0	0
Ge2	0.0110(3)	0.0095(3)	0.0131(3)	0.0001(2)	0.0006(2)	-0.0011(2)
Ge3	0.0115(3)	0.0092(3)	0.0140(3)	0.0001(2)	0.0018(2)	-0.0012(2)
Ag1	0.0106(3)	0.0106(3)	0.0134(4)	0	0	0
Ag2	0.0124(2)	0.0113(2)	0.0146(2)	0.0015(2)	-0.0015(2)	0.0004(2)
Li2	0.009(4)	0.027(6)	0.014(5)	-0.006(4)	0.004(3)	-0.012(4)
Li3	0.017(5)	0.018(5)	0.013(4)	-0.003(3)	0.004(4)	-0.003(4)

Figure S-1. Coordination environment of Li2 (a) and Li3 (b) for Li₂AgGe. Li Ag and Ge are shown as thermal ellipsoids at 90% probability level in grey, white and black respectively. Ag – Ge contacts are represented in thick black and Li – Li contacts in thin grey lines.
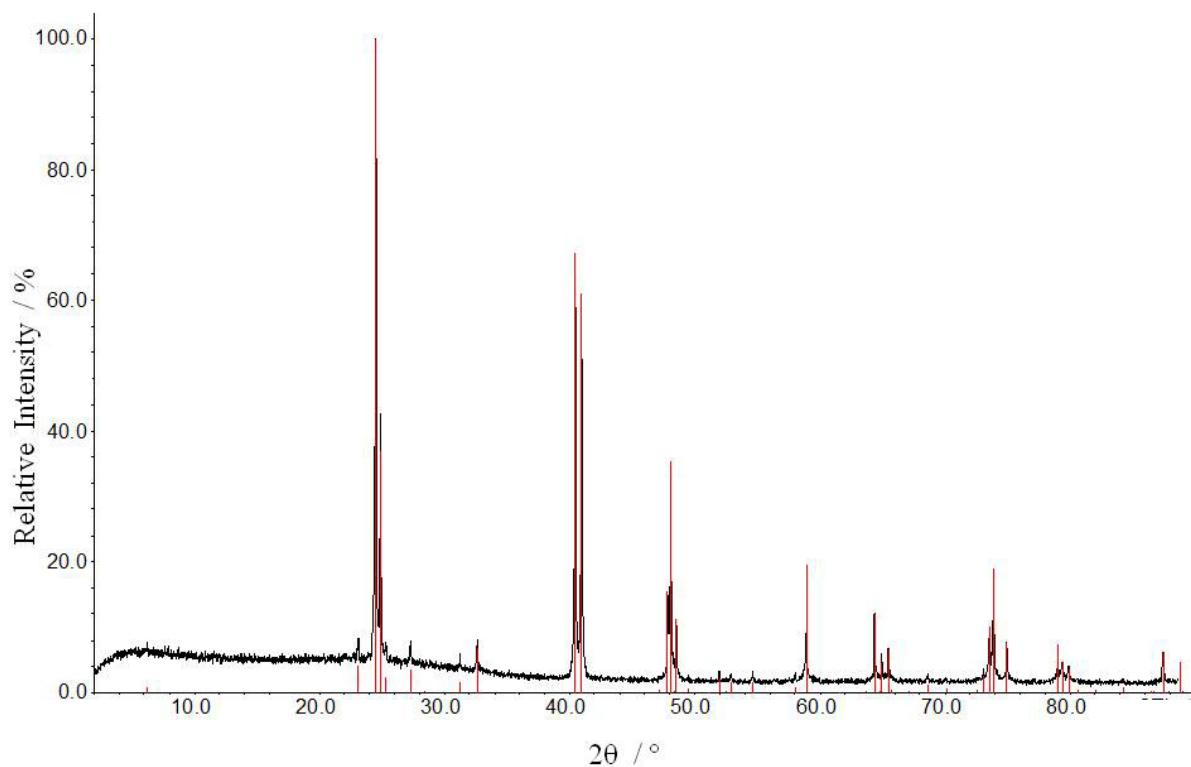
Figure S-2. Experimental X-ray powder diffractogram (black) with the theoretical pattern of Li_2AgGe (red).
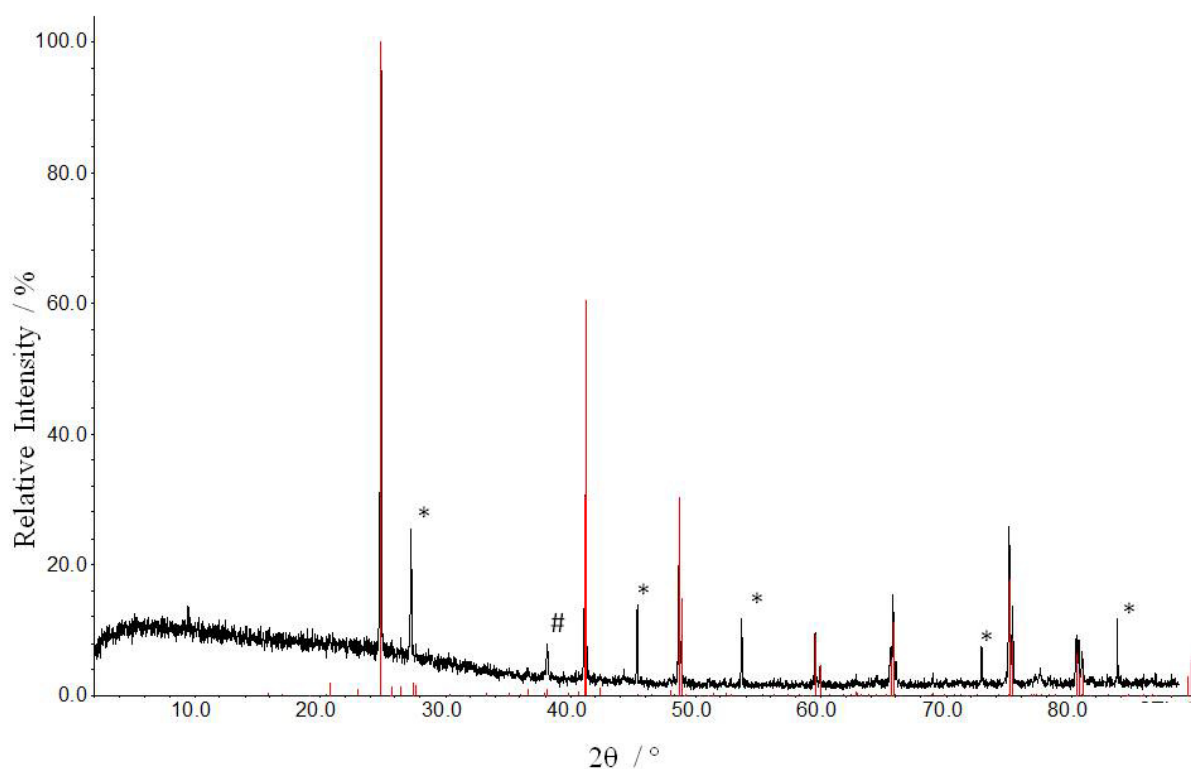

Figure S-3. Experimental X-ray powder diffractogram (black) with the theoretical pattern of $Li_{2.8-x}AgGe$ (x = 0.27) (red). Impurities of Ge and Ag are marked with an * and # respectively.
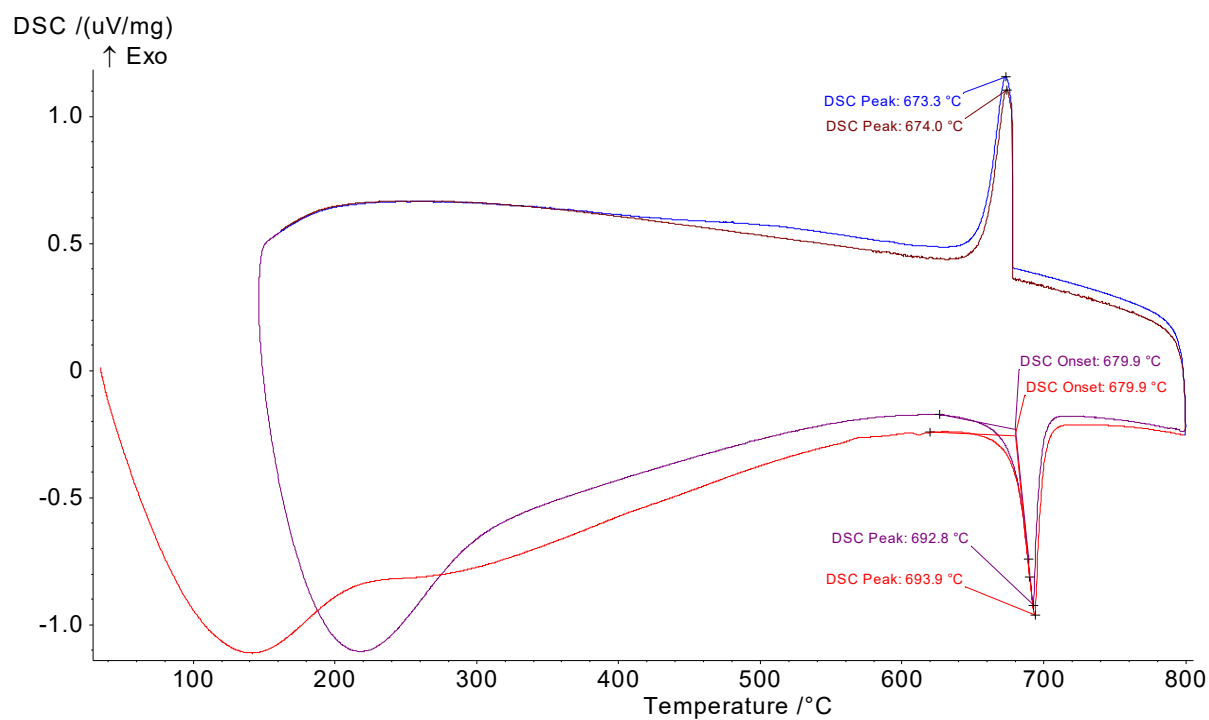
Figure S-4. Thermogram of a phase pure sample of Li2AgGe. The heating traces are shown in red and purple, the cooling traces in blue and brown respectively.

6.3 Synthesis and Structural Characterization of $Li_2Ag_{1-x}Ge_{1+x}$ (x = 0.06)

Alexander Henze, Thomas F. Fässler

manuscript for publication

Abstract

Extending our investigations in the Li-Ag-Ge system, the novel ternary phase $LiAg_{1-x}Ge_{1+x}$ (x = 0.06) was synthesized using high-temperature methods and characterized crystallographically. The compound crystallizes in the space group I4(1)/amd (Nr. 141) with lattice parameters of a = 4.3735(4) and c = 6.2895(13). The structure consists of a nearly undistorted diamond-like polyanionic network of non-ordered Ag and Ge atoms. The resulting channels in this network are filled with Li atoms resulting in a structure derived from the NaTl-type. Therefore the compound $LiAg_{1-x}Ge_{1+x}$ (x = 0.06) represents now the third compound in the system Li-Ag-Ge exhibiting a Li filled polyanionic network. The degree of distortion of these networks can be controlled by the deployed Ag/Ge ratio.

Introduction

The ever-increasing demand for portable electronic devices drives the search for new materials with improved features for rechargeable solid state Li-ion batteries. Especially binary and ternary Li and tetrel element consisting materials have drawn a lot of attention and are investigated for the purpose to serve as electrode materials. As commonly used graphite suffers from a relatively low capacity,[1, 2] higher tetrelides have become interesting for research, especially Si and Ge.[3-6] While silicon offers a high natural abundance and the highest theoretical capacity (4200 $mAhg^{-1}$ compared to 1564 $mAhg^{-1}$ for the formation of $Li_{21}Si_5$ and $Li_{16.95}Ge_4$ respectively)[7, 8] Ge impresses with a 400 times higher Li diffusivity at room temperature compared to Si.[9, 10] The addition of a late transition metal (T) to the binary Li tetrelides leads to the formation of Li-filled 2- and 3-dimensional polyanionic networks which were first discovered by the groups of H.-U. Schuster[11] and A. Weiss[12], but have recently drawn attention due to the high Li mobility, e.g. of Li_2AuSn_2 and $LiAg_2Sn$.[13, 14] The recently discovered Li_2AgSn_2 with a diamond-like polyanionic network shows an even improved Li ion mobility and therefore proved, that Li-filled diamond-like polyanionic networks might be interesting as electrode materials.[15] We focused our investigations on the lighter Li-Ag-Ge system where up to our investigations only the two Heusler phases $LiAg_2Ge$ and $Li_3Ag_2Ge_3$ as well as $Li_3Ag_3Ge_2$ which crystallizes in the Cu_3Au structure type were known.[16] Our investigations led to the discovery of the very Li rich compound $Li_{12}AgGe_4$, as well as the two compounds Li_2AgGe and $Li_{2.53}AgGe_2$, both featuring distorted diamond-like polyanionic networks with Li occupying the hexagonal channels in a and b direction.[17, 18] Further investigations aiming at a less distorted Ag-Ge network now led to the discovery of the phase $Li_2Ag_{1-x}Ge_{1+x}$ (x = 0.06) exhibiting this kind of network. All positions in the polyanionic network are mixed-occupied by Ag and Ge.

Experimental Section

Synthesis

To synthesize the title compounds, all materials were handled in an argon atmosphere using an argon filled glove box (MBraun 20 G, argon purity 99.996%). Starting materials for the synthesis were Li rods (99.9%, Sigma Aldrich), Ag wire (99.9%, Sigma Aldrich) and Ge pieces (99.999%, ChemPur). The 254 mg (2.36 mmol) of the Ag wire and 209 mg (2.88 mmol) of the Ge pieces were pre-melted in an arc furnace (Mini Arc Melting System, MAM-1, Johanna Otto GmbH) to obtain a binary regulus with the expected stoichiometry. 36 mg (5.24 mmol) of Li were given into a niobium ampoule with the corresponding binary regulus. The ampoule was sealed by arc-welding and transferred into a silica tube. The silica tube was evacuated and put into a vertical resistance tube furnace. The samples were heated to 750 °C and tempered for 24 hours. Afterwards they were slowly cooled to room temperature with a degree of −0.1 K/min. After opening the ampoules, the product appeared as metallic lustrous silver powder, which was sensitive to air and moisture.

Powder and Single Crystal X-ray diffraction and structural refinement

For powder diffraction analysis, the sample was finely ground to a powder, sealed in glass capillaries and measured at room temperature using a STOE Stadi P powder diffractometer with Cu-K$_\alpha$ radiation (λ = 1.54056 Å, Ge(111) monochromator) and a position sensitive detector (Mython 1K). The STOE WINXPOW program package was used for phase analysis.[19] The diffractogram reveals a nearly phase pure sample of the compound Li$_2$Ag$_{0.94}$Ge$_{1.06}$ (Figure S-1). It was not possible to identify the side phase.

For the structure determination, a single crystal was mounted on the tip of a glass capillary using perfluoropolyalkylether. The data collection was carried out on an OXDORD Xcalibur3 diffractometer system (Sapphire3 CCD detector; Mo K$_\alpha$ radiation, λ = 0.71073 Å, graphite monochromator, sealed tube X-ray source) with crystal cooling in a 120 °C cold nitrogen stream. For data processing, the Oxford CrysAlis RED software[20] was used. A empirical absorption correction was performed using the STOE X-RED/X-SHAPE software[21, 22] X-Prep[23] was used for space group determination and data merging (identical indices only). For structure solution (direct methods) and

refinement the programs XS[24] and XL[25] were used. Selected crystallographic data a given in Table 1 and 2.

Table 1:   crystal data and structure refinement

Formula	$Li_2Ag_{0.94}Ge_{1.06}$
Formula weight (g·mol^{-1})	192.22
Space group	*I4(1)/amd* (Nr. 141)
Z	2
Unit cell parameters (Å)	a = 4.3735(4) c = 6.2895(13)
Volume (Å^3)	120.30(3)
P_{calc} g·cm^{-3}	5.173
abs. coeff.	20.19
F(000)	164.0
Crystal shape/color	block/silver
Temperature (K)	130
Θ range	5.68 – 35.63
Range in hkl	−7/7 −7/7 −10/9
Reflections collected	1262
Unique reflections	84
Data / parameter	84 / 7
GOF on F^2	1.149
R$_1$, wR$_2$ ($I \geq 2\sigma(I)$)	0.0168, 0.0328
R$_1$, wR$_2$ (all data)	0.0207, 0.0334
Largest diff. peak and hole	0.905 and −1.427

Table 2:   Atomic coordinates and equivalent isotropic displacement parameters for $LiAg_{0.94}Ge_{1.06}$

Atom	Wyck.	*sof*	x	y	z	U_{eq}/Å^2
Ge1/Ag1	4*a*	53 / 47(11)	0	3/4	1/8	0.012(1)
Li1	4*b*		1/2	3/4	7/8	0.019(3)

EDX Measurements

EDX analysis was carried out on single crystals of the title compounds $LiAg_{0.94}Ge_{1.06}$ using a JEOL 5900LV scanning electron microscope equipped with an OXFORD INSTRUMENTS INCA energy dispersive X-ray microanalysis system. The unit cells of the crystals were determined by single crystal XRD. The quantitative analysis for both compounds showed the presence of the elements Ag and Ge with no other element heavier than Na detectable.

Differential Thermal Analysis

Investigations of the thermal behavior of $Li_2Ag_{0.94}Ge_{10.6}$ were carried out in order to find out if any phase transitions occurs at higher temperatures. The DTA experiment was carried out on a Netzsch DSC 404 Pegasus apparatus. In an argon-filled glove box 70 mg of a crystallographically almost phase pure sample were loaded in a Nb crucible. The ampoule was closed by crimping and subsequent sealing by arc-welding of the ampoule inside of the glove box. Afterwards it was transferred into the DTA apparatus. An empty, sealed Nb crucible was used as a reference. During the measurement, the sample was heated and cooled in a constant argon flow with a rate of 10 K·min^{-1} respectively. The sample was recovered in an argon-filled glove box. For data processing the program Proteus Thermal Analysis[26] was used. Both recorded cycles are almost identical. In the courses of heating two exothermic effects are visible, a smaller one at an onset temperature of 568.5° C (peaks at 577.1° C and 580.6° C, respectively) and a bigger one at an onset temperature of about 676° C (peaks at 690.3° C and 691.8° C, respectively). In the cooling courses the equivalent endothermic signals are visible at 647° C (peaks at 662.4° C and 662.7° C) for the bigger effect and 545.6° C (peak at 556.9° C) for the smaller thermal effect. Clearly both effects are reversible. While the thermal effect at about 676° C should be a congruent melting point, the effect at about 579° C could be a melting point of the side-phase which is visible in the powder diffractogram, or a sign for a phase transition. We were not able to isolate any other phases by rapid cooling of the title phase from temperatures above 580° C, though. The melting point of $Li_2Ag_{1-x}Ge_{1+x}$ is very close to the melting point of the related compound Li_2AgGe with an onset temperature of 679.9° C which should not be surprising regarding the similar structure and composition of both compounds. The powder diffractogram of the recovered sample

shows no significant difference to the one of the original sample. The DTA graph is shown in Figure 3.

Results

Our resent investigations in the Li-Ag-Ge phase diagram led to the discovery of the two new compounds Li_2AgGe and $Li_{2.53}AgGe_2$.[18] Both of these compounds exhibit a distorted diamond like polyanionic substructure filled with Li atoms. As the structure especially of Li_2AgGe appeared rather unusual forming a very long c axis, we were looking for some kind of basic structure to these compounds. The thermal analysis of Li_2AgGe showed no transformations of the structure up to the melting point. Further investigations now aimed at the tolerance of different Ag:Ge ratios in this compound. We found that a ratio of more than 1:1.05 of Ag:Ge leads to a collapsing of the long c axis of Li_2AgGe and a new compound with less ordering on the Ag and Ge positions is formed. This compound crystallizes in the structure type of low-temperature LiAl[27] in the space group $I4_1/amd$ cell parameters of a = 4.3735 Å and c = 6.2895(13). The composition of this compound was refined to $Li_2Ag_{1-x}Ge_{1+x}$ (x = 0.06(11)). The structure of this compound consists of two interpenetrating diamond-like networks build by Li and Ag/Ge atoms respectively. The structure derives from the NaTl structure and therefore represents a half-Heusler phase. There are no signs of ordering on the Ag/Ge position. The Ag/Ge-Ag/Ge distance is 2.6934(2) Å which is longer than Ge-Ge contacts in α-Ge (2.45 Å)[28] and Ge-Ge contacts in $Li_{13}Ge_4$ (2.62 Å)[29]. It is slightly longer than the sum of the covalent radii of Ag and Ge (2.65 Å)[30] and in the range of Ag-Ge bond lengths in Li_2AgGe (2.73 Å)[18], indicating the slight excess of Ge in the occupation of the positions in the polyanionic network. Accordingly, the Ag/Ge-Ag/Ge bond is much shorter than Ag-Ag contacts in the elemental structure (2.889 Å)[31]. The Li-Li distance is 2.6934(2) Å as well and therefore much shorter than in Li-Li contacts in the elemental structure (3.05 Å)[32] which is due to the highly ionic character of the Li atoms. It is well in the range of Li-Li distances in related Li_2AgGe (2.64 Å – 2.75 Å) and other polar intermetallic compounds like $Li_3Ag_2Ge_3$ (2.68 Å)[16] and LiGe (2.66 Å)[33]. In contrast to the related compounds Li_2AgGe and $Li_{2.53}AgGe_2$ the distortion of the polyanionic network is much smaller, but can be seen in the angles of any Ag/Ge position to the neighboring Ag/Ge positions which are 108.56° and 109.93° compared with 107.62° and 111.26° in stronger distorted Li_2AgGe and the perfect tetrahedral angle of 109.47 in cubic NaTl. This distortion indicates, that the Ag/Ge positions is not occupied by Ag and Ge at a rate of 50% each which would be

66

possible regarding the standard deviation of the refined value for x in the sum formula. Crystallization in the cubic NaTl structure type would be expected in this case though. The fact that this compound results from experiments in which Ge was weighed in excess to Ag indicates that Ge should be the element that occupies the mixed Ag/Ge position in slight excess as is indicated by the structural refinement of this position. Therefore, in the system Li-Ag-Ge three compounds with Li-filled, diamond-like polyanionic networks with varying levels of distortion that can be controlled by the Ag:Ge ratio in the synthesis are now known. As these polyanionic networks can provide low E_A for Li ion mobility which is not only dependent on the size of the channels, but of a variety of factors as shown for polyanionic networks containing stanides,[15] investigations in the Li-ion mobility of these three compounds might lead to a closer insight on these factors, especially on the influence of the distortion of the network.
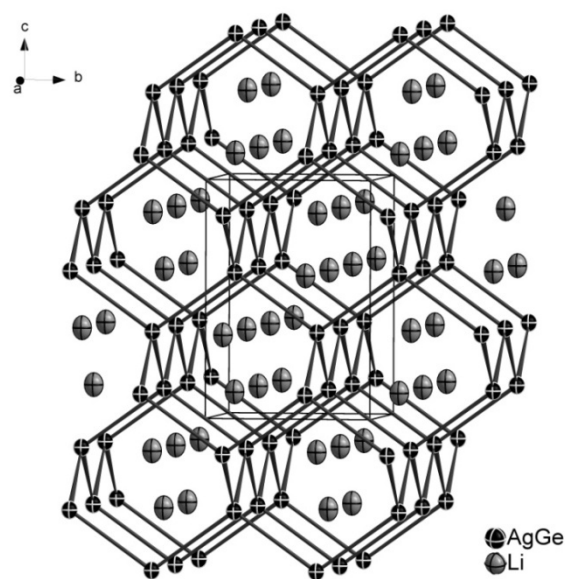

Figure 1: Li-filled polyanionic Ag/Ge network of $Li_2Ag_{1-x}Ge_{1+x}$. Ag/Ge and Li atoms are represented as black and grey ellipsoids at 90% probability level respectively.
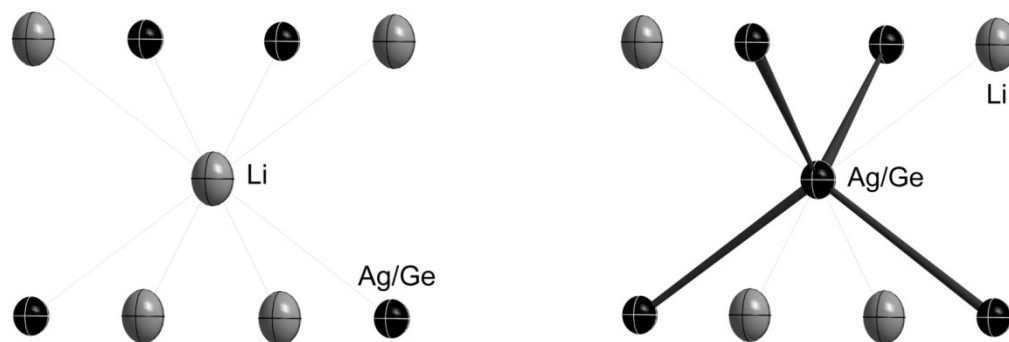
Figure 2: Surrounding of the Ag/Ge and Li position in the respective tetrahedral surrounding. Ag/Ge and Li atoms are represented as black and grey ellipsoids at 70% probability level respectively.
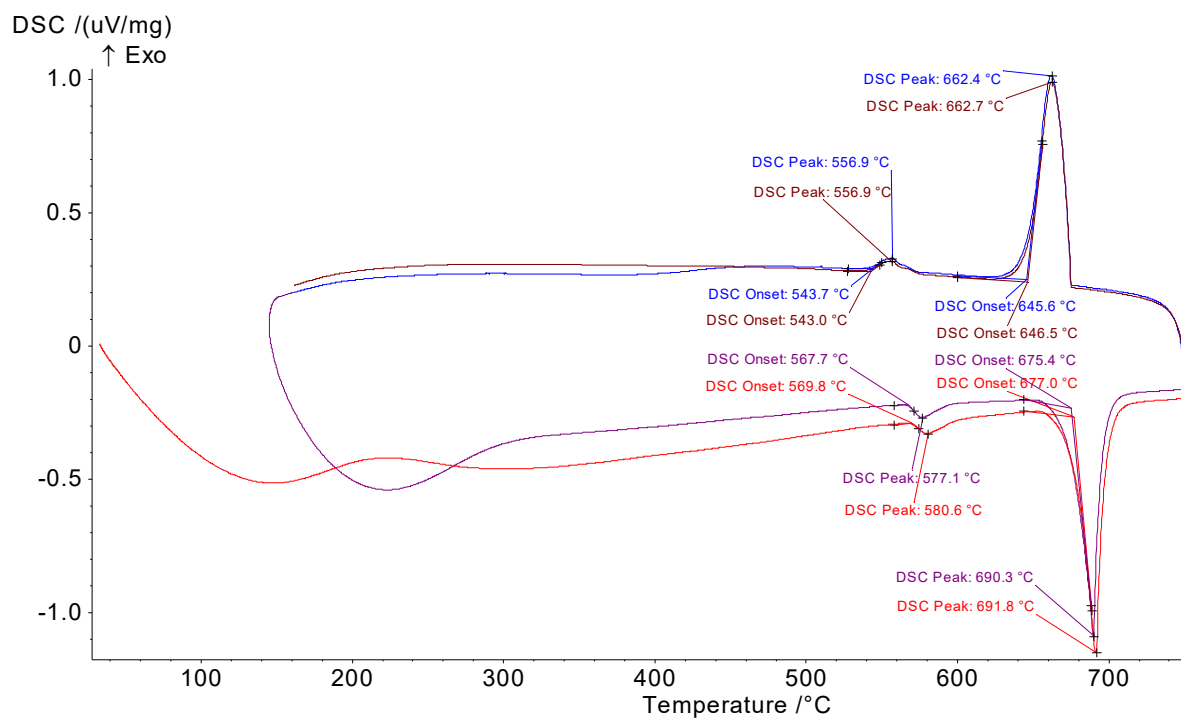

Figure 3: Thermogram of a nearly phase pure sample of $Li_2Ag_{1-x}Ge_{1+x}$. The heating traces are shown in red and purple, the cooling traces in blue and brown respectively.

Associated content

Supporting Information available: X-ray crystallographic files in CIF format

Author information

Corresponding Author: Prof. Dr. Thomas F. Fässler, Department Chemie, Technische Universität München, Lichtenbergstr. 4, D-85747 Garching, Germany

*E-mail: Thomas.Faessler@lrz.tum.de.

Notes: The authors declare no competing financial interest.

References

(1)   Obrovac, M. N.; Christensen, L. *Electrochem. Solid-State Lett.* **2004,** *7*, A93–A96.

(2)   Hatchard, T. D.; Dahn, J. R. *J. Electrochem. Soc.* **2004,** *151*, A838–A842.

(3)   Iwamura, S.; Nishihara, H.; Ono, Y.; Morito, H.; Yamane, H.; Nara, H.; Osaka, T.; Kyotani, T. *Sci. Rep.* **2015,** *5*, 8085.

(4)   Wang, X.; Yang, A.; Xia, S. *J. Electrochem. Soc.* **2016,** *163*, A90-A95.

(5)   Tian, H.; Xin, F.; Wang, X.; He, W.; Han, W. *Journal of Materiomics* **2015,** *1*, 153-169.

(6)   Song, T.; Jeon, Y.; Samal, M.; Han, H.; Park, H.; Ha, J.; Yi, D. K.; Choi, J.-M.; Chang, H.; Choi, Y.-M.; Paik, U. *Energy Environ. Sci.* **2012,** *5*, 9028-9033.

(7)   Wen, C. J.; Huggins, R. A. *J. Solid State Chem.* **1981,** *37*, 271-278.

(8)   Goward, G. R.; Taylor, N. J.; Souza, D. C. S.; Nazar, L. F. *J. Alloys Comp.* **2001,** *329*, 82-91.

(9)   Fuller, C. S.; Severiens, J. C. *Phys. Rev.* **1954,** *96*, 21–24.

(10)   Graetz, J.; Ahn, C. C.; Yazami, R.; Fultz, B. *J. Electrochem. Soc.* **2004,** *151*, A698–A702.

(11)   Schuster, H.-U.; Thiedemann, D.; Schönemann, H. *Z. Anorg. Allg. Chem.* **1969,** *370*, 160-170.

(12)   Pauly, H.; Weiss, A.; Witte, H. *Z. Metallkd.* **1968,** *59*, 47-58.

(13)   Wu, Z.; Mosel, B. D.; Eckert, H.; Hoffmann, R. D.; Pöttgen, R. *Chem. Eur. J.* **2004,** *10*, 1558–1564.

(14) Wu, Z.; Hoffmann, R.-D.; Johrendt, D.; Mosel, B. D.; Eckert, H.; Pottgen, R. *J. Mater. Chem.* **2003,** *13*, 2561-2565.

(15) Winter, F.; Dupke, S.; Eckert, H.; Rodewald, U. C.; Pöttgen, R. *Z. Anorg. Allg. Chem.* **2013,** *639*, 2790-2795.

(16) Kevorkov, D. G.; Pavlyuk, V. V.; Bodak, O. I. *Pol. J. Chem.* **1997,** *71*, 712–715.

(17) Henze, A.; Fässler, T. F. *Inorg. Chem.* **2015,** *submitted*.

(18) Henze, A.; Hlukhyy, V.; Fässler, T. F. *Inorg. Chem.* **2015,** *54*, 1152-1158.

(19) Stoe *WinXPOW*, 2.08; Stoe & Cie GmbH: Darmstadt, 2003.

(20) Stoe *CrysAlis RED*, 1.171.33.34; Oxford Diffraction Ltd.: 2009.

(21) Stoe *X-RED32*, 1.48; STOE & Cie GmbH: Darmstadt, 2008.

(22) Stoe *X-Shape*, 2.11; Stoe & Cie GmbH: Darmstadt, 2008.

(23) Sheldrick, G. M. *XPREP-97*, University of Göttingen (Germany), 1997.

(24) Sheldrick, G. M. *SHELXS-97*, University of Göttingen (Germany), 1997.

(25) Sheldrick, G. M. *SHELXL-97*, University of Göttingen (Germany), 1997.

(26) *Netzsch Proteus Thermal Analysis*, 4.8.2; Netzsch-Gerätebau GmbH: Selb, Germany, 2006.

(27) Ehrenberg, H.; Pauly, H.; Knapp, M.; Gröbner, J.; Mirkovic, D. *J. Solid State Chem.* **2004,** *177*, 227-230.

(28) Pauling, L., *The Nature of the Chemical Bond*. Ithaca, NY, 1960.

(29) Nesper, R. Habilitation, University of Stuttgart, 1988.

(30) Pauling, L.; Kamb, B. *Proc. Natl. Acad. Sci. U S A* **1986,** *83*, 3569-3571.

(31) Swanson, H. E.; Tatge, E. *Phys. Rev.* **1955,** *99*, 1737 - 1743.

(32) Donohue, J., *The Structures of the Elements*. Wiley: New York, 1974.

(33) Menges, E.; Hopf, V.; Schäfer, H.; Weiss, A. *Z. Naturforsch. B* **1969,** *21*, 1351–1352.

Supporting Information

for

Synthesis and Structural Characterization of $Li_2Ag_{1-x}Ge_{1+x}$ (x = 0.06)

Alexander Henze, Thomas F. Fässler

manuscript for publication

Contents

Crystal structures

Table S-1. Interatomic distances for $Li_2Ag_{0.94}Ge_{1.06}$

Table S-2. Anisotropic displacement parameters for $Li_2Ag_{0.94}Ge_{1.06}$

Powder and Single Crystal X-ray diffraction and structural refinement.

Figure S-1. Powder diffractogram of a nearly phase pure sample of $Li_2Ag_{1-x}Ge_{1+x}$ (x = 0.06).

Table S-1: Interatomic distances for $Li_2Ag_{0.94}Ge_{1.06}$

Atoms		Distances (Å)
Ge1/Ag1	Ge1/Ag1	2.6934(2)
Ge1/Ag1	Li1	2.6934(2)
Li1	Li1	2.6934(2)

Table S-2: Anisotropic displacement parameters for $Li_2Ag_{0.94}Ge_{1.06}$

Atom	U_{11}	U_{22}	U_{33}	U_{12}	U_{13}	U_{23}
Ge1/Ag1	0.0113(6)	0.0113(6)	0.0134(6)	0	0	0
Li1	0.0160(32)	0.0160(32)	0.0254(54)	0	0	0
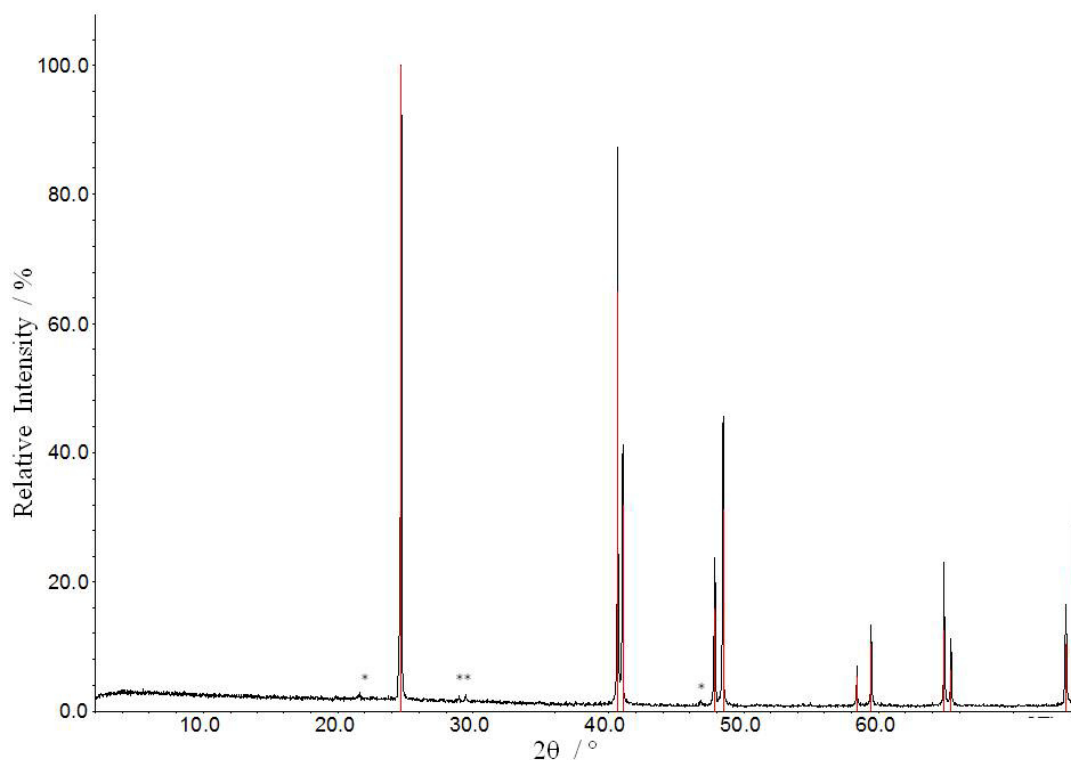
Figure S-1: Experimental X-ray powder diffractogram of a nearly phase pure sample of $Li_2Ag_{1-x}Ge_{1+x}$ (x = 0.06) (black) with the theoretical pattern of $Li_2Ag_{1-x}Ge_{1+x}$ (red). The possible side phase is marked with an asterisk.

6.4 The Copper Stannide with the Highest Lithium Content: Synthesis and Structural Characterization of Li_6CuSn_2

Alexander Henze, Thomas F. Fässler

manuscript for publication

Abstract

In view of the interest into new intermetallic Li containing compounds for Li-ion batteries, the ternary phase diagram of Li-Cu-Sn has been investigated. High-temperature synthesis using a premelted alloy of Cu and Sn and elemental Li yielded the compound Li_6CuSn_2 which is now the Li-richest in this phase system. The structure of the compound was investigated using single-crystal X-ray diffraction. Li_6CuSn_2 crystallizes in its own structure type in the space group $P6_3/mmc$ (No. 194) with lattice parameters of $a = 4.5484(1)$ and $c = 8.4532(1)$. The compound consists of two types of layers. The polyanionic layers formed by Cu and Sn arrange in nearly planar six-membered rings with only heteroatomic contacts between the atoms. Intercalated between these layers are two layers of Li, which arranged in six-membered rings as well. An ordered model of the compound regarding the half-occupation of the Cu and Li2 positions reveals chains of Cu and Sn in a layered arrangement.

Introduction

Intermetallic compounds containing Li are in the focus of research due to their potential application in intermetallic alloy electrodes in Li-ion batteries (LIBs). Although weight is an important issue, compounds containing the heavy group 14 element Sn have drawn some attention and are already used in commercialized LIBs.[1, 2] This is due to the low specific capacity of graphite (372 mAh/g)[3] which represents the most common anode material. In comparison, the lithiation of Sn to the compound $Li_{17}Sn_4$[4] offers a specific capacity of 960 mAh/g. But the tremendous volume change on lithiation which is up to 200% remains a main problem, not only for tin, but also for its lighter homologues. A solution to this problem is the introduction of transition metals (T) into these binary systems. This leads to an increase of mechanical stability and therefore less volume change during charging/discharging processes combined with beneficial safety improvements. One of the most promising transition metals for this purpose seems to be Cu. The first two compounds in the Li-Cu-Sn system, Li_2CuSn and $LiCu_2Sn$ were first described almost 50 years ago.[5-7] But due to their potential regarding anode materials in LIBs they were recently reinvestigated.[8] Following these investigations, new compounds in the Li-Cu-Sn system were discovered and investigated regarding their Li-ion mobility namely the compounds Li_2CuSn_2[9] and $Li_3Cu_6Sn_4$[10] as well as Li_3CuSn and $Li_6Cu_3Sn_2$.[11] Inspired by our recent investigations in the Li-rich part of the Li-Ag-Ge system,[12, 13] we extended our investigations into the Li-rich part of the Li-Cu-Sn system using high-temperature syntheses. During these investigations the compound Li_6CuSn_2 was discovered and its structure was analyzed using single-crystal X-ray diffraction. The compound crystallizes in the space group $P6_3/mmc$ (no. 194) with a cell parameters of $a =$ 4.5485 and $c =$ 8.4532. Li_6CuSn_2 therefore now represents the Li-richest compound in this system. This compound contains polyanionic layers of Cu and Sn with intercalated layers of Li. Although its composition reminds on the recently found Li_7CuSi_2,[14] the structures are build completely different and are not related.

Experimental Section

Synthesis

All steps of the synthesis and sample preparation were carried out using an argon filled glove box and other standard inert gas techniques. The starting materials were Li rods (99%, Rockwood Lithium), Cu wire (99.9%, Sigma Aldrich) and Sn granules (99.999%, ChemPur) were used as received. The preparation of the Cu/Sn alloy was performed by pre-melting 93 mg (1.464 mmol) of the Cu wire with 347 mg (2.92 mmol) of the Sn granules in an arc furnace (Mini Arc Melting System, MAM-1, Johanna Otto GmbH) installed in a glove box to obtain a binary regulus with the expected stoichiometry. 61 mg (8.76 mmol) of Li was provided in a niobium ampoule and the binary regulus was added on top. The niobium ampoule was sealed by arc welding and transferred into a silica tube. The silica tube was evacuated and placed into a vertical resistance tube furnace. The sample was heated to 750 °C and tempered for 24 hours. Afterwards it was cooled with a cooling rate of 0.1 K to 450 °C and tempered for another 24 hours. Finally the sample was cooled to room temperature with a cooling rate of 0.1 K. After the ampoule was opened in an argon atmosphere, the sample was gained as lustrous silver powder which was sensitive to air and moisture.

Powder and Single Crystal X-ray diffraction and structural refinement

For powder diffraction analysis, the sample was finely ground to a powder, sealed in a glass capillary and measured at room temperature using a STOE Stadi P powder diffractometer with Cu-K$_\alpha$ radiation (λ = 1.54056 Å, Ge(111) monochromator) and a position sensitive detector (Mythen 1K). The STOE WINXPOW program package was used for phase analysis.[15]

For the structure determination of Li$_6$CuSn$_2$ a suitable single crystal was selected in an argon-filled glove box equipped with a microscope. The lustrous, block shaped crystal was mounted on the tip of a glass capillary using perfluoropolyalkylether. Single crystal XRD data were collected using an OXDORD Xcalibur3 diffractometer system (Sapphire3 CCD detector; Mo K$_\alpha$ radiation, λ = 0.71073 Å, graphite monochromator, sealed tube X-ray source) with crystal cooling in a 120 °C cold nitrogen stream. For data processing, the Oxford CrysAlis RED software[16] was used. A empirical absorption correction was

performed using the STOE X-RED/X-SHAPE software.[17, 18] The program X-Prep[19] was used for space group determination and data merging (identical indices only). For the structure solution (direct methods) and the refinement the programs XS[20] and XL[21] were used. Selected crystallographic data are given in Table 1 to 4.

Table 1: crystal data and structure refinement

Formula	**Li_6CuSn_2**
Formula weight (g·mol^{-1})	271.14
Space group	$P6_3/mmc$ (no. 194)
Z	2
Unit cell parameters (Å)	$a = 4.5484(1)$ $c = 8.4532(1)$
Volume (Å^3)	151.46(4)
$D_{calcd.}$ (g·cm^{-3})	4.148
Abs. coeff. (mm^{-1})	14.91
$F(000)$ (e)	164.0
Crystal shape/color	block/silver
Temperature (K)	130
Θ range (deg)	4.82 – 39.26
Range in hkl	−7/8 −7/7 −14/12
Reflections collected	3635
Unique reflections	195
Data / parameter	195 / 16
GOF on F^2	1.095
R_1, wR_2 ($I > 2\,\sigma(I)$)	0.0143, 0.0304
R_1, wR_2 (all data)	0.0174, 0.0313
Largest diff. peak/hole (e Å^{-3})	1.29 and −0.88

Table 2:   Atomic coordinates and equivalent isotropic displacement parameters for Li_6CuSn_2

Li_6CuSn_2

Atom	Wyck.	*sof*	*x*	*y*	*z*	$U_{eq}/Å^2$
Sn1	2*c*	1	1/3	2/3	1/4	0.007(1)
Cu1	2*b*	0.55(1)	0	0	1/4	0.026(1)
Li1	4*f*	1	2/3	1/3	0.09294	0.017(2)
Li2	4*e*	0.49(2)	0	0	0.08172	0.045(6)

Table 3:   Interatomic distances for Li_6CuSn_2

Li_6CuSn_2

Atoms		Distances (Å)
Sn1	Cu1	2.6261(1)
	Li1	2.899(9)
	Li2	2.987(11)
Cu1	Li1	2.943(4)
	Li2*	1.423(22)
	Li2	2.804(22)
Li1	Li1	2.655(18)
	Li2	2.628(1)
Li2	Li2*	1.382(44)
	Li2	2.845(44)

* distance to nearest unoccupied Li2 position

Table 4: Anisotropic displacement parameters for Li_6CuSn_2

Li_6CuSn_2

Atom	U_{11}	U_{22}	U_{33}	U_{12}	U_{13}	U_{23}
Sn1	0.0061(2)	0.0061(2)	0.0078(2)	0.0030(1)	0	0
Cu1	0.0049(3)	0.0049(3)	0.0669(9)	0.0024(2)	0	0
Li1	0.016(2)	0.016(2)	0.020(3)	0.008(1)	0	0
Li2	0.013(3)	0.013(3)	0.109(17)	0.007(2)	0	0

EDX Measurements

EDX analysis was carried out on single crystals of the title compound Li_6CuSn_2 using a JEOL 5900LV scanning electron microscope equipped with an OXFORD INSTRUMENTS INCA energy dispersive X-ray microanalysis system. The unit cells of the crystals were determined by single crystal XRD. The quantitative analysis for this compound showed the presence of the elements Cu and Sn with no other element heavier than Na detectable.

Results

Structure description of Li_6CuSn_2

The compound Li_6CuSn_2 crystallizes in its own structure type in the space group $P6_3/mmc$ (no. 194) with lattice parameters of $a = 4.5485$ and $c = 8.4532$. The structure can be described consisting of two types of layers extending in *ab* direction and stacked in *c* direction, one build by Cu and Sn atoms and one build by Li atoms (Figure 1). Both types of layers consist of nearly planar 6-membered rings. While the Sn and Li1 atoms in these layers show an occupancy of 100%, the Cu and Li2 atoms only show an occupancy of 50% each. This results from the special positions of these atoms on the edge of the unit cell. These positions lead to a representation of both sequences the Cu and Li2 atoms are able to occupy on the *c* edge of the unit cell next to each other. This leads to significantly too short interatomic distances (Figure 2a). The Li2-Li2 distance on the cell edge is 1.382(1) Å, the Li2-Cu distance is 1.423(1) Å. An ordered model of the compound occurs if only every second of the half-occupied atomic positions of the unit cell is regarded at a time. In this ordered model, Li2 and Cu atoms present reasonable interatomic distances

(Figure 2b). The Li2-Li2 distance increases to 2.845(1) Å which is smaller than Li-Li distances in body-centered cubic Li (3.05 Å)[22] and in Li_2CuSn_2 (2.93 Å) but considerably longer than Li-Li distances in highly ionic compounds like Li_7Sn_2 and $Li_{17}Sn_4$ with 2.61 Å and 2.41 Å respectively.[4, 23] The Li-Cu distance increases to 2.804(1) Å. This is slightly longer than Li-Cu distances in Li_2CuSn and Li_2CuSn_2 with 2.71 Å and 2.66 Å. The sequence of the two possible variants of the Li-Cu strings seems to be statistical, as it was not possible to find any superlattice reflections in the crystallographic data. The resulting structure consists of interwined strings of Cu and Sn where every Cu atom is surrounded by three Sn atoms, while the Sn atoms are connected to two Cu atoms if they are in the chain or one Cu atom if they are not (Figure 3). This kind of chains are known from the numerous compounds of the La_3NiGe_2 structure type.[24]

The synthesis of an ordered variant of this compound might be possible by variations of the reaction parameters. The Li1-Li2 distance in the compound is 2.628(1) Å which is very close to Li-Li distances in Li_7Sn_2 mentioned above. The Cu-Sn distances in the compound is 2.626(1) Å which is very close to Cu-Sn distances in Cu_6Sn_5 and Cu_3Sn with 2.63 Å and 2.65 Å respectively.[25, 26] A different crystallographic peculiarity besides the half-occupied positions on the c axis of the unit cell is their long anisotropic replacement parameters in c direction (Figure 4). This might be a hint to an incommensurability of the structure. If this is the case, this would require a modulation of the Li2 and Cu2 positions which has not been done yet. The long ellipsoids of the Cu atoms can as well be observed in the Electron Density Contour Fourier Map along the cell edge (Figure S-2, S-3). This map shows the two Cu positions with an electron density of 83 e/Å which corresponds to the half-occupation of these positions. The Li positions on the cell edge in c direction are not visible in this map due to their low electron density. A Difference Fourier Map with implemented Sn1, Cu and Li1 positions reveals the Li2 positions though with an electron density of 3.6 e/Å each (Figure S-4, S-5). The ellipsoidal shape of the electron density can be observed for Li2 as well. In contrast, the fully occupied Li1 positions are visible in the respective Fourier Map with 11 e/Å (Figure S-6, S-7). The Sn1 position in this map is clearly visible with 403 e/Å. This shows that the structure model of this compound should be correct. The unsatisfying occupation of the cell edge by two possible sequences for Cu and Li might therefore be avoided by different conditions in the synthesis, but is present in the described compound.
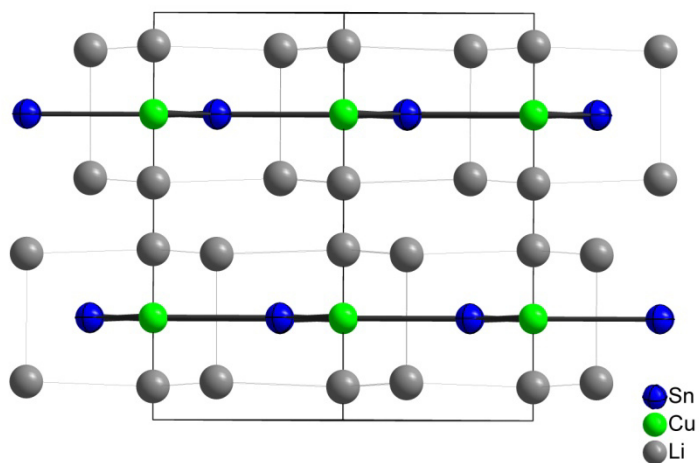
Figure 1: Layers of Cu/Sn and Li in Li_6CuSn_2. Li, Cu and Sn are represented as spheres in blue, green and grey respectively. Thick black lines mark Cu-Sn bonds, thin black lines show the coordination of the Li atoms.
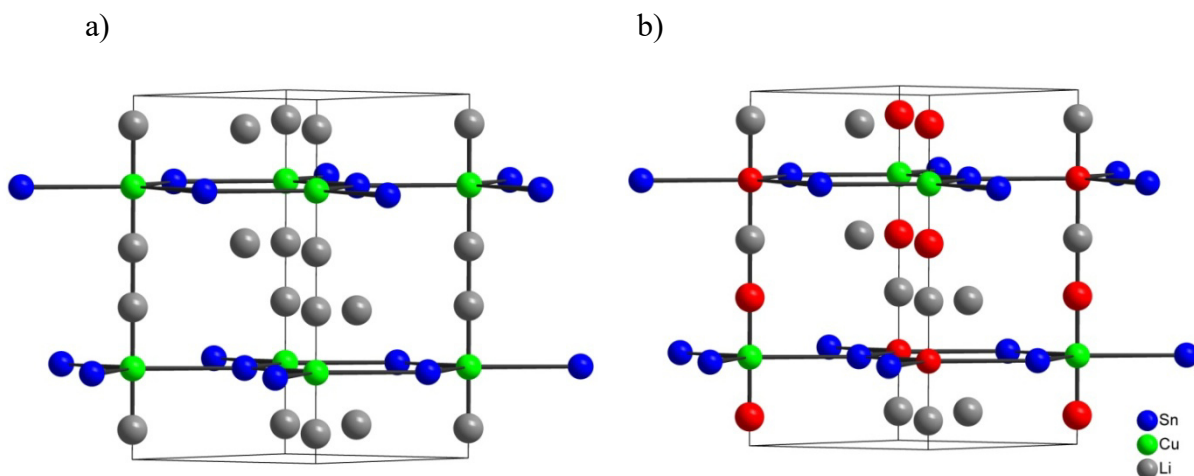
a)   b)

Figure 2: Unit cell Li_6CuSn_2. Li, Cu and Sn are represented as spheres in blue, green and grey respectively. a) All occupied atomics positions in their respective color. b) 50% of the half-occupied positions are marked in red to depict a model which might be present in parts of the structure.

a)　　　　　　　　　　　　b)
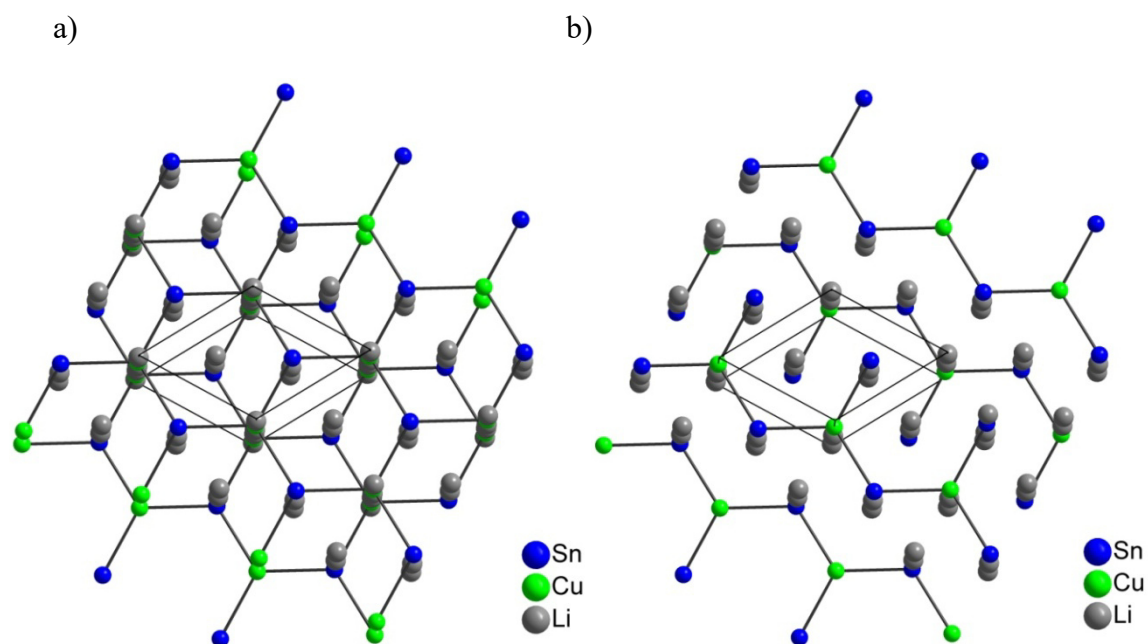
Figure 3: View on the structure of Li_6CuSn_2 nearly along the c-axis. a) all half-occupied positions are depicted emphasizing the graphite-like stacking of the layers. b) half of the half-occupied atomic positions are removed emphasizing the resulting structure of interwined strings. Li, Cu and Sn are represented as spheres in blue, green and grey respectively.
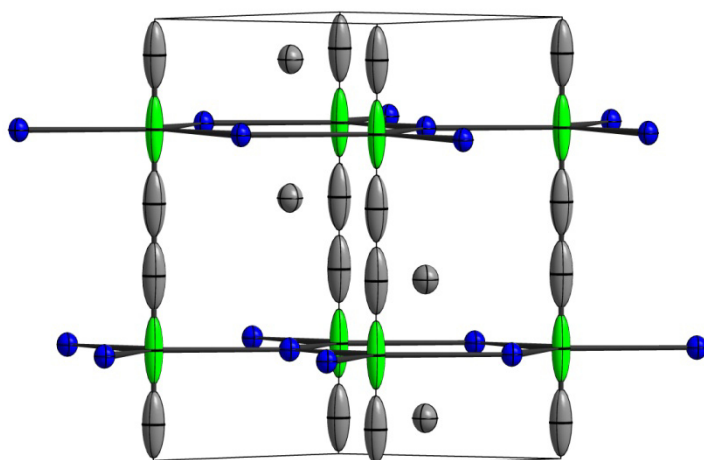
Figure 4: Unit cell Li_6CuSn_2. Li, Cu and Sn are represented as ellipsoids with 90% probability level in blue, green and grey respectively.

Conclusion

Our investigations in the Li-Cu-Sn phase diagram led to the discovery of the new polar intermetallic compound Li_6CuSn_2. This compound now represents the Li richest compound in this phase diagram and consists of two-dimensional layers of Cu and Sn

with intercalated Li atoms. The polyanionic Cu-Sn layers are build of nearly planar six-membered rings, which reminds on the structure of graphite. There are considerably more Li atoms between the polyanionic layers though, as the Li atoms themselves form two layers of six-membered rings between the polyanionic layers. Currently, we are working on improvements in the synthesis leading to a phase pure compound as well as an ordered variant of the structure.

Associated content

Supporting Information available: X-ray crystallographic files in CIF format, powder diffractogram and figures of the Fourier and Difference Fourier Maps.

Author information

Corresponding Author: Prof. Dr. Thomas F. Fässler, Department Chemie, Technische Universität München, Lichtenbergstr. 4, D-85747 Garching, Germany

*E-mail: Thomas.Faessler@lrz.tum.de.

Notes: The authors declare no competing financial interest.

References

(1)   Idota, Y.; Kubota, T.; Matsufuji, A.; Maekawa, Y.; Miyasaka, T. *Science* **1997,** *276*, 1395-1397.

(2)   Fan, Q.; Chupas, P. J.; Whittingham, M. S. *Electrochem. Solid-State Lett.* **2007,** *10*, A274-A278.

(3)   Nagaura, T.; Tozawa, K. *Prog. Batteries Solar Cells* **1990,** *9*, 209.

(4)   Lupu, C.; Mao, J.-G.; Rabalais, J. W.; Guloy, A. M.; Richardson, J. W. *Inorg. Chem.* **2003,** *42*, 3765-3771.

(5)   Pauly, H.; Weiss, A.; Witte, H. *Z. Metallkd.* **1968,** *59*, 47-58.

(6)   Schuster, H.-U.; Thiedemann, D.; Schönemann, H. *Z. Anorg. Allg. Chem.* **1969,** *370*, 160-170.

(7)   Kripyakevich, P. I.; Oleksiv, G. I. *Dopovidi Akademii Nauk Ukrains'koi RSR, A* **1970**, 63-65.

(8)   Fürtauer, S.; Effenberger, H. S.; Flandorfer, H. *J. Solid State Chem.* **2014,** *220*, 198-205.

(9)   Winter, F.; Dupke, S.; Eckert, H.; Rodewald, U. C.; Pöttgen, R. *Z. Anorg. Allg. Chem.* **2013,** *639*, 2790-2795.

(10)   Fürtauer, S.; Effenberger, H. S.; Flandorfer, H. *Z. Kristallogr.* **2015,** *230*, 97-105.

(11)   Fürtauer, S.; Effenberger, H. S.; Flandorfer, H. *Z. Kristallogr.* **2016,** *231*, 79-87.

(12)   Henze, A.; Hlukhyy, V.; Fässler, T. F. *Inorg. Chem.* **2015,** *54*, 1152-1158.

(13)   Henze, A.; Fässler, T. F. *Inorg. Chem.* **2015**.

(14)   Slabon, A.; Budnyk, S.; Cuervo-Reyes, E.; Wörle, M.; Mensing, C.; Nesper, R. *Angew. Chem.* **2012,** *124*, 11762–11764.

(15)   Stoe *WinXPOW*, 2.08; Stoe & Cie GmbH: Darmstadt, 2003.

(16)   Stoe *CrysAlis RED*, 1.171.33.34; Oxford Diffraction Ltd.: 2009.

(17)   Stoe *X-RED32*, 1.48; STOE & Cie GmbH: Darmstadt, 2008.

(18)   Stoe *X-Shape*, 2.11; Stoe & Cie GmbH: Darmstadt, 2008.

(19)   Sheldrick, G. M. *XPREP-97*, University of Göttingen (Germany), 1997.

(20)   Sheldrick, G. M. *SHELXS-97*, University of Göttingen (Germany), 1997.

(21)   Sheldrick, G. M. *SHELXL-97*, University of Göttingen (Germany), 1997.

(22)   Donohue, J., *The Structures of the Elements*. Wiley: New York, 1974.

(23)   Frank, U.; Müller, W.; Schäfer, H. *Z. Naturforsch. B* **1975,** *30*, 10–13.

(24)   Bodak, O.; Bruskov, V.; Pecharskij, V. **1982**.

(25)   Gangulee, A.; Das, G.; Bever, M. *Metallurgical Transactions* **1973,** *4*, 2063-2066.

(26)   Hendus, H.; Knödler, H. *Acta Cryst.* **1956,** *9*, 1036-1036.

<div align="center">

Supporting Information

for

The Copper Stannide with the Highest Lithium Content: Synthesis and Structural Characterization of Li_6CuSn_2

</div>

Alexander Henze, Thomas F. Fässler

manuscript for publication

Contents

Powder and Single Crystal X-ray diffraction and structural refinement.

Figure S-1. Powder diffractogram of a sample with Li_6CuSn_2 as the main component.

Crystal structures

Figure S-2. Electron Density Contour Fourier Map of the cell edge of Li_6CuSn_2.

Figure S-3. 3D image of the Electron Density Contour Fourier Map of the cell edge of Li_6CuSn_2.

Figure S-4. Difference Fourier Map of the cell edge of Li_6CuSn_2 with implemented Cu atoms.

Figure S-5. 3D image of the Difference Fourier Map of the cell edge of Li_6CuSn_2 with implemented Cu atoms.

Figure S-6. Electron Density Contour Fourier Map of the full occupied Sn1 and Li1 positions.

Figure S-7. 3D image of the Electron Density Contour Fourier Map of the fully occupied Sn1 and Li1 positions.
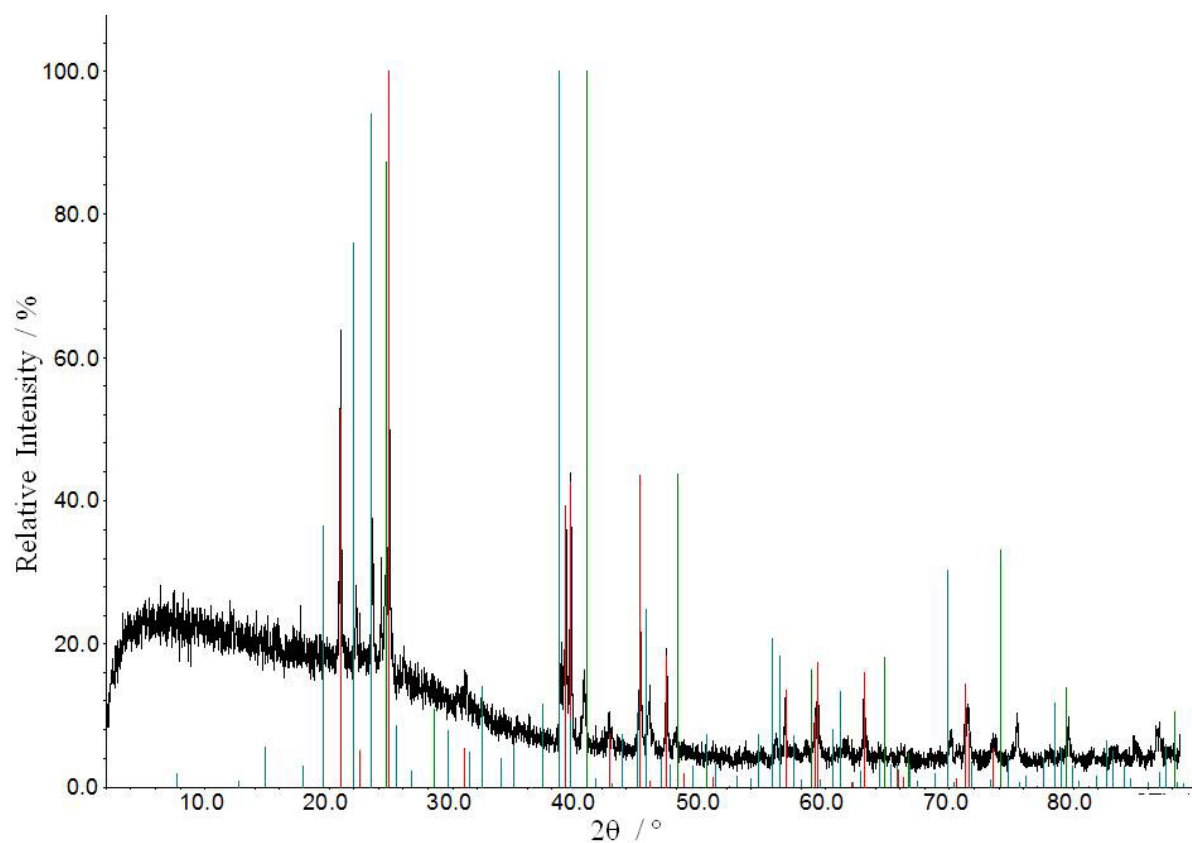
Figure S-1: Experimental X-ray powder diffractogram of a sample of Li_6CuSn_2 (black) with the theoretical pattern of Li_6CuSn_2 (red) as well as of $Li_{22}Sn_5$ (green) and Li_2CuSn (blue), which are side phases.
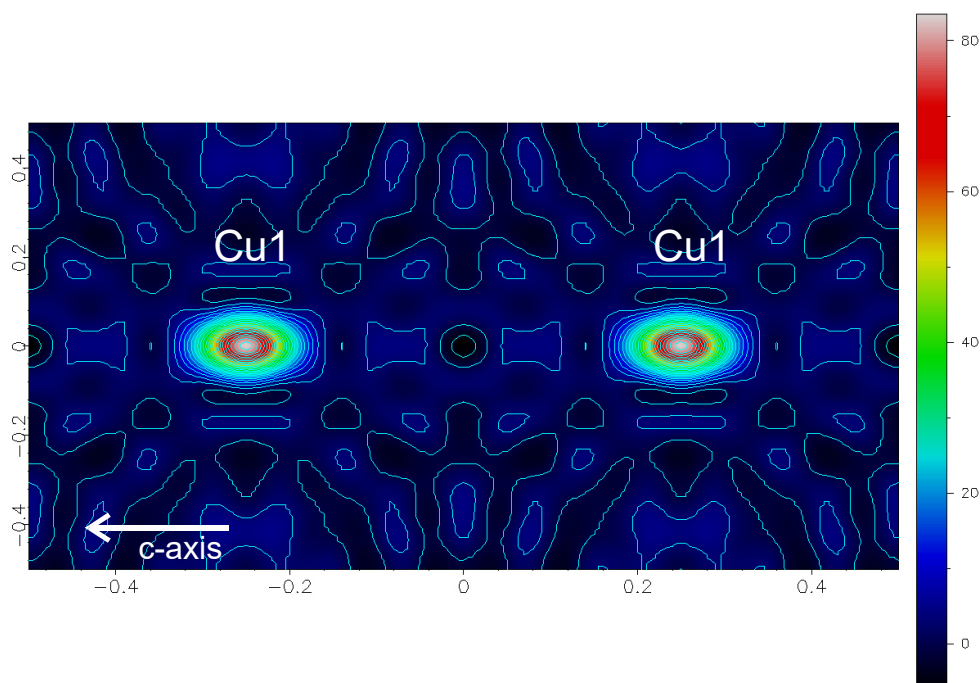
a)
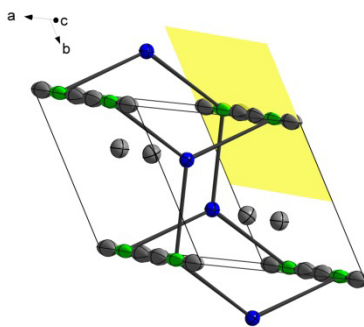
b)

Figure S-2: Electron Density Contour Fourier Map of the cell edge in *c* direction of Li_6CuSn_2 marked yellow in a) and actual map in b). The Cu positions and their ellipsoidal shape are clearly visible.
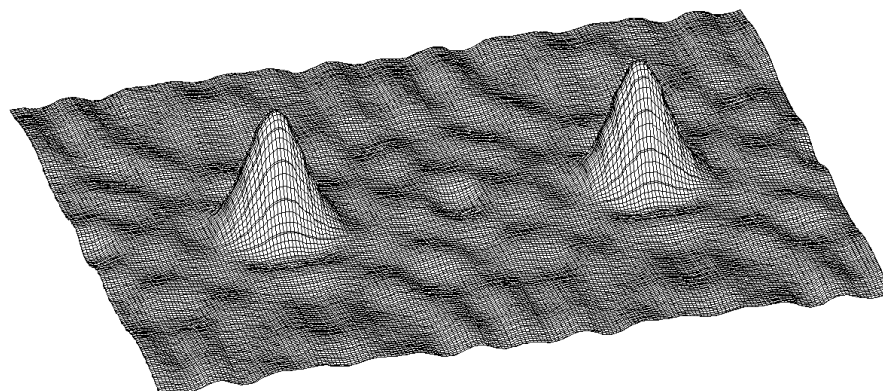

Figure S-3: 3D image of the Electron Density Contour Fourier Map of the cell edge in *c* direction of Li_6CuSn_2.
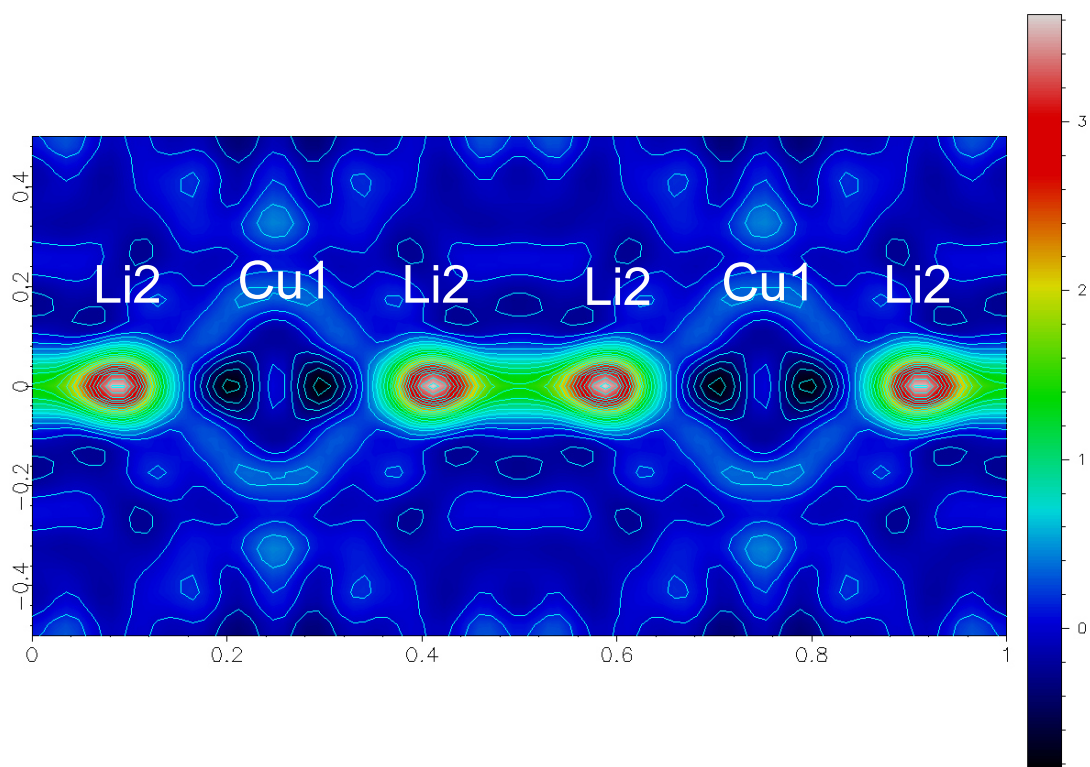
Figure S-4 Difference Fourier Map of the cell edge in *c* direction of Li_6CuSn_2 with implemented Cu positions. The half occupied positions of the Li2 atoms are clearly visible with 3.6 e/Å.
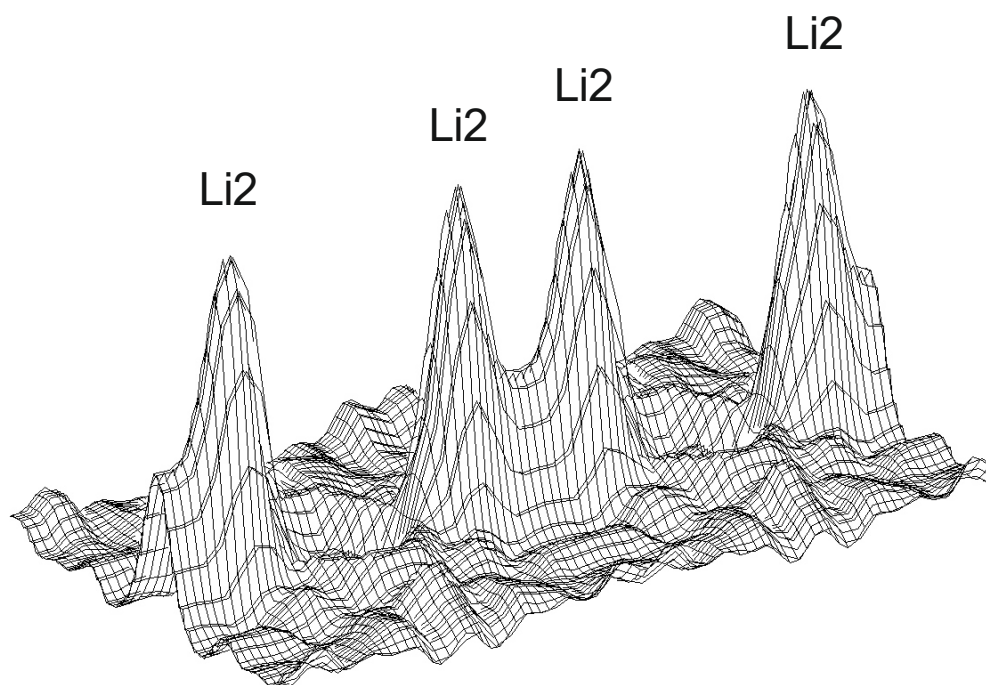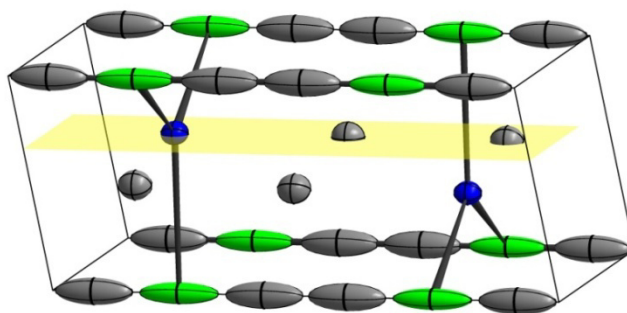

Figure S-5: 3D image of the Difference Fourier Map of the cell edge in *c* direction of Li_6CuSn_2.
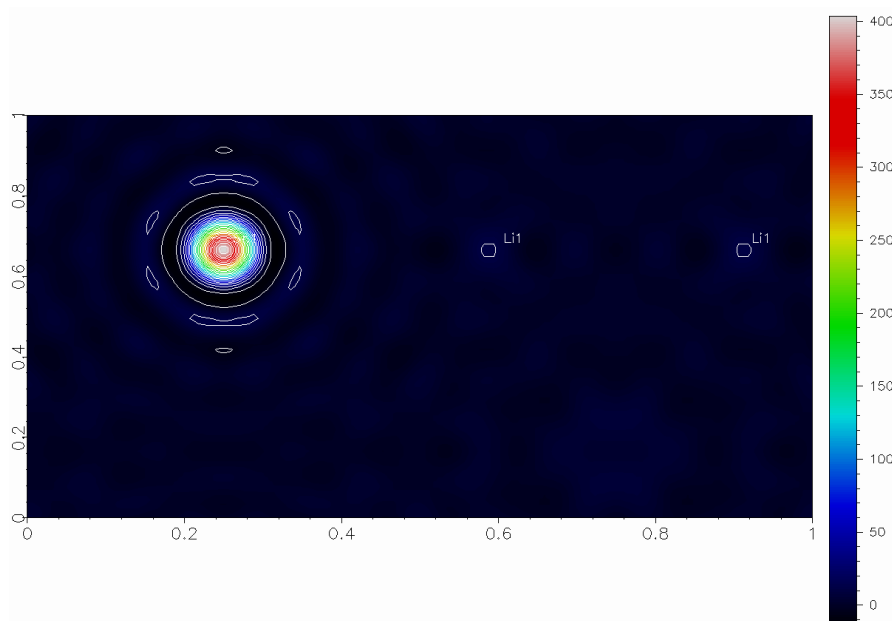
a)

b)

Figure S-6: Electron Density Contour Fourier Map of the full occupied Sn1 and Li1 positions. a) Layer in the unit cell in yellow. b) Actual map. Sn1 is visible with 403 e/Å, Li1 positions are visible with 11 e/Å.
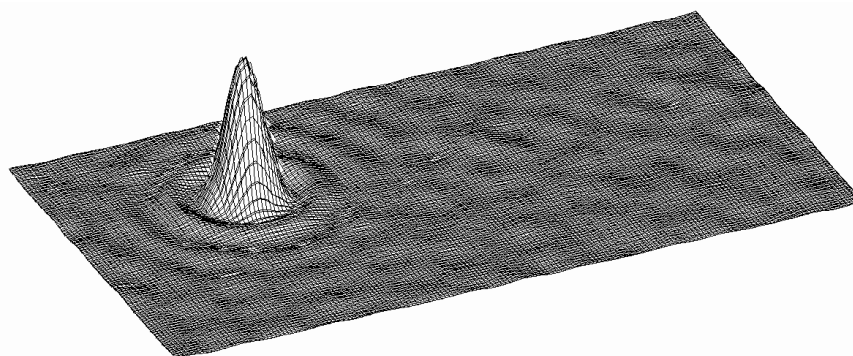

Figure.S-7: 3D image of the Electron Density Contour Fourier Map of the fully occupied Sn1 and Li1 positions. The Li1 positions are not visible in this image.

6.5 Synthesis and Structural Characterization of $Li_{14}Ni_{8+x}Ge_{9-x}$ (x = 0.3) featuring the First Rhombic Dodecahedral Cluster in a Solid State Compound

Alexander Henze, Thomas F. Fässler

manuscript for publication

Abstract

Regarding the excellent properties of intermetallic compounds as anode materials in Li-ion batteries and the highly interesting clusters found in Li-rich parts of intermetallic systems, the Li-rich part of the system Li-Ni-Ge was investigated. High-temperature solid state synthesis led to the formation of the new compound $Li_{14}Ni_{8+x}Ge_{9-x}$ (x = 0.3) whose structure was characterized using single crystal X-ray diffraction. The compound crystallizes in the space group $Fm\bar{3}m$ (Nr. 225) with a lattice parameter of a = 11.7219. The structure of this compound consists of a 3D network of Ge bridged $[Ni_8Ge_6]^{6-}$ clusters in form of rhombic dodecahedra and interstitial Li^+ cations. The clusters are filled with Ni and Ge atoms with a probability of 30% and 70% respectively. Therefore, this represents the first solid state synthesis of rhombic dodecahedra which up to now were only known from solution syntheses. Furthermore, $Li_{14}Ni_{8+x}Ge_{9-x}$ (x = 0.3) represents only the second compound containing main group filled rhombic dodecahedra. The tube shaped voids in *ac* and *bc* direction in this 3D polyanionic network are filled with Li atoms raising the question of Li-ion mobility. The compound as a whole is electron precise and can be viewed as a Zintl compound.

Keywords: Li, rhombic dodecahedron, cluster chemistry

Introduction

One of the main aspects for the investigation of metal clusters is to take an insight into the chemistry lying between isolated molecules and extended three-dimensional networks in solid state compounds.[1] The most common cluster units in solvent and solid state chemistry are the tetrahedral $[E]^{4-}$ and the $[E]_9^{n-}$ cluster units (E = main group element). But also bigger clusters like icosahedra, Friauf-polyhedra[2] and rhombic dodecahedra are known and have raised some attention. Rhombic dodecahedral cluster, in opposition to the other mentioned clusters, are only known from solution based chemistry though. In solid state chemistry only rhombic dodecahedral coordination spheres are known as in the 26 atom clusters (M_{26}) known from γ-brass and structures derived from this polyhedron. This occurs for example in $Li_{17}Si_4$.[3] The rhombic dodecahedron presents itself as a combination of six octahedrally arranged atoms capping the six sides of a cube. The six positions of the octahedron in such clusters are usually occupied by E atoms and the eight positions of the cube by transition metals (T). This cluster exists in an empty version with P as the main group element as in $Ni_8(\mu_4\text{-}PPh)_6(L)_8$ (L = CO, PPh_3/Cl)[4, 5] and a filled version with a tendency of the central atomic position to be occupied by the transition metal building the cube around it. This is represented by the general formula $[T@T_8(\mu_4\text{-}E_6]L_8$.[6-8] But also the cluster $[As@Ni_8(\mu_4\text{-}E_6](CO)_8$ and a $[Si@Al_{14}](Cp)_6$ cluster with a main group element in the center are known.[9, 10] The increase in stability of clusters by centering with a main group element has also been suggested by *Wheeler* based on extended Hückel calculations[11] and more theoretical work confirms the enhanced stability of these compounds.[12] The element Ni seems to have a special addiction to the rhombic dodecahedra. It was not only found in the first isolated such cluster $Ni_8(\mu_4\text{-}PPh)_6(CO)_8$ but also in $[Ni@Ni_8((\mu_4\text{-}GeEt)_6](CO)_8$, which is the only such compound containing a group 14 element.[4, 13] But also clusters containing Pd and Co are known.[6, 7, 14] In this work we present the compound $Li_{14}Ni_{8+x}Ge_{9-x}$ (x = 0.3) containing the first rhombic dodecahedron synthesized in a solid state reaction. The rhombic dodecahedra are filled with Ni and Ge respectively and are connected via Ge atoms to form a three-dimensional network exhibiting wide Li filled channels. $Li_{14}Ni_{8.3}Ge_{8.7}$ represents the third compound in the Li-Ni-Ge phase system in addition to $LiNi_2Ge$ and $LiNi_6Ge_6$,[15, 16] but the first one that includes clusters in its structure.

Experimental Section

Synthesis

To synthesize the title compounds, all materials were handled in an argon atmosphere using an argon filled glove box (MBraun 20 G, argon purity 99.996%). Starting materials for the synthesis were Li rods (99.9%, Sigma Aldrich), Ni wire (99.9%, Johnson-Matthey) and Ge pieces (99.999%, ChemPur). 204 mg (3.48 mmol) of the Ni wire and the 253 mg (3.48 mmol) of the Ge pieces were pre-melted in an arc furnace (Mini Arc Melting System, MAM-1, Johanna Otto GmbH) to obtain a binary regulus with the expected stoichiometry. 43 mg (6.15 mmol) of Li were given into a niobium ampoule with the corresponding binary regulus. The ampoule was sealed by arc-welding and transferred into a silica tube. The silica tube was evacuated and put into a vertical resistance tube furnace. The samples were heated to 750 °C and tempered for 24 hours. Afterwards they were slowly cooled to room temperature with a degree of −0.1 K/min. After opening the ampoules, the product appeared as metallic lustrous silver powder, which was sensitive to air and moisture.

Powder and Single Crystal X-ray diffraction and structural refinement

For powder diffraction analysis, the sample was finely ground to a powder, sealed in glass capillaries and measured at room temperature using a STOE Stadi P powder diffractometer with Cu-K$_\alpha$ radiation (λ = 1.54056 Å, Ge(111) monochromator) and a position sensitive detector (Mythen 1K). The STOE WINXPOW program package was used for phase analysis.[17] The powder diffractogram shows Li$_{14}$Ni$_{8.3}$Ge$_{8.7}$ as the main phase, while at least one different phase is present. It was not possible to identify the side phases.

For the structure determination, a single crystal was mounted on the tip of a glass capillary using perfluoropolyalkylether. The data collection was carried out on an OXDORD Xcalibur3 diffractometer system (Sapphire3 CCD detector; Mo K$_\alpha$ radiation, λ = 0.71073 Å, graphite monochromator, sealed tube X-ray source) with crystal cooling in a 150 °C cold nitrogen stream. For data processing, the Oxford CrysAlis RED software[18] was used. A empirical absorption correction was performed using the STOE X-RED/X-SHAPE software[19, 20] X-Prep[21] was used for space group determination and

data merging (identical indices only). For structure solution (direct methods) and refinement the programs XS[22] and XL[23] were used. Selected crystallographic data a given in Table 1 and 2.

Table 1:   crystal data and structure refinement

Formula	$Li_{14}Ni_{8.3}Ge_{8.7}$
Formula weight (g·mol^{-1})	1220.16
Space group	$Fm\bar{3}m$ (Nr. 225)
Z	1
Unit cell parameters (Å)	$a = 11.7219$
Volume (Å^3)	1631.95
P_{calc} g·cm^{-3}	4.949
abs. coeff.	25.04
F(000)	2211.2
Crystal shape/color	block/silver
Temperature (K)	150
Θ range	3.46 – 32.39
Range in hkl	−17/17 −16/17 −9/17
Reflections collected	10366
Unique reflections	185
Data / parameter	185 / 18
GOF on F^2	1.349
R$_1$, wR$_2$ ($I \geq 2\sigma(I)$)	0.0222, 0.0583
R$_1$, wR$_2$ (all data)	0.0243. 0.0589
Largest diff. peak and hole	1.02 and −0.69

Table 2:   Atomic coordinates and equivalent isotropic displacement parameters for $Li_{14}Ni_{8.3}Ge_{8.7}$

Atom	Wyck.	x	y	z	U_{eq}/Å^2
Ge1	24e	0	0.22368	0.52957	0.007(1)
Ge2/Ni2^a	4a	0	0	0	0.005(1)

Ge3	8c	1/4	1/4	1/4	0.007(1)
Ni1	32f	0.12721	0.12721	0.12721	0.006(1)
Li1	32f	0.37845	0.12155	0.12155	0.020(3)
Li2	24d	1/4	1/4	0	0.020(4)

^{a}The occupancy factor for Ge2/Ni2 is 0.69 / 0.31(9).

EDX Measurements

EDX analysis was carried out on single crystals of the title compounds $Li_{14}Ni_{8.3}Ge_{8.7}$ using a JEOL 5900LV scanning electron microscope equipped with an OXFORD INSTRUMENTS INCA energy dispersive X-ray microanalysis system. The unit cells of the crystals were determined by single crystal XRD. The quantitative analysis for both compounds showed the presence of the elements Ni and Ge with no other element heavier than Na detectable.

Results

Structure description and discussion

The compound $Li_{14}Ni_{8.3}Ge_{8.7}$ crystallizes in its own structure type in the space group $Fm\bar{3}m$ (Nr. 225). The compound exhibits a network derivative of Heusler alloys, in which rhombic dodecahedral (Ni_8Ge_6) clusters form a face-centered cubic (fcc) packing (Figure 1). The rhombic dodecahedra are each build by eight Ni1 atoms arranging in a cube with six Ge1 atoms capping each side of it. The central positions inside of the rhombic dodecahedra are occupied by Ni2/Ge2 with an occupation ratio of 0.69 / 0.31(9). There are no signs of ordering on this central Ni2/Ge2 position. The occupation with solely Ni or Ge led to significantly worse solutions in the structure refinement. Each of the eight Ni atoms in the rhombic dodecahedra is connected to a Ge3 position, which occupies all tetrahedral voids of the fcc analogue packing and bridges the filled (Ni_8Ge_6) clusters to an interconnected network. This leads to a polyanionic substructure which derives from the fluorite structure. The octahedral voids of the framework are filled with cubes of Li atoms (Figure 2a). No electron density could be found inside of these cubes. The rest of the Li atoms form a cuboctahedral surrounding of the (Ni_8Ge_6) cluster thus building a filled M_{26} unit known from γ-brass (M = metal atom). These filled M_{26} units consist of two

tetrahedra, one octahedron and an outer shell of 12 cuboctahedrally arranged atoms (Figure 3). In $Li_{14}Ni_{8.3}Ge_{8.7}$ these units are not crystallographically independent, but corner connected to the neighboring M_{26} units (Figure 2b). The two tetrahedra occupied by Ni and the octahedron occupied by Ge of the M_{26} unit in $Li_{14}Ni_{8.3}Ge_{8.7}$ are building an undistorted rhombic dodecahedral cluster, which has never resulted from a solid state synthesis before.

It is noteworthy though, that the Ge1 and the Ni2 position in the ternary intermetallic compound $CaNi_5Ge_3$ show distorted coloring variants of these M_{26} coordination spheres.[24] The Ge1 position in $CaNi_5Ge_3$ is surrounded by a cube of eight Ni atoms with the octahedron being occupied by four Ni and two Ca positions. The 12 positions cuboctahedral surrounding this inner part are occupied by Ge. The Ni2 position also forms the center of a (Ni_8) cube, while the faces of this cube are capped by Ge atoms as in $Li_{14}Ni_{8.3}Ge_{8.7}$. The cuboctahedral surrounding positions are occupied with Ni and Ca atoms. These coordination spheres overlap in $CaNi_5Ge_3$ in ab-direction forming the layers the compound is build of (Figure 4). In $Li_{14}Ni_{8.3}Ge_{8.7}$, the high amount of Li atoms leads to a strong separation of the core rhombic dodecahedron of the filled M_{26} unit through the occupation of the surrounding cuboctahedral positions by Li atoms. Accordingly, the filled (Ni_8Ge_6) units do not build 2-dimensional layers anymore but instead are weakly interconnected through bridging Ge atoms forming a 3-dimensional network. This results in the formation of rhombic dodecahedral $(Ni/Ge@Ni_8Ge_6)$ clusters. While this type of cluster has never been obtained through a solid state reaction before, it is known from solution based syntheses.

In the $(Ni/Ge@Ni_8Ge_6)$ cluster all bonds are heteroatomic and show a Ni1-Ge1 bond length of 2.403(1) Å which is in the range Ni-Ge bond lengths in NiGe with 2.33 to 2.49 Å.[25] In comparison, the Ni1-Ge3 bond length to the bridging Ge atoms in the tetrahedral voids is 2.504(1) Å and should be considered rather weak. The Ni-Ni distances are 2.995(1) Å which is very long compared to Ni-Ni distances of 2.49 Å in metallic Ni and no bonds should be considered.[26] This is also in good accordance with the cluster in $[Ni@Ni_8(GeEt)_6](CO)_8$, in which the Ni-Ge bond length is 2.36 Å, while Ni-Ni distances are 2.67.[13] Calculations on the bond lengths in a theoretical $[Ge@Ni_8Ge_6(CO)_8]^{4-}$ cluster were optimized to 2.42 Å for Ni-Ge and 2.79 Å for Ni-Ni distances. Calculations concerning the influence of the ligand atom on the Ni-Ni distances show, that the substitution of neutral ligands (like CO) by isoelectronic, but positively charged ligands

leads to less electron-electron repulsion between the Ni atoms and consequently shorter Ni-Ni distances by about 0.2 Å. As the atomic positions of the ligand atoms in $Li_{14}Ni_{8.3}Ge_{8.7}$ are occupied by Ge atoms with a formal charge of 4− the longer Ni-Ni distances should be a result of the additional electron-electron repulsion induced by the electron donating function of the Ge3 atoms. The interatomic distances in $Li_{14}Ni_{8.3}Ge_{8.7}$ also fit well to those in $[As@Ni_8As_6](PH_3)_8$ and the $[Ni@Ni_8Te_6](PH_3)_8$ cluster, with bond lengths of 2.32 Å for Ni-As and 2.55 Å for Ni-Te distances. The respective Ni-Ni distances of 2.89 Å and 2.87 Å are also non-binding. The ethyl ligands are probably very important to the stability of that compound as they donate electrons necessary for the stability of the compound. This is probably the reason why it is the only compound featuring a group 14 element, while the main group element in all other clusters is of the more electron rich groups 15 and 16. For $Li_{14}Ni_{8.3}Ge_{8.7}$ the additional electrons are provided by the surrounding Li atoms, which make the $[Ni/Ge@Ni_8Ge_6]$ cluster the first charged rhombic dodecahedra, while all other clusters are charge balanced due to their solution based synthesis.

The distance between the Ni2/Ge2 position in the center of the (Ni_8Ge_6) to the cluster atoms is 2.594(1) Å for Ni2/Ge2-Ni1 and 2.634(1) Å for Ni2/Ge2-Ge1 respectively. The high coordination number of the Ni2/Ge2 position already shows that no 2-center 2-electron bonds of this position to the cluster shell should be considered. The high interatomic distances emphasize this fact. The Li-Li distances in the compound range from 2.57(1) Å for Li1-Li2 to 2.86(2) Å for Li1-Li1. This is much shorter than Li-Li distances in body-centered-cubic Li with 3.05 Å,[27] but longer than Li-Li distances in highly ionic compounds like $Li_{2.53}AgGe_2$ with 2.49 Å[28] or $Li_{12}Ge_7$ with 2.41 Å.[29] This might be due to the space the Li atoms are given in the large channels between the clusters (Figure 5). This might also explain the in one direction enlarged anisotropic replacement parameter for Li2 (Figure S-2f). The ellipsoids of this atom point towards the unoccupied octahedral voids, which is also where the lone pairs of the Ge1 atoms in the cluster are directed to. This may cause additional attraction to the cationic Li besides the given space in this direction.

Regarding the electronic situation of the cluster, the ligand substituting Ge3 atoms which bridge the clusters should be considered with a formal charge of −4. With 14 positive charges from the Li atoms, this leaves the cluster at a formal charge of −6. The Ni filled cluster $[Ni@Ni_8Ge_6]^{6-}$ is consequently isoelectronic to cluster valence electron (CVE)

counts of 124 in clusters like $[Ni@Ni_8(GeEt)_6](CO)_8$ and the $[Ni@Ni_8As_6](PPh_3)_8$ cluster. This is true if the bridging Ge^{4-} atoms that occupy the same positions as ligands like CO or PPh_3 are also viewed as a formal 2-electron donor. This seems possible, as the four electrons that these Ge atoms formally received originate from Li atoms and not the Ni atoms they are coordinated at. The Ge filled variant $[Ge@Ni_8Ge_6]^{6-}$ would possess a CVE count of 118 accordingly and is therefore almost isoelectronic to the $[As@Ni_8As_6](PPh_3)_8$ cluster with a CVE count of 119, lacking one electron. Both clusters do not match the favored electron count predicted by general electron counting rules (114, 120). However, this is true for most of the observed rhombic dodecahedral clusters (Table 7). The existence of a $[Ge@Ni_8Ge_6]^{6-}$ should not be surprising, as it extends the series of main group element filled $[E@Ni_8E_6]$ clusters regarding the Te centered $[Te@Ni_8Te_6](L_8)$ cluster which was proposed based on theoretical work.[11] As both clusters show the same charge it seems reasonable that they are able to coexist in one compound. In conclusion the compound $Li_{14}Ni_{8.3}Ge_{8.7}$ is expected to be a diamagnetic, charge balanced Zintl phase.

Table 3: Selected rhombic dodecahedral clusters, their valence electron counts and interatomic distances in the rhombic dodecahedra

cluster	CVEs	$M\text{-}E$ (Å)	$M\text{-}M$ (Å)	ref
$[Ni_8(PPh)_6](PPh_3)_4Cl_4$	116	2.21	2.61	4
$[Ni_8S_6](PPh_3)_6Cl_2$	118	2.21	2.68	30
$[Ge@Ni_8Ge_6]^{6-}(Ge^{4-})_{8/4}$	118	2.40	3.00	a
$[As@Ni_8As_6](PPh_3)_8$	119	2.32	2.89	12
$[Ni_8(PPh)_6](CO)_8$	120	2.18	2.65	5
$[Ni@Ni_8Ge_6]^{6-}(Ge^{4-})_{8/4}$	124	2.40	3.00	a
$[Ni@Ni_8(GeEt)_6](CO)_8$	124	2.36	2.67	13
$[Pd@Pd_8As_6](PPh_3)_8$	124	2.49	3.11	6
$[Pd@Pd_8Sb_6](PPh_3)_8$	124	2.61	3.26	7
$[Ni@Ni_8Te_6](PEt_3)_8$	130	2.55	2.86	8

[a] = this publication

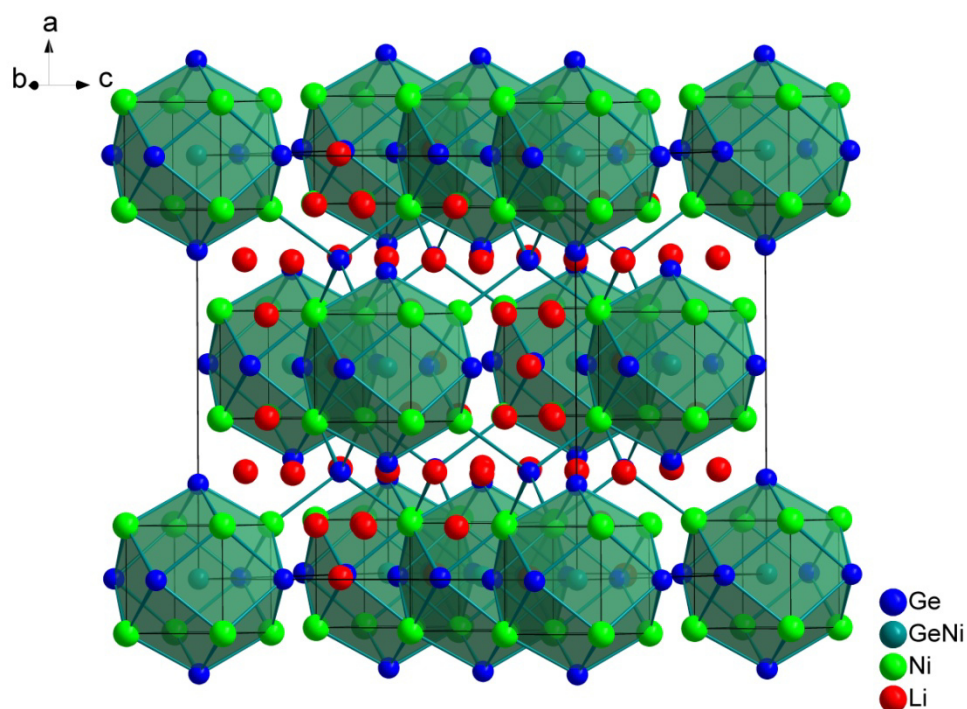**Figure 1:** Unit cell with highlighted Ni_8Ge_6 clusters of the compound $Li_{14}Ni_{8.3}Ge_{8.7}$. Li, Ni, Ge and Ni/Ge mixed positions are represented as spheres in red, green, blue and teal respectively.
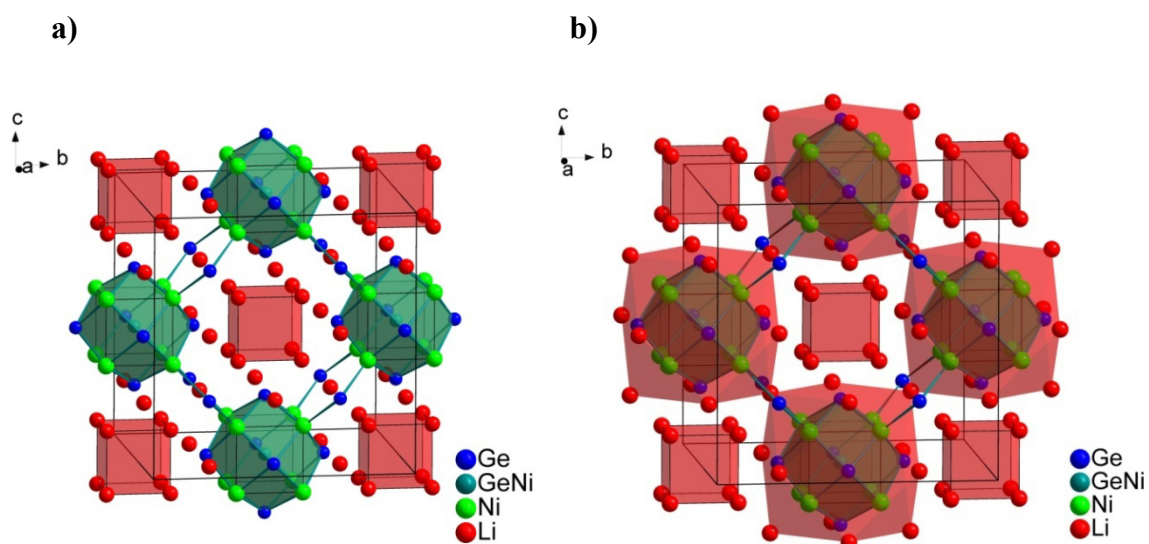

Figure 2: a) One layer in the compound $Li_{14}Ni_{8.3}Ge_{8.7}$. Li, Ni, Ni/Ge and Ge positions are represented as spheres in red, green, teal and blue respectively. Covalent bonds are marked with thick teal lines. Thin lines represent the coordination of Li atoms. b) The cuboctahedral coordination sphere of Li2 atoms as well as the Li1 cubes in the octahedral voids are marked with red polyhedra. Li, Ni, Ni/Ge and Ge positions are represented as spheres in red, green, teal and blue respectively. Covalent bonds are marked with thick teal lines. Thin lines represent the coordination of Li atoms.
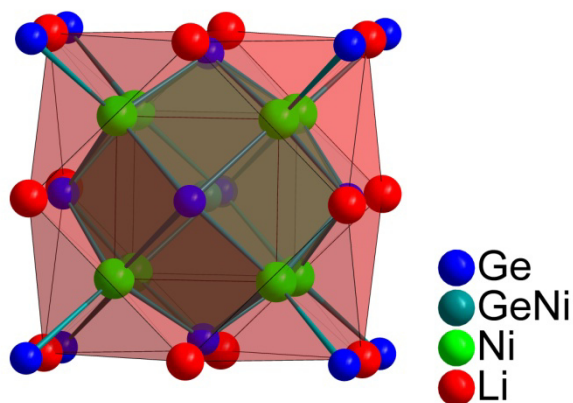
Figure 3: (Ni/Ge@Ni$_8$Ge$_6$) cluster (teal polyhedron) with cuboctahedral surrounding of Li2 atoms (red polyhedron) and Ge3 atoms capping the triangular faces of the coboctahedron in the compound Li$_{14}$Ni$_{8.3}$Ge$_{8.7}$. Li, Ni, Ni/Ge and Ge positions are represented as spheres in red, green, teal and blue respectively. Covalent bonds are marked with thick teal lines. Thin lines represent the coordination of Li atoms.
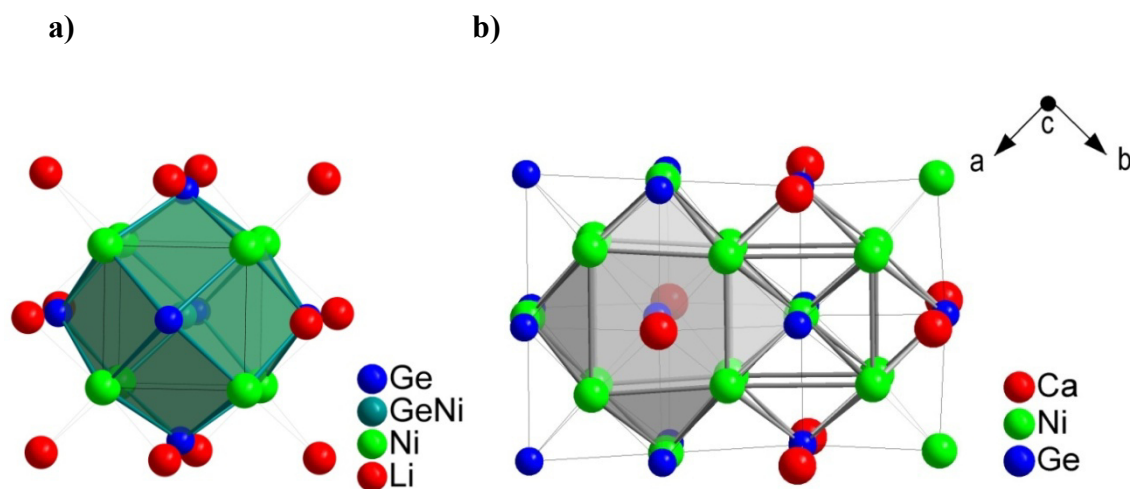
a)   **b)**

Figure 4: a) Ni2/Ge2 filled M$_{26}$ unit in Li$_{14}$Ni$_{8.3}$Ge$_{8.7}$. Li, Ni, Ni/Ge and Ge positions are represented as spheres in red, green, teal and blue respectively. Covalent bonds are marked with thick lines. Thin lines represent the coordination of Li atoms. b) Ni and Ge filled overlapping M_{26} units in CaNi$_5$Ge$_3$. Ca,Ni and Ge are represented as spheres in red, green and blue respectively. Bonds in the direct coordination of the core atom are marked with thick lines, bonds between and to the surrounding cuboctahedral atoms are marked with thin lines.
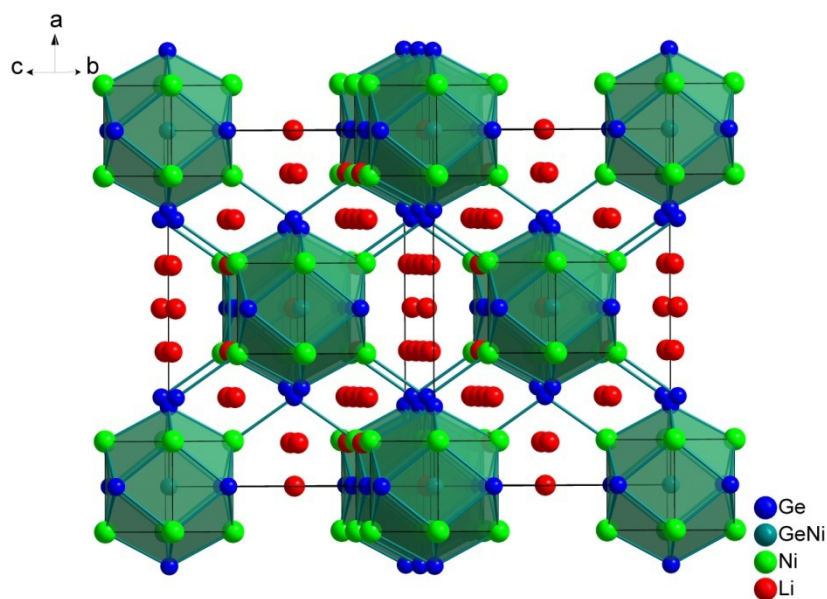
Figure 5. Unit cell of $Li_{14}Ni_{8.3}Ge_{8.7}$ in nearly *bc*-direction highlighting the Li filled channels in the structure. Li, Ni, Ge and Ni/Ge mixed positions are represented as spheres in red, green, blue and teal respectively.

Conclusion

Our investigations in the system Li-Ni-Ge led to the discovery of the new compound $Li_{14}Ni_{8.3}Ge_{8.7}$. This compound represents the third compound in this system and includes Ge bridged rhombic dodecahedra of eight Ni and six Ge atoms and which are filled with Ni and Ge atoms respectively. These clusters represent the first example of rhombic dodecahedra synthesized by a solid state reaction and only one different compound with a main group element in the center of such a cluster is known up to date. Currently, we are working on a phase pure synthesis of this compound for investigations on the Li-ion mobility in the extraordinary wide Li-filled channels.

Associated content

Supporting Information available: X-ray crystallographic files in CIF format, powder diffractogram and tables of anisotropic displacement parameters for the title compound.

Author information

Corresponding Author: Prof. Dr. Thomas F. Fässler, Department Chemie, Technische Universität München, Lichtenbergstr. 4, D-85747 Garching, Germany

*E-mail: Thomas.Faessler@lrz.tum.de.

Notes: The authors declare no competing financial interest.

References

(1)   Mingos, D. M. P.; Wales, D. J., *Introduction to cluster chemistry*. Prentice Hall: 1990.

(2)   Scherf, L. M.; Zeilinger, M.; Fässler, T. F. *Inorg. Chem.* **2014,** *53*, 2096-2101.

(3)   Zeilinger, M.; Kurylyshyn, I. M.; Häussermann, U.; Fässler, T. F. *Chem. Mater.* **2013,** *25*, 4623-4632.

(4)   Fenske, D.; Basoglu, R.; Hachgenei, J.; Rogel, F. *Angew. Chem. Int. Ed.* **1984,** *23*, 160–162.

(5)   Lower, L. D.; Dahl, L. F. *J. Am. Chem. Soc.* **1976,** *98*, 5046-5047.

(6)   Fenske, D.; Fleischer, H.; Persau, C. *Angew. Chem. Int. Ed.* **1989,** *28*, 1665-1667.

(7)   Fenske, D.; Persau, C. *Z. Anorg. Allg. Chem.* **1991,** *593*, 61-68.

(8)   Brennan, J.; Siegrist, T.; Stuczynski, S.; Steigerwald, M. *J. Am. Chem. Soc.* **1989,** *111*, 9240-9241.

(9)   Vogt, K. Ph.D. Thesis. University of Karlsruhe, Germany, 1994.

(10)   Purath, A.; Dohmeier, C.; Ecker, A.; Köppe, R.; Krautscheid, H.; Schnöckel, H.; Ahlrichs, R.; Stoermer, C.; Friedrich, J.; Jutzi, P. *J. Am. Chem. Soc.* **2000,** *122*, 6955-6959.

(11)   Wheeler, R. A. *J. Am. Chem. Soc.* **1990,** *112*, 8737-8741.

(12)   Gautier, R.; Ogliaro, F.; Halet, J.-F.; Saillard, J.-Y.; Baerends, E. J. *Eur. J. Inorg. Chem.* **1999,** *1999*, 1161-1168.

(13)   Zebrowski, J. P.; Hayashi, R. K.; Bjarnason, A.; Dahl, L. F. *J. Am. Chem. Soc.* **1992,** *114*, 3121-3123.

(14)   Christou, G.; Hagen, K.; Bashkin, J.; Holm, R. *Inorg. Chem.* **1985,** *24*, 1010-1018.

(15)   Schuster, H. U.; Mewis, A. *Z. Naturforsch, B* **1969,** *24*, 1190.

(16)   Buchholz, W.; Schuster, H. U. *Z. Anorg. Allg. Chem.* **1981,** *482*, 40-48.

(17)   Stoe *WinXPOW*, 2.08; Stoe & Cie GmbH: Darmstadt, 2003.

(18)   Stoe *CrysAlis RED*, 1.171.33.34; Oxford Diffraction Ltd.: 2009.

(19)   Stoe *X-RED32*, 1.48; STOE & Cie GmbH: Darmstadt, 2008.

(20)   Stoe *X-Shape*, 2.11; Stoe & Cie GmbH: Darmstadt, 2008.

(21)   Sheldrick, G. M. *XPREP-97*, University of Göttingen (Germany), 1997.

(22)   Sheldrick, G. M. *SHELXS-97*, University of Göttingen (Germany), 1997.

(23)   Sheldrick, G. M. *SHELXL-97*, University of Göttingen (Germany), 1997.

(24)   Siggelkow, L.; Hlukhyy, V.; Wahl, B.; Fässler, T. F. *Eur. J. Inorg. Chem.* **2011,** *2011*, 4012-4024.

(25)   Pfisterer, H.; Schubert, K. *Z. Metallkd.* **1950,** *41*, 358-367.

(26)   Swanson, H. E.; Tatge, E. *Acta Crystallogr. A* **1954,** *7*, 464-464.

(27)   Donohue, J., *The Structures of the Elements*. Wiley: New York, 1974.

(28)   Henze, A.; Hlukhyy, V.; Fässler, T. F. *Inorg. Chem.* **2015,** *54*, 1152-1158.

(29)   Gruttner, A.; Nesper, R.; Schnering, H. *Acta Crystallogr. A* **1981,** *37*, 161.

(30)   Fenske, D.; Hachgenei, J.; Ohmer, J. *Angew. Chem. Int. Ed.* **1985,** *24*, 706-709.

<div align="center">

Supporting Information

for

Synthesis and Structural Characterization of $Li_{14}Ni_{8+x}Ge_{9-x}$ (x = 0.3) featuring the First Rhombic Dodecahedral Cluster in a Solid State Compound

</div>

Alexander Henze, Thomas F. Fässler

manuscript for publication

Contents

Crystal structures

Table S-1. Interatomic distances for $Li_{14}Ni_{8.3}Ge_{8.7}$.

Table S-2. Anisotropic displacement parameters for $Li_{14}Ni_{8.3}Ge_{8.7}$.

Powder and Single Crystal X-ray diffraction and structural refinement.

Figure S-1. Powder diffractogram of a sample of $Li_{14}Ni_{8.3}Ge_{8.7}$.

Crystal structure

Figure S-2. Anisotropic replacement parameter for $Li_{14}Ni_{8.3}Ge_{8.7}$.

Table S-1. Interatomic distances for $Li_{14}Ni_{8.3}Ge_{8.7}$

$Li_{14}Ni_{8.3}Ge_{8.7}$		
atoms		**Distance (Å)**
Ge1	Ge2/Ni2	2.634 (1)
	Ni1	2.403 (1)
	Li1	2.723 (1)
	Li2	2.960 (1)
Ge2/Ni2	Ni1	2.594 (1)
Ge3	Ni1	2.504 (1)
	Li1	2.619 (1)
	Li2	2.943 (1)
Ni1	Ni1	2.995 (1)
	Li1	2.959 (1)
	Li2	2.534 (1)
Li1	Li1	2.862 (1)
	Li2	2.573 (1)

Table S-2. Anisotropic displacement parameters for $Li_{14}Ni_{8.3}Ge_{8.7}$

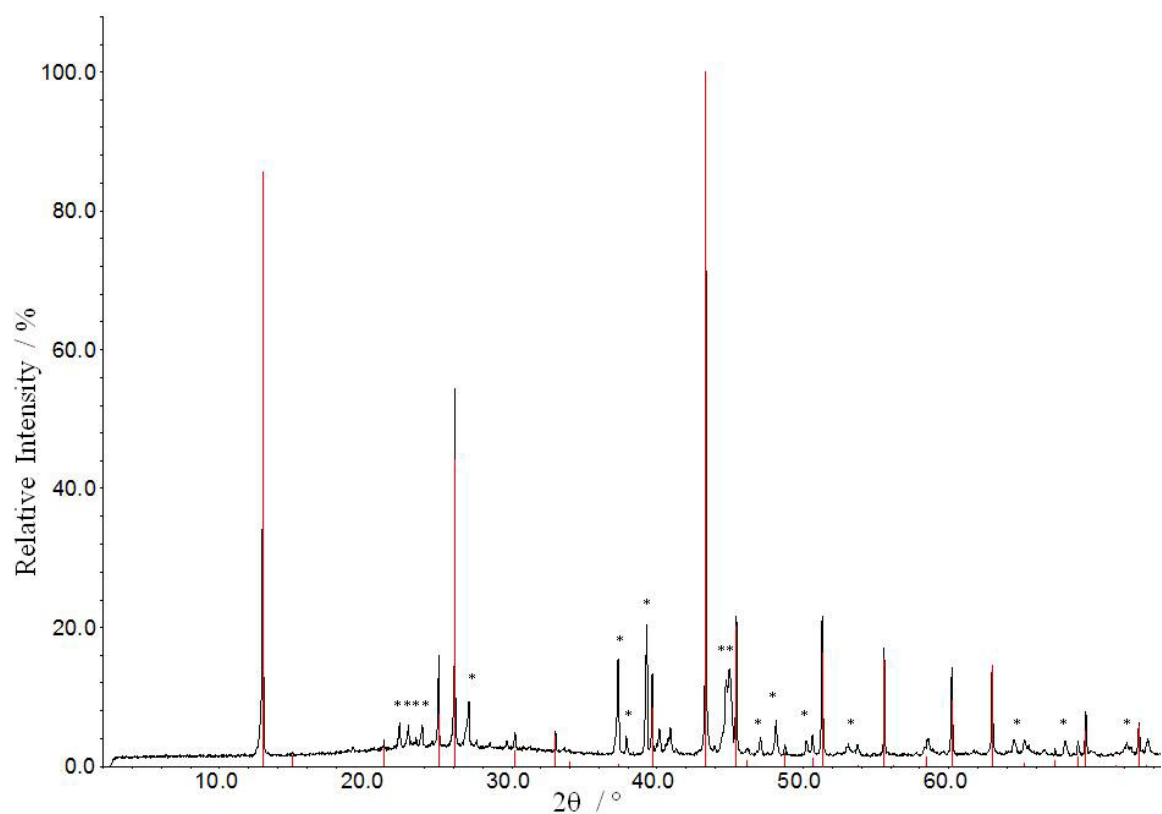| $Li_{14}Ni_{8.3}Ge_{8.7}$						
Atom	U_{11}	U_{22}	U_{33}	U_{12}	U_{13}	U_{23}
Ge1	0.0060(3)	0.0084(5)	0.0060(3)	0	0	0
Ge2/Ni2	0.0051(8)	0.0051(8)	0.0051(8)	0	0	0
Ge3	0.0069(4)	0.0069(4)	0.0069(4)	0	0	0
Ni1	0.0065(3)	0.0065(3)	0.0065(3)	-0.0002(2)	-0.0002(2)	-0.0002(2)
Li1	0.020(4)	0.020(4)	0.020(4)	-0.001(3)	-0.001(3)	0.001(3)
Li2	0.025(6)	0.025(6)	0.011(7)	-0.011(7)	0	0

Figure S-1. Experimental X-ray powder diffractogram (black) with the theoretical pattern of $Li_{14}Ni_{8.3}Ge_{8.7}$ (red). Minor sidephases are marked with an asterisk.
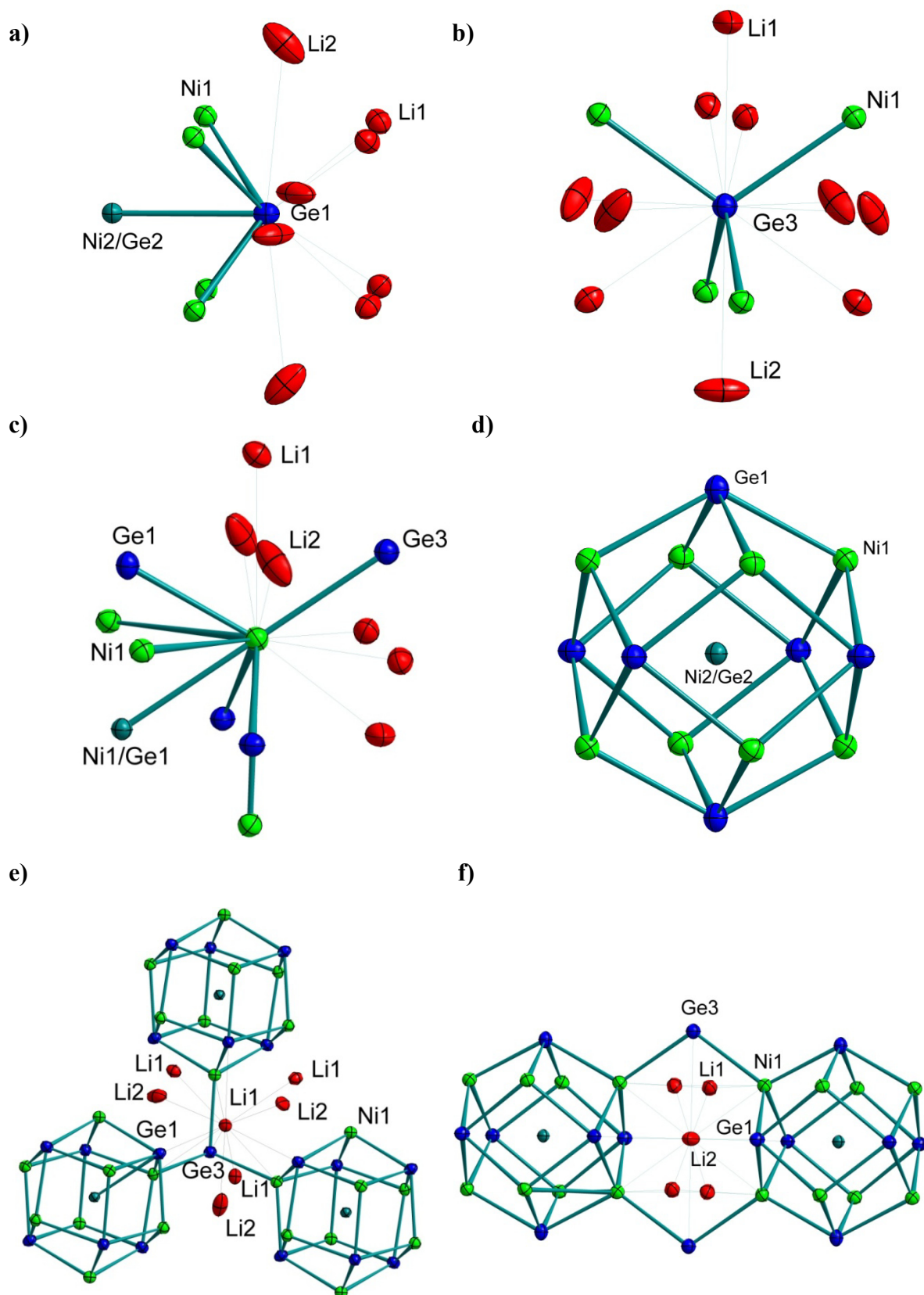
Figure S-2. Coordination polyhedral of a) – b) Ge atoms c) – d) Ni containing atomic positions and e) –f) Li atoms. Li, Ni, Ni/Ge and Ge positions are shown as ellipsoids at the 90% probability level in red, green, teal and blue respectively. Covalent bonds are marked with thick lines. Thin lines represent the coordination of Li atoms.

6.6 Synthesis and Structural Characterization of $Na_{29}Ag_{17.8}Sn_{43}$ and $Na_{13}Ag_{2.7}Sn_{24}$

Alexander Henze, Thomas F. Fässler

manuscript for publication

Abstract

Investigations in the system Na-Ag-Sn led to the discovery of the compounds $Na_{29}Ag_{17.8}Sn_{43}$ and $Na_{13}Ag_{3-x}Sn_{24}$ (x = 0.3) representing the first ternary compounds in this system. Both compounds were obtained by high-temperature synthesize from a binary alloy and Na and characterized by single-crystal X-ray diffraction methods as well as thermal and magnetic measurements. The compounds crystallize in the space groups P6/mmm and $Im\bar{3}$ respectively with lattice parameters of a = 15.9283(4) and c = 9.7914(4) for $Na_{29}Ag_{17.8}Sn_{43}$ and a = 15.333(1) for $Na_{13}Ag_{3-x}Sn_{24}$ (x = 0.3). Both compounds exhibit 3-dimensional networks of condensated clusters compensating the electron deficiency induced by the introduction of the electron poor Ag in the binary Na-Sn system. $Na_{29}Ag_{17.8}Sn_{43}$ crystallizes in its own structure type exhibiting strings of Na centered ($Ag_{13}Sn_7$) clusters, Sn_3 triangles and (Ag_2Sn_{10}) icosahedra. The $Na_{13}Ag_{2.7}Sn_{24}$ structure derives from the Bergman structure expressing a 3-dimensional Sn network of distorted Sn_{12} icosahedra interconnected by Na centered double-Friauf polyhedra with additional Na atoms and Ag_2 dumbbells filling the voids of this network.

Keywords: Cluster chemistry, silver, stannide

Introduction

Homo- and heteroatomic clusters mark a frontier area between solid state, solution based and gas phase chemistry.[1] Among others, their investigation leads to a closer understanding of the transition from aggregates of a few atoms to bulk solid state compounds when it comes to bonding situation, structure and properties. If these clusters suffer by electron deficiency, they compensate this situation by condensation of the clusters. This has been shown for cluster of group 13 elements, where although a few naked clusters are known,[2-4] especially Ga and In containing compounds show this kind of behavior.[5-7] This electron deficiency can also be introduced in Group 14 element (*T*) containing systems by partly substitution of the group 14 element with a transition metal (*M*). This has been shown for example in $Na_{29}Zn_{24}Sn_{32}$,[8] $Na_{13}Cd_{20}E_7$ (*E* = Sn/Pb)[9] and $Na_{49}Cd_{58.5}Sn_{37.5}$.[10] However, the formation of these structural motifs depends on a high *M*/*T* ratio, which should be near one or higher. For low *M*/*T* ratios, a transition as known from the tin rich side of the binary Na-Sn phase diagram should be expected. In that phase diagram isolated tin clusters in Na_4Sn_4[11] emerge through two- and three dimensional networks in Na_7Sn_{12},[12] $NaSn_2$[13] and Na_5Sn_{13}[14] to metallically bonded Sn atoms in $NaSn_5$.[15] For further proof of this concept, we regarded systems where the group 14 element is substituted by a group 11 element. The substitution with the large Au only results in the formation of different kinds of three-dimensional networks in the three known compounds in the Na-Au-Sn system $NaAuSn$,[16] Na_2AuSn_3[17] and $Na_{30}Au_{39}Sn_{12}$[18] even at high Au/Sn rates. Recently we investigated the Na-Cu-Sn system where the small Cu atom should have a formal charge of +1. The concept seems to work in this case, as the compound $Na_{2.8}Cu_5Sn_{5.6}$[19] with a Cu/Sn ratio of almost one shows linear tubes of Cu and Sn which can be realized as condensed form of the discrete, onion-like $[Cu_{12}Sn_{21}]^{21-}$ cluster in $Na_{12}Cu_{12}Sn_{21}$.[20] The formation of these clusters can be explained by the higher Cu/Sn ratio and therefore lower electron deficiency. To further prove this concept we now investigated the Na-Ag-Sn system where Ag with a formal charge of 1+ should lead to severe electron deficiency and therefore corresponding structural motifs. It is noteworthy that no ternary compounds have been found in this system up to now. We were able to determine the structure of two new compounds with the composition $Na_{29}Ag_{17.8}Sn_{43}$ and $Na_{13}Ag_{3-x}Sn_{24}$ (x = 0.3). The compounds crystallize in the space group P6/mmm and $Im\bar{3}$ respectively with $Na_{29}Ag_{17.8}Sn_{43}$ exhibiting the expected interconnected cluster units,

while in $Na_{13}Ag_{2.7}Sn_{24}$ a structure of stronger condensated clusters and isolated Ag_2 dumbbells is found.

Experimental Section

Synthesis

All materials were handled in an argon atmosphere using an argon filled glove box and other standard inert gas techniques. The starting materials were Na rods, Ag wire (99.9%, Sigma Aldrich) and Sn granules (99.999%, ChemPur) were used as received. The preparation of the Ag/Sn alloys was performed by pre-melting Ag and Sn in an arc furnace (Mini Arc Melting System, MAM-1, Johanna Otto GmbH) to obtain a binary regulus with the expected stoichiometry. The amount of Ag and Sn used for the synthesis of $Na_{29}Ag_{17.8}Sn_{43}$ were 140 mg (1.30 mmol) and 316 mg (2.67 mmol), respectively. For the synthesis of $Na_{13}Ag_{2.7}Sn_{24}$ 47 mg (0.43 mmol) of Ag and 410 mg (3.46 mmol) of Sn were used. The respective binary reguli were added to 43 mg (1.88 mmol) of Na for the synthesis of $Na_{29}Ag_{17.8}Sn_{43}$ as well as for the synthesis of $Na_{13}Ag_{2.7}Sn_{24}$ which was in each case provided in a niobium ampoule. The niobium ampoule was sealed by arc welding and transferred into a silica tube. The silica tube was evacuated and placed into a vertical resistance tube furnace. The samples were heated to 750 °C and tempered for 24 hours. Afterwards the samples were cooled with a cooling rate of 0.1 K to 450 °C and tempered for another 24 hours. Finally the samples were cooled to room temperature with a cooling rate of 0.1 K. After the ampoules were opened in an argon atmosphere, the samples were gained as lustrous silver powders which were sensitive to air and moisture.

Powder and Single Crystal X-ray diffraction and structural refinement

For powder diffraction analysis, each sample was finely ground to a powder, sealed in a glass capillary and measured at room temperature using a STOE Stadi P powder diffractometer with Cu-K$_\alpha$ radiation (λ = 1.54056 Å, Ge(111) monochromator) and a position sensitive detector (Mythen 1K). The STOE WINXPOW program package was used for phase analysis.[21] Both powder X-ray diffraction patterns show that we were able to synthesize the respective compound as a phase pure sample.

For the structure determination of $Na_{29}Ag_{17.8}Sn_{43}$ a suitable single crystal was selected in an argon-filled glove box equipped with a microscope. The lustrous, block shaped crystal was mounted on the tip of a glass capillary using perfluoropolyalkylether. Single crystal XRD data were collected using an OXDORD Xcalibur3 diffractometer system (Sapphire3 CCD detector; Mo K_{α} radiation, $\lambda = 0.71073$ Å, graphite monochromator, sealed tube X-ray source) with crystal cooling in a 130 °C cold nitrogen stream. For data processing, the Oxford CrysAlis RED software[22] was used. A empirical absorption correction was performed using the STOE X-RED/X-SHAPE software.[23,24]

The structure determination of $Na_{13}Ag_{2.7}Sn_{24}$ was carried out at 123 K using a Bruker AXS X-ray diffractometer equipped with a CCD detector (APEX II, κ-CCD), a rotating anode FR591 with Mo Kα radiation ($\lambda = 0.71073$ Å), and a MONTEL optic monochromator. Data collection was controlled with the Bruker APEX software package.[25] Integration, data reduction, and absorption correction were performed with the SAINT[26] and SADABS[27] packages.

For both compounds X-Prep[28] was used for space group determination and data merging (identical indices only). The programs XS[29] and XL[30] were used for the solution (direct methods) and refinement of the structure. Selected crystallographic data a given in Table 1 and 2. For $Na_{29}Ag_{17.8}Sn_{43}$ a split model was applied for one Sn position (Sn4A/Sn4B).

Table 1:   crystal data and structure refinement

Formula	$Na_{29}Ag_{17.8}Sn_{43}$	$Na_{13}Ag_{2.7}Sn_{24}$
Formula weight (g·mol^{-1})	334.26	271.14
Space group	*P6/mmm* (no. 191)	*Im$\bar{3}$* (no. 204)
Z	23	2
Unit cell parameters (Å)	*a* = 16.0532(4)	*a* = 15.333(1)
	c = 9.7362(4)	
Volume (Å^3)	2172.92(14)	3604.66(4)
$D_{\text{calcd.}}$ (g·cm^{-3})	5.875	3.198
Abs. coeff. (mm^{-1})	16.09	9.01
F(000) (e)	3305	2968
Crystal shape/color	block/silver	block/silver

Temperature (K)	130	123
Θ range (deg)	3.29 – 27.49	1.88 – 27.47
Range in hkl	−20/20 −18/20 −12/12	19 19 19
Reflections collected	31794	14433
Unique reflections	1031	770
Data / parameter	1031 / 61	770 / 41
GOF on F^2	0.939	1.034
R_1, wR_2 ($I > 2\,\sigma(I)$)	0.0341, 0.0952	0.0183, 0.0294
R_1, wR_2 (all data)	0.0427. 0.0981	0.0289, 0.0313
Largest diff. peak/hole (e Å^{-3})	2.39 and −1.85	0.79 and −0.88

Table 2:   Atomic coordinates and equivalent isotropic displacement parameters for Na$_{29}$Ag$_{17.8}$Sn$_{43}$ and Na$_{13}$Ag$_{2.7}$Sn$_{24}$.

Na$_{29}$Ag$_{17.8}$Sn$_{43}$

Atom	Wyck.	sof	x	y	z	U_{eq}/Å^2
Sn1	6m	1	0.60478	0.20955	1/2	0.019(1)
Sn2	12p	1	0.49083	0.15933	0	0.022(1)
Sn3	12n	1	0.34616	0	0.15983	0.024(1)
Sn4A	12q	0.5	0.24856	0.10896	1/2	0.040(1)
Sn5/Ag5	12o	0.56/0.44(6)	0.55106	0.10211	0.25152	0.023(1)
Sn6/Ag6	2e	0.60/0.40(16)	0	0	0.14687	0.042(2)
Ag7	12n	0.90(1)	0.17889	0	0.26707	0.039(1)
Na1	4h	1	2/3	1/3	0.18901	0.021(2)
Na2	1b	1	0	0	1/2	0.022(2)
Na3	12o	1	0.42911	0.21455	0.69716	0.025(2)
Na4	6l	1	0.26481	0.13240	0	0.029(2)
Na5	6k	1	0.38167	0	1/2	0.034(2)

Na$_{13}$Ag$_{2.7}$Sn$_{24}$

Atom	Wyck.		x	y	z	U_{eq}/Å^2
Sn1	24g	1	0.15345(3)	0.09416(3)	0	0.009(1)

Sn2	24g	1	0.31096(3)	0.18161(3)	0	0.013(1)
Sn3	48h	1	0.30984(2)	0.34378(2)	0.09402(2)	0.012(1)
Ag1	12e	0.90(1)	0.40420(5)	1/2	0	0.014(1)
Na1	16f	1	0.1883(2)	0.18826(11)	0.1883(2)	0.011(1)
Na2	12e	1	0.1981(2)	1/2	0	0.011(1)
Na3	24g	1	0.3057(2)	0	0.1160(2)	0.011(1)

EDX Measurements

An EDX analysis was carried out on single crystals of the title compounds $Na_{29}Ag_{17.8}Sn_{43}$ and $Na_{13}Ag_{2.7}Sn_{24}$. A JEOL 5900LV scanning electron microscope equipped with an OXFORD INSTRUMENTS INCA energy dispersive X-ray microanalysis system was used for this. The unit cells of the crystals were determined by single crystal XRD. The quantitative analysis showed the presence of the elements Na, Ag and Sn with no other element heavier than Na detectable for both compounds.

Differential Thermal Analysis

The thermal behavior of the compound $Na_{29}Ag_{17.8}Sn_{43}$ was investigated to see, if any kind of transition is visible for this compound regarding the existence of mixed occupied and ordered positions next to each other. A Netzsch DSC 404 Pegasus apparatus was used for this. In an argon filled glove box 65mg of a phase pure sample of the respective compound were filled into a cylindrical niobium ampoule. The ampoule was closed by crimping and sealing inside of the glove box. An empty niobium crucible was used as a reference. During the experiment the sample was heated in an argon flow with a heating/cooling rate of 10 K·min^{-1}. The sample was recovered in an argon-filled glove box. For data processing the program Proteus Thermal Analysis[31] was used. Both recorded cycles were almost identical. In the courses of heating, one strong exothermic effect is visible at 502.5 and 506.0 °C respectively. This effect should be due to the congruent melting of the investigated phase. In the courses of cooling, one corresponding endothermic effect is found at 462.7 °C which results from the crystallization of the compound (Figure S-4). No signs of any kind of phase transition were visible.

Magnetic Measurements

Magnetic measurements were performed using a Quantum Design MPMS 5 XL SQUID magnetometer. Therefore, 61.7 mg of a phase pure sample of $Na_{13}Ag_{2.7}Sn_{24}$ were measured at applied fields of 500 and 10000 Oe over a temperature range of 2 – 300 K. All data were corrected for the corresponding sample holder and for ion-core diamagnetism using Pascal's constants.[32] The molar susceptibility X_m for this compound is negative and temperature independent as expected for diamagnetic compounds. The increasing values for X_m at temperatures below 50K indicates the presence of paramagnetic impurities, which may results from small amounts of elemental Sn which is not detectable in the powder X-ray diffractograms. The graph is shown in Figure S-5 in the supporting information.

Results

The two new compounds $Na_{29}Ag_{17.8}Sn_{43}$ and $Na_{13}Ag_{2.7}Sn_{24}$ were synthesized by high temperature reaction of Na with a binary alloy of Ag and Sn. Both compounds feature a polyanionic network of interconnected clusters and represent the first known compounds in the system Na-Ag-Sn. These compounds emphasize our previous finding that the implementation of electron poor transition metals in binary A_xT_y compounds leads to the formation of interconnected clusters. For Ag as particularly electron poor element, this applies at even smaller amounts in the compound than for other transition metals.

Structure description of $Na_{29}Ag_{17.8}Sn_{43}$

The compound $Na_{29}Ag_{17.8}Sn_{43}$ crystallizes in its own structure type in the space group P6/mmm (no. 191) with lattice parameters of a = 15.9283(4) and c = 9.7914(4). The main structural features of this compound are Ag_2Sn_{10} icosahedra, Sn_3 triangles and $Ag_{13}Sn_7$ clusters which attend at a ratio of 3:2:1 in the compound as seen in Figure 1. The icosahedra are building a Kagomé net which expands in *ab*-direction while it is primitively stacked in *c* direction forming larger hexagonal and smaller triangular channels in *c* direction. The $Ag_{13}Sn_7$ clusters and the Sn_3 triangles are located between each two layers of the Kagomé net in the hexagonal and triangular channels respectively (Figure 2). The polyanionic substructure of $Na_{29}Ag_{17.8}Sn_{43}$ can therefore be described as a hierarchical relative of the $CaCu_5$ structure type[33] in which specific atoms are replaced by

certain cluster units. In this case, the Ag_2Sn_{10} icosahedra lie on the Cu1 positions of the $CaCu_5$ structure type, while the Sn_3 triangles lie on the Cu2 positions and the $Ag_{13}Sn_7$ cluster occupy the Ca positions. This type of polyanionic network has been observed before, e.g. in the compounds $Na_8K_{23}Cd_{12}In_{48}$, $Na_{29}Zn_{24}Sn_{32}$ or $Na_{30.5}Ag_{6.4}Ga_{53.6}$.[8, 34, 35] While in all these compounds the Cu1 position is occupied by icosahedra and the Cu2 position by E_3 triangles (E = main group element) the cluster occupying the Ca position differ. The $Ag_{13}Sn_7$ cluster described in this compound has not been observed before.

The icosahedra in $Na_{29}Ag_{17.8}Sn_{43}$ consist of three 4-fold atomic positions. Two of these positions are fully occupied by Sn (Sn2, Sn3) while one position is Sn/Ag mixed-occupied with a ratio of 0.56/0.44(6). As in the range of the standard deviation this position is statistically occupied by two Sn and two Ag atoms the icosahedra will be referred to as Ag_2Sn_{10} (Figure 3a). The Sn2 position connects the icosahedra to the Kagomé net via Sn2-Sn2 exobonds, with a bond length of 2.763(2) Å each, which is a strong covalent bond considering the Sn-Sn distance in α-Sn of 2.81 Å. The Sn3 position forms an exobond (2.881(2) Å) to the Ag7 position of the $Ag_{13}Sn_7$ cluster and the mixed-occupied Sn5/Ag5 position connects the icosahedra via an exobond (2.843(2)) with the Sn1 position of the Sn_3 triangle. Therefore all of the atoms of the Ag_2Sn_{10} icosahedra are exobonded. The interatomic distances in the icosahedra range from 2.763(2) Å for Sn2-Sn2 to 3.113(2) Å for Sn3-Sn3 which is in the range of Sn-Sn distances in β-Sn (3.016 and 3.175 Å)[36]. The Sn_3 triangles occupy the smaller voids of the Kagomé net neighboring six icosahedra each connected via a Sn1-Sn5/Ag5 bond to the Sn_3 triangle. This results in the formation of strings of stacked slightly distorted Friauf polyhedra in c direction which share alternately the Sn_3 triangle and the hexagonal ring build by Sn2 atoms of the icosahedra. These Friauf polyhedra are all centered by a Na1 position (Figure 3b). The Sn1-Sn1 distance in the Sn_3 triangle is 2.981(2) Å which is slightly shorter than the Sn1-Sn1 distance in the Sn_3 triangle in $Na_{29}Zn_{24}Sn_{32}$ with 3.02 Å which was considered covalent.[8] The $Ag_{13}Sn_7$ cluster which occupies the hexagonal voids of the Kagomé net has not been described before. It can be generated by an elongated hexagonal prism formed by Ag atoms with the addition of six Sn atoms capping the rectangular faces slightly outside of the hexagonal prism and additionally capping the hexagonal faces of this unit with a mixed-occupied Ag6/Sn6 position (Figure 3c). The occupation ratio of this Ag6/Sn6 position is 0.60/0.40(16) and will be viewed as a statistic occupation with one Ag and one Sn atom which is in the range of the standard deviation. Therefore

the composition of the cluster is described as "$Ag_{13}Sn_7$" which disregards that the Ag7 position is only occupied by 90(1) %, but reveals the 20 atomic positions of the cluster. Each $Ag_{13}Sn_7$ cluster is surrounded by 12 pentagonal faces of the Ag_2Sn_{10} icosahedra (Figure 4). In the $Ag_{13}Sn_7$ cluster every Sn4 atom is coordinated by four Ag7 atoms. Due to a high anisotropic displacement parameter (adp) for the Sn4 position a split of this position was conducted, leading to a 12q position for Sn4 with an occupancy of 50% each. The distance between the two split positions is 0.492 Å. This split leads to a Sn4-Sn4' distance of 3.030(3) Å which is well in the range of Sn-Sn distances in β-Sn and significant Sn-Sn bonding should be considered (Figure5). The two possible positions for the Sn4 atoms resulting from the split on the 6m position should also be the reason for increased adps on the neighbouring 12n positions observed for Ag in this compound as well as the respective atoms in the compounds $Na_8K_{23}Cd_{12}In_{48}$ and $Na_{30.5}Ag_{6.4}Ga_{53.6}$. The form of the Ag7 ellipsoid pointing directly at the possible Sn4-Sn4 bond indicates a slightly distant position in the case that this bond is formed and a slightly closer position in the case it is not. The adp for Ag7 is not as high as in the mentioned examples due to the underoccupancy of 10% on this position. A partial occupation of Na on this site was considered but rejected due to the low averaged Ag7-Sn4 and Ag7-Sn3 distances of 2.849(1) Å and 2.881(2) Å which is between the Ag-Sn distance of 2.78 Å to 2.81 Å for polar $Li_{17}Ag_3Sn_6$[37] and the 2.93 Å to 3.02 Å in metallic Ag_3Sn,[38] but do not match typical Na-Sn distances of usually well above 3.0 Å.[13, 39] The $Ag_{13}Sn_7$ cluster has never been described before, it is related to the 18 atom clusters found in $Na_8K_{23}Cd_{12}In_{48}$ and $Na_{30.5}Ag_{6.4}Ga_{53.6}$ though.[34, 35] These 18 atom cluster can be built as well from a hexagonal prism by capping the rectangular faces with additional atoms. In the $Ag_{13}Sn_7$ cluster these capping atoms are outside of the cluster though which leads to a bigger diameter for the waist hexagonal ring compared to the hexagonal prism, while in the 18 atom clusters the capping atoms are inside of the hexagonal prism. Additionally, the hexagonal faces of the 18 atom clusters are open and they inhabit two alkali-metal atoms while the hexagonal faces of the $Ag_{13}Sn_7$ are capped by the mixed-occupied Ag6/Sn6 position and the cluster is only centered by one Na atom. The cationic partial structure of $Na_{29}Ag_{17.8}Sn_{43}$ consists of a Na_{20} cluster capping the triangular faces of the icosahedra, therefore forming a pentagonal dodecahedron as well as a Na_{30} cluster with six hexagonal, 12 pentagonal and 12 triangular faces encapsulating the $Ag_{13}Sn_7$ cluster. The Na_{30} clusters are stacked along the c axis by sharing their hexagonal faces with each other while the pentagonal faces are shared with the Na_{20} cluster. The Sn3 triangle is encapsulated by a Na_{14} cluster with six

116

pentagonal and six triangular faces which are shared with the Na_{20} and Na_{30} cluster respectively (Figure 6). Therefore a complete space-filling is achieved. Additionally the Na2 position which is not part of these Na clusters is centering the $Ag_{13}Sn_7$ cluster. This cationic partial structure corresponds to the cationic partial structure of $Na_{29}Zn_{24}Sn_{32}$.

The mixed-occupied atomic positions in the $Ag_{13}Sn_7$ cluster and the Icosahedra as well as the small underoccupancy of the Ag7 position make it difficult to put reasonable formal charges on the clusters the structure of $Na_{29}Ag_{17.8}Sn_{43}$ is build of. The Sn_3 triangle should formally be neutral, as every Sn atom is tetrahedral coordinated. The Ag_2Sn_{10} icosahedron needs according to Wades' rules $2n+2 = 26$ skeletal electrons to be stable. The eight Sn atoms with exobonds provide three electrons each. The mixed occupied position can be viewed as two Sn and two Ag atoms in terms of the standard deviation. The two Sn atoms with exobonds provide three electrons each as well, while the two Ag atoms with exobonds provide formally zero electrons. This adds up to 30 electrons giving each icosahedron a formal charge of +4 to fulfil Wades' rules. In view of the composition of the compound consisting of three icosahedra, two Sn_3 triangles and one $(Ag_{13}Sn_7)$ cluster per 29 Na atoms, the $(Ag_{13}Sn_7)$ cluster should posses a formal charge of $3*(-4)+2*0+(-29)= -41$ to charge balance the compound. If the $(Ag_{13}Sn_7)$ cluster is regarded as a hypho cluster in view of the three squares between the three central Sn-Sn bonds, $2n+8 = 48$ skeletal electrons are needed to stabilize this cluster. The six Sn atoms of the central six-membered ring without exobonds provide 2 electrons each. The Ag atoms, all with exobonds connected to the icosahedra provide zero electrons. The Ag/Sn capping atomic position can be view as approximately occupied by one Ag and one Sn atom in terms of the standard deviation, each with an exobonds. Accordingly, the Sn atom provides three electrons, while the Ag atom provides none. In addition, 15 skeletal electrons of this cluster are formally provided by the participating atoms, leading to a formal charge of -33. According to this, the compound $Na_{29}Ag_{17.8}Sn_{43}$ is not charge balanced. The same results are obtained by electron counting on the related $M_{12}E_6$ clusters which is off by 7 electrons for In_6Cd_{12} while the Ag_xGa_{18-x} (x =2.6 and 6.4) cluster would lead to a charge balanced compound for x = 3. In general, it seems questionable though if Wades' rules can be applied like this to these clusters. In view of the metallic appearance of the compound, a charge balanced compound should anyways not be expected.

A comparison of the valence electron concentration (VEC) of the network atoms with related compounds forming Kagomé layers of icosahedra shows, that the VEC of 3.60 for

$Na_{29}Ag_{17.8}Sn_{43}$ fits nice to other compounds with some, but not exclusively E-E bonds in the voids of the Kagomé net as $Na_{16}Zn_{13.54}Sn_{13.46}$ (VEC = 3.59) and $Na_{22}Zn_{20}Sn_{19}$ (VEC = 3.54).[40] In comparison, compounds with a covalent bonded substructure of exclusively Sn atoms in the hexagonal voids of the Kagomé net show a higher VEC (3.66 for $Na_{29}Zn_{24}Sn_{32}$), while compounds with no E-E bonds in the respective partial structure show a lower VEC (3.06 for $Na_{34}Zn_{66}Sn_{38}$).
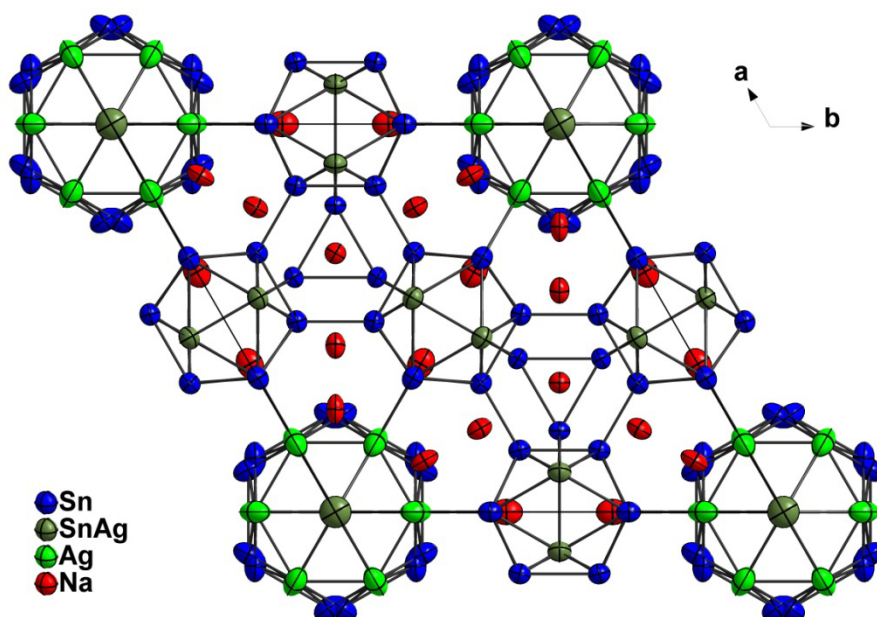
Figure 1: Unit cell of $Na_{29}Ag_{17.8}Sn_{43}$. Na, Ag, Ag/Sn mixed positions and Sn are represented as ellipsoids with 90% probability level in red, green, dark green and blue respectively.
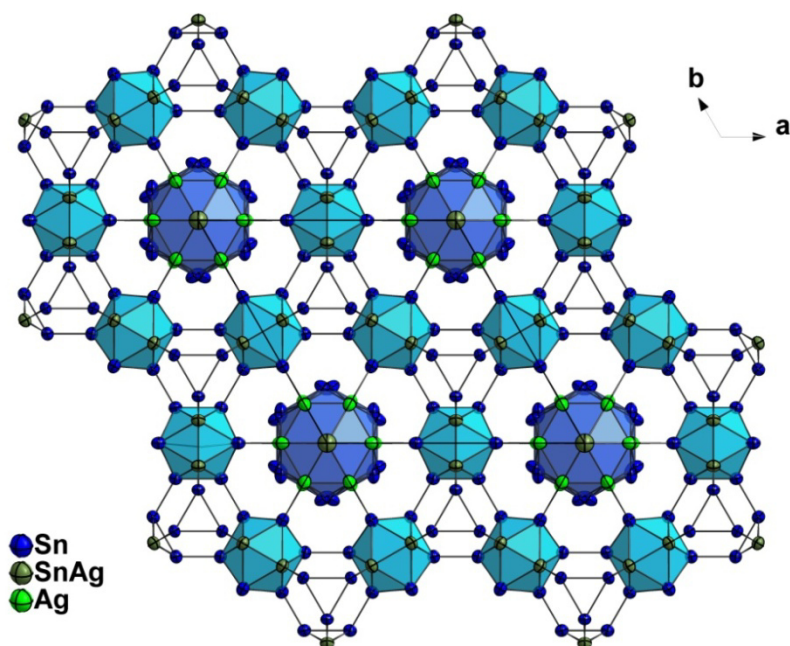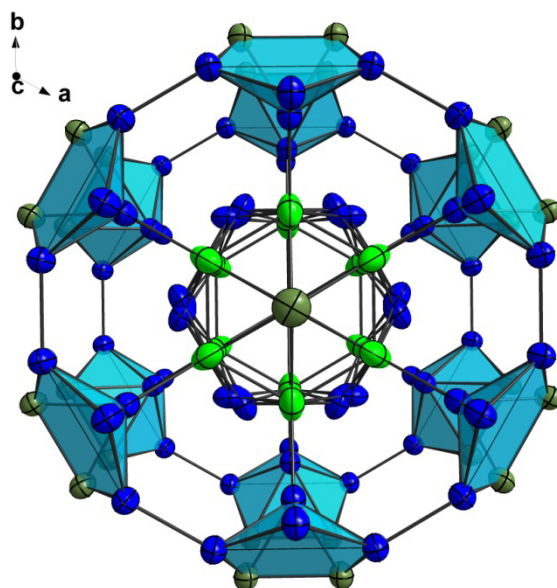
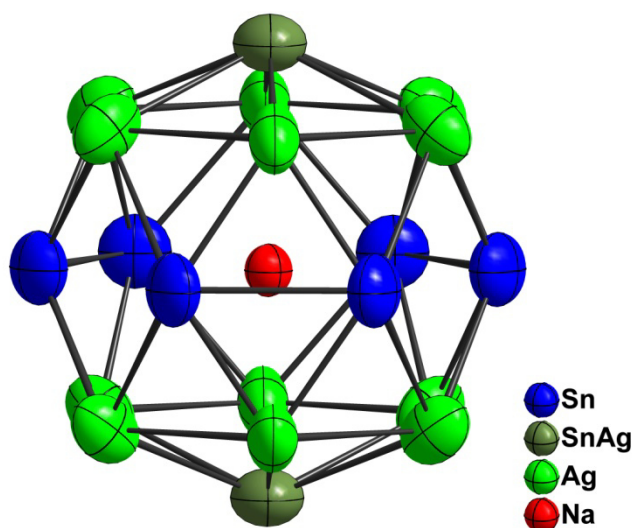**Figure 2:** Kagome net of the compound $Na_{29}Ag_{17.8}Sn_{43}$. Ag, Ag/Sn mixed positions and Sn are represented as ellipsoids with 90% probability level in green, dark green and blue respectively.
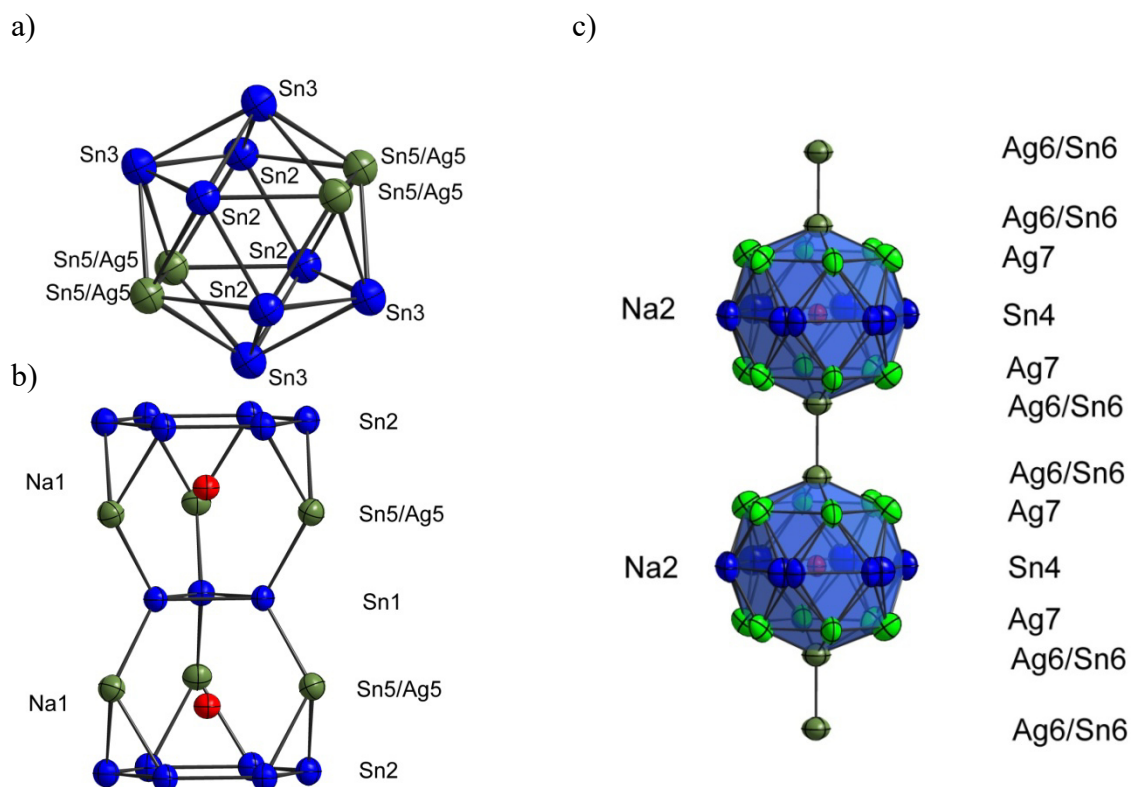

Figure 3: (a) Icosahedron with a Sn/Ag mixed position. Sn:Ag ratio on this position is 52:48. (b) Sn_3 triangel bridging two Na centered Friauf polyhedra. (c) Two $(Ag_{12}Sn_6)$ clusters interconnected by Ag/Sn – Ag/Sn dumbbells. Na, Ag, Ag/Sn mixed positions and Sn are represented as ellipsoids with 90% probability level in red, green, dark green and blue respectively.

Figure 4: View along the c-axis with the surrounding of the central cluster string. Ag, Ag/Sn mixed positions and Sn are represented as ellipsoids with 90% probability level in green, dark green and blue respectively.

Figure 5: Resonance structure of the $(Ag_{13}Sn_7)$ cluster with three Sn-Sn bonds in the waist hexagon. Ag, Ag/Sn mixed positions and Sn are represented as ellipsoids with 90% probability level in green, dark green and blue respectively.
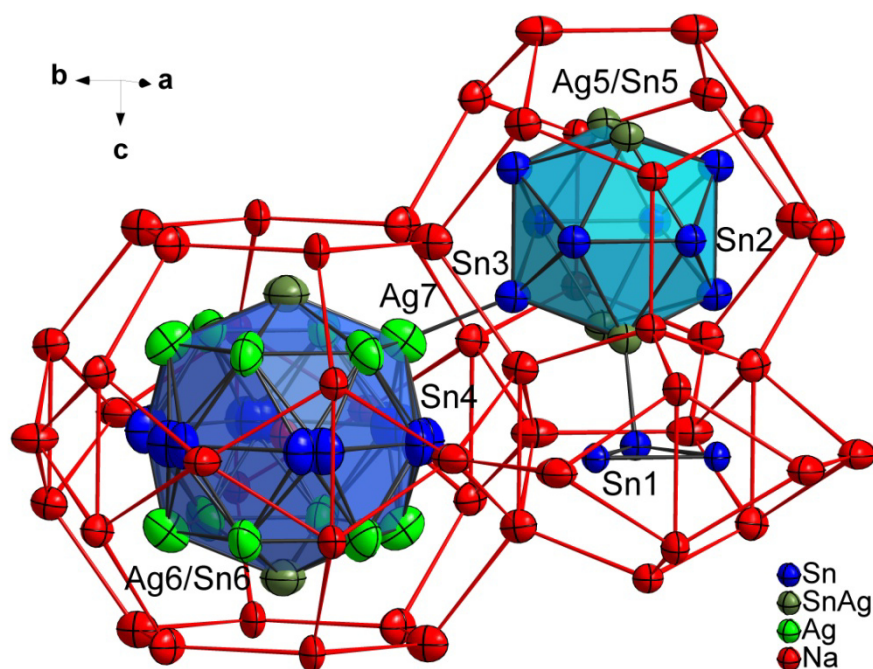
Figure 6: The three different interconnected anionic clusters with the (Na_{30}), (Na_{20}) and (Na_{14}) cages surrounding them. The red lines between the Na atoms do not indicate any kind of bonding interaction between the Na atoms. Na, Ag, Ag/Sn mixed positions and Sn are represented as ellipsoids with 90% probability level in red, green, dark green and blue respectively.

Structure description of $Na_{13}Ag_{2.7}Sn_{24}$

The compound $Na_{13}Ag_{2.7}Sn_{24}$ crystallizes in the space group $Im\bar{3}$ (no. 204) with $a =$ 15.333(1) in its own structure type. This structure type represents a coloring variant of the $Li_{52}Cu_{57}Si_{51}$ structure type,[18] a variant of the Bergman phase $Mg_{32}(Zn,Al)_{49}$.[41] All atomic positions in the structure are fully ordered. The structure consists of a body centered cubic arrangement of Sn_{12} icosahedra formed by Sn1 positions (Figure 7). These icosahedra are octahedrally distorted, resulting in eight of the 20 triangular faces of the central icosahedra to point at the eight cubic surrounding icosahedra, while of the 12 remaining triangular faces each two are edge connected and pointing at the center of every face of the surrounding unit cell (Figure 8a).The interatomic Sn1-Sn1 distance is 2.906(1) Å for all bonds forming the triangular faces pointing in the corner of the unit cell, while it is 2.888(1) Å for all Sn1-Sn1 bonds pointing at the center of the faces of the unit cell. As in the Ag_2Sn_{10} icosahedra in $Na_{29}Ag_{17.8}Sn_{43}$ all Sn positions of the Sn_{12} icosahedra are exobonded. All of the exobonds are Sn1-Sn2 bonds with a bond length of 2.807(1) Å which results in the Sn2 positions to form a bigger icosahedron with the same octahedral

distortion around the central $(Sn1)_{12}$ icosahedron (Figure 8b). The resulting Sn2-Sn2 distances are of course far too long to expect any kind of bonding in the outer $(Sn2)_{12}$ icosahedron. The eight triangular faces of the $(Sn2)_{12}$ icosahedra pointing in the corners of the unit cell are each connected to a planar hexagonal ring of Sn3 atoms via Sn2-Sn3 bonds with interatomic distances of 2.806(1) Å and 2.874(1) Å. These hexagonal rings connect all $(Sn2)_{12}$ icosahedra to a three-dimensional polyanionic network (Figure9a). The Sn3-Sn3 distances in the hexagonal ring are 2.883(1) Å. In general, all Sn-Sn distance are in the narrow range from 2.762(1) – 2.906(1) which is well in the range of covalent Sn-Sn bonding distances with the shortest distance nearly equal to the shortest Sn-Sn distance in $Na_{29}Ag_{17.8}Sn_{43}$ (2.763(1) Å). A different view on the structure reveals that the icosahedra in the center and the corners of the unit cell are each interconnected via two Friauf polyhedra that share one hexagonal face and are each centered by a Na1 atom (Figure 9b). The same structural unit appears in $Na_{29}Ag_{17.8}Sn_{43}$ though the Friauf polyhedra are stacked in c direction there and form a one-dimensional string by additionally sharing the $(Sn1)_3$ triangle (Figure 3a). If the Ag_2 dumbbells are also regarded as part of the polyanionic substructure, the structure can as well be rationalized as packing of Samson polyhedral (Figure 10) with 13-vertex spacer polyhedral. This view on the structure is analogue to $Li_{13}Cu_6Ga_{21}$,[42] a different coloring variant of the Bergman structure. The central $(Sn1)_{12}$ icosahedra is therefore surrounded by 12 pentagonal faces all capped on the inside by Sn2 positions and 20 hexagonal faces which do not occur in the surrounding of the $Ag_{13}Sn_7$ cluster in $Na_{29}Ag_{17.8}Sn_{43}$ (Figure 6). Regarding the Ag_2 dumbbells as part of the cationic substructure, the voids in the polyanionic substructure build by Sn atoms are located in the center of each face and cell edge of the unit cell. These voids are centered by Ag_2 dumbbells and oriented in the direction of the respective dumbbell (Figure 11). The Ag-Ag distance in the dumbbell is 2.938(1) Å which matches very well with Ag-Ag distances in Ag_3Sn with 2.93 to 2.98 Å[38] though the occupation factor for the Ag position was refined to only 0.90(1). It is not quite clear what causes the underoccupation of this position as the nearest neighbors are quite far away with interatomic distances of 3.148(1) for Ag1-Sn3 and 3.160(1) for Ag1-Na2 whereby the Ag_2 dumbbell appears quite isolated. The surrounding of the Ag_2 dumbbells reminds on the $Ag_{13}Sn_7$ clusters of $Na_{29}Ag_{17.8}Sn_{43}$ as it can be build by a hexagonal prism of Sn atoms by capping the rectangular and hexagonal faces with Na atoms (Figure 12). The four Na2 atoms are shared with the neighboring Ag_2 dumbbells while the four Na3 atoms are not shared. In contrast to $Ag_{13}Sn_7$, this 20 atom unit inhabits two instead of one atom.
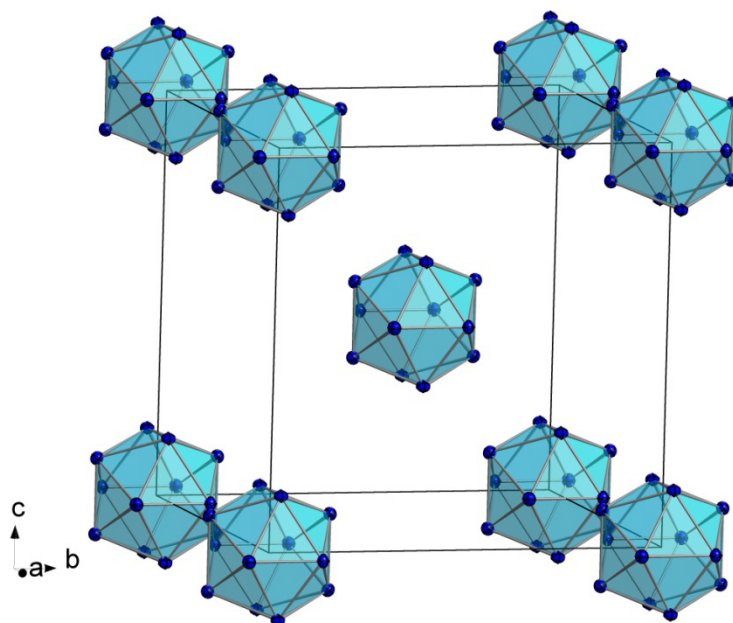
Figure 7: Body centered cubic arrangement of distorted Sn_{12} icosahedra in $Na_{13}Ag_{2.7}Sn_{24}$. Sn atoms are represented as ellipsoids with 90% probability level.
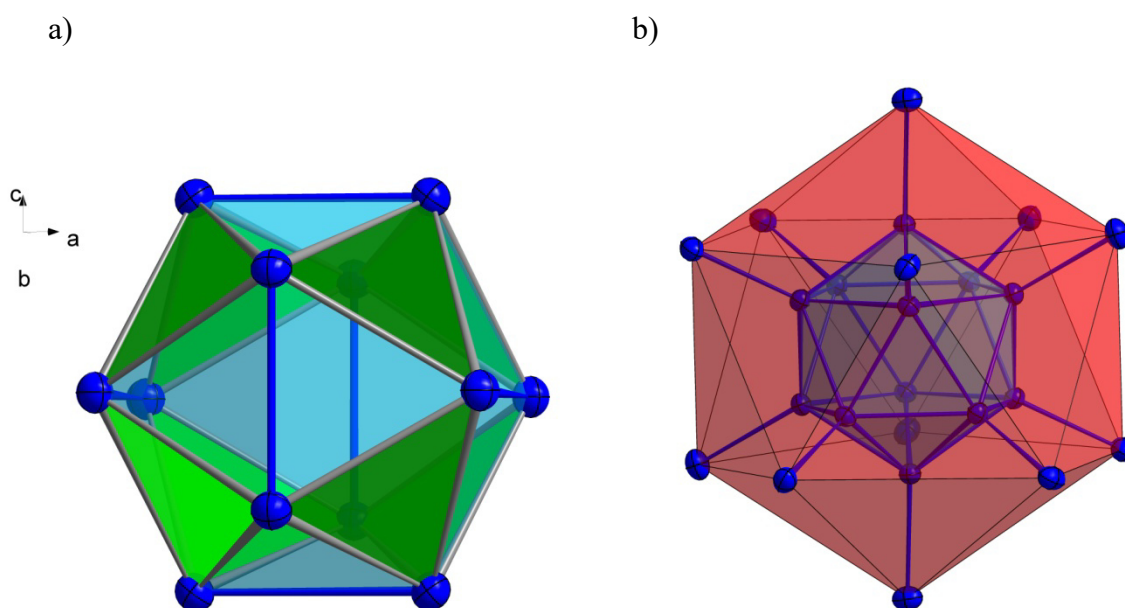
a)

b)

Figure 8: a) $(Sn1)_{12}$ icosahedron in $Na_{13}Ag_{2.7}Sn_{24}$ showing the octahedral distortion of the short Sn1-Sn1 bonds (blue, longer Sn1-Sn1 bonds grey) and the resulting orientation of the green triangular faces in the corner of a surrounding cube. b) Distorted $(Sn1)_{12}$ icosahedron (blue cluster) and surrounding $(Sn2)_{12}$ icosahedron (red cluster) in $Na_{13}Ag_{2.7}Sn_{24}$. Covalent bonds are marked with thick blue lines. Sn atoms are represented as ellipsoids with 90% probability level.

a)   b)
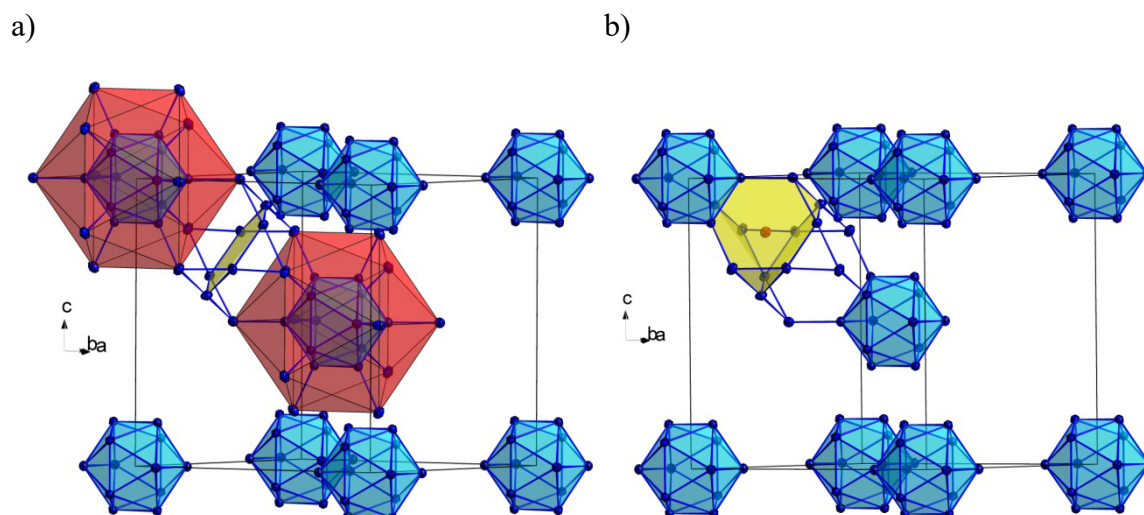
Figure 9: Body centered cubic arrangement of distorted Sn_{12} icosahedra in $Na_{13}Ag_{2.7}Sn_{24}$. a) Additional Sn2 positions around two icosahedra (red cluster) and the connecting planar hexagonal ring of Sn3 positions (yellow). b) Two Friauf polyhedra (one marked in yellow and Na centered) sharing a hexagonal ring connecting the icosahedra in the center and at the corner. Covalent bonds are marked with thick blue lines. Sn atoms are represented as ellipsoids with 90% probability level.
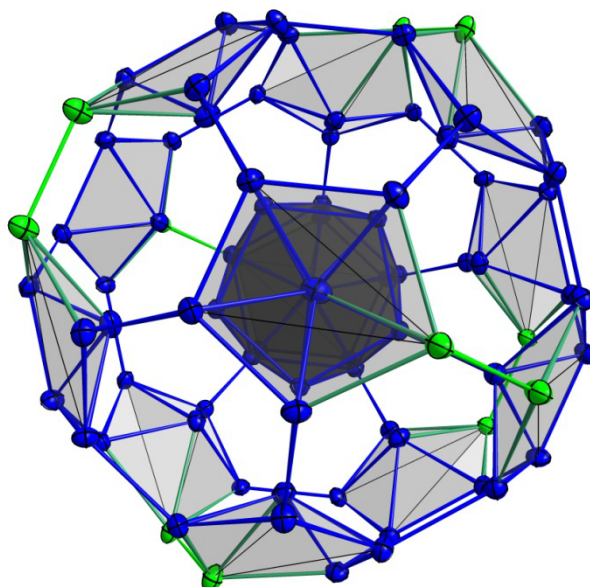
Figure 10: Samsons polyhedron as coordination sphere of the central Sn-icosahedron. Ag and Sn are represented as ellipsoids with 90% probability level in green and blue respectively. Sn-Sn, Sn-Ag and Ag-Ag bonds are represented as thick blue, dark green and green lines.
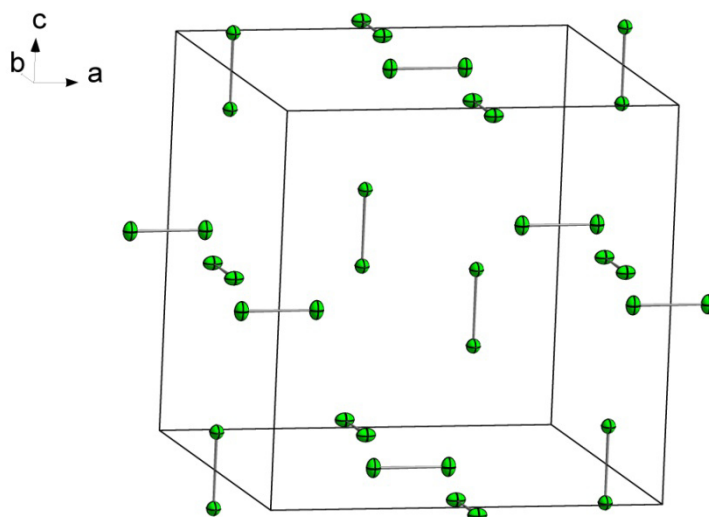
Figure 11: Unit cell of the compound $Na_{13}Ag_{2.7}Sn_{24}$ showing all Ag_2 dumbbells which center the voids in the polyanionic network and are located at the center of all edges and faces and their orientation. Ag atoms are represented as ellipsoids with 90% probability level in green.
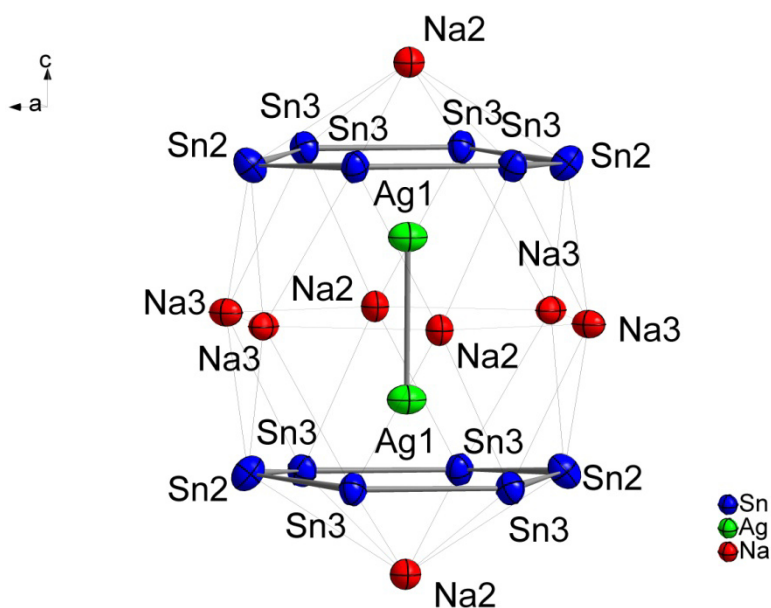

Figure 12: Coordination sphere of the Ag_2 dumbbell. Na, Ag and Sn are represented as ellipsoids with 90% probability level in red, green and blue respectively. Sn-Sn and Ag-Ag contacts are draws as thick grey, Na-Sn and Na-Ag contacts as thin grey lines.

Conclusion

Our investigations on structures build by partial substitution of Sn in binary Na-Sn compounds with electron poor transition metals led to the synthesis of the phase pure

compounds $Na_{29}Ag_{17.8}Sn_{43}$ and $Na_{13}Ag_{2.7}Sn_{24}$. These compounds represent the first known compound in the Na-Ag-Sn phase diagram with $Na_{29}Ag_{17.8}Sn_{43}$ exhibiting a network of interconnected clusters including the unique ($Ag_{13}Sn_7$) cluster. The Ag poorer $Na_{13}Ag_{2.7}Sn_{24}$ exhibits an interconnected cluster like 3-dimensional Sn network with encapsulated Na atoms and isolated Ag_2 dumbbells.

Associated content

Supporting Information available: X-ray crystallographic files in CIF format, powder diffractograms and tables of anisotropic displacement parameters for the title compound as well as results of the magnetic susceptibility measurement.

Author information

Corresponding Author: Prof. Dr. Thomas F. Fässler, Department Chemie, Technische Universität München, Lichtenbergstr. 4, D-85747 Garching, Germany

*E-mail: Thomas.Faessler@lrz.tum.de.

Notes: The authors declare no competing financial interest.

References

(1)   Oro, L. A.; Braunstein, P.; Raithby, P. R., *Metal clusters in chemistry*. Wiley-vch Weinheim, Germany: 1999; Vol. 3.

(2)   Sevov, S. C.; Corbett, J. D. *J. Am. Chem. Soc.* **1993,** *115*, 9089-9094.

(3)   Sevov, S. C.; Corbett, J. D. *Inorg. Chem.* **1993,** *32*, 1612-1615.

(4)   Zhao, J.-T.; Corbett, J. D. *Inorg. Chem.* **1995,** *34*, 378-383.

(5)   Belin, C.; Tillard-Charbonnel, M. *Prog. Solid St. Chem.* **1993,** *22*, 59-109.

(6)   Corbett, J. D. *Angew. Chem. Int. Ed.* **2000,** *39*, 670-690.

(7)   Corbett, J. D. *Struct. Bonding (Berlin)* **1997,** *87*, 158.

(8)   Kim, S.-J.; Hoffman, S. D.; Fässler, T. F. *Angew. Chem.* **2007,** *119*, 3205-3209.

(9)   Todorov, E.; Sevov, S. C. *Inorg. Chem.* **1997,** *36*, 4298-4302.

(10)   Todorov, E.; Sevov, S. C. *J. Am. Chem. Soc.* **1997,** *119*, 2869-2876.

(11)   Müller, W.; Volk, K. *Z. Naturforsch. B* **1977,** *32*, 709-710.

(12)   Fässler, T. F.; Hoffmann, S. *Inorg. Chem.* **2003,** *42*, 5474-5476.

(13)   Dubois, F.; Schreyer, M.; Fässler, T. F. *Inorg. Chem.* **2005,** *44*, 477-479.

(14)   Vaughey, J. T.; Corbett, J. D. *Inorg. Chem.* **1997,** *36*, 4316-4320.

(15)   Fässler, T. F.; Kronseder, C. *Angew. Chem.* **1998,** *110*, 1641-1644.

(16)   Wrobel, G.; Schuster, H. U. *Z. Anorg. Allg. Chem.* **1977,** *432*, 95-100.

(17)   Zachwieja, U. *Z. Anorg. Allg. Chem.* **2001,** *627*, 353-356.

(18)   Döring, W.; Seelentag, W.; Buchholz, W.; Schuster, H. U. *Z. Naturforsch. B* **1979,** *34*, 1715-1718.

(19)   Stegmaier, S.; Fässler, T. F. *Angew. Chem.* **2012,** *124*, 2701 –2704.

(20)   Stegmaier, S.; Fässler, T. F. *J. Am. Chem. Soc.* **2011,** *133*, 19758–19768.

(21)   Stoe *WinXPOW*, 2.08; Stoe & Cie GmbH: Darmstadt, 2003.

(22)   Stoe *CrysAlis RED*, 1.171.33.34; Oxford Diffraction Ltd.: 2009.

(23)   *X-RED32* Version 1.26; STOE & Cie GmbH: Darmstadt, 2004.

(24)   Stoe *X-Shape*, 2.11; Stoe & Cie GmbH: Darmstadt, 2008.

(25)   Inc., B. A. *APEX2: APEX Suite of Crystallographic Software*, 2008.4; Madison, WI, USA, 2008.

(26)   Inc., B. A. *SAINT*, Madison, WI, USA, 2001.

(27)   Inc., B. A. *SADABS*, Madison, Wi, USA, 2001.

(28)   Sheldrick, G. M. *XPREP-97*, University of Göttingen (Germany), 1997.

(29)   Sheldrick, G. M. *SHELXS-97*, University of Göttingen (Germany), 1997.

(30)   Sheldrick, G. M. *SHELXL-97*, University of Göttingen (Germany), 1997.

(31)   *Netzsch Proteus Thermal Analysis*, 4.8.2; Netzsch-Gerätebau GmbH: Selb, Germany, 2006.

(32)   Bain, G. A.; Berry, J. F. *J. Chem. Educ.* **2008,** *85*, 532–536.

(33)   Hauke, W. *Z. anorg. allg. Chem* **1940,** *244*.

(34)   Flot, D. M.; Tillard-Charbonnel, M. M.; Belin, C. H. E. *J. Am. Chem. Soc.* **1996,** *118*, 5229-5235.

(35)   Henning, R. W.; Corbett, J. D. *Z. Anorg. Allg. Chem.* **2002,** *628*, 2715-2723.

(36)   Donohue, J., *The Structures of the Elements*. Wiley: New York, 1974.

(37)   Lupu, C.; Downie, C.; Guloy, A. M.; Albright, T. A.; Mao, J.-G. *J. Am. Chem. Soc.* **2004,** *126*, 4386-4397.

(38)   Fairhurst, C. W.; Cohen, J. B. *Acte Cryst. B* **1972,** *28*, 371-378.

(39)   Fässler, T. F.; Kronseder, C. *Angew. Chem. Int. Ed.* **1998,** *37*, 1571-1575.

(40)   Kim, S.-J.; Fässler, T. F. *J. Solid State Chem.* **2009,** *182*, 778-789.

(41)   Bergman, G.; Waugh, J. L. T.; Pauling, L. *Acta Cryst.* **1957,** *10*, 254-259.

(42)   Tillard-Charbonnel, M.; Belin, C. *J. Solid State Chem.* **1991,** *90*, 270-278.

Supporting Information

for

Synthesis and Structural Characterization of $Na_{29}Ag_{17.8}Sn_{43}$ and $Na_{13}Ag_{2.7}Sn_{24}$

Alexander Henze, Thomas F. Fässler

manuscript for publication

Contents

Crystal structures

Powder and Single Crystal X-ray diffraction and structural refinement.

Differential Thermal Analysis

Magnetic measurements

Table S-1. Interatomic distances for $Na_{29}Ag_{17.8}Sn_{43}$ and $Na_{13}Ag_{2.7}Sn_{24}$

	$Na_{29}Ag_{17.8}Sn_{43}$	
atoms		**Distance (Å)**
Sn1	Sn1	2.981 (2)
	Sn5/Ag5	2.843 (2)
	Na1	3.483 (8)
	Na3	3.446 (5)
	Na5	3.479 (5)
Sn2	Sn2	2.763 (2)
	Sn3	2.902 (1)
	Sn5/Ag5	2.943 (2)
	Na1	3.357 (5)
	Na3	3.367 (6)
	Na4	3.430(10)
Sn3	Sn3	3.113 (2)
	Sn5/Ag5	2.986 (1)
	Ag7	2.880 (2)
	Na3	3.314 (4)
	Na4	3.378 (3)
	Na5	3.360 (2)
Sn4	Sn4	3.443 (3)
	Ag7	2.849 (2)
	Na2	3.443 (2)
	Na3	3.169 (6)
	Na5	3.585 (8)
Sn5/Ag5	Sn5/Ag5	2.840 (2)
	Na1	3.271 (2)
	Na3	3.298 (7)
	Na5	3.389 (5)
Sn6/Ag6	Sn6/Ag6	2.861 (5)
	Ag7	3.101 (2)
	Na2	3.438 (3)
Ag7	Ag7	2.871 (2)

	Na4	3.203 (4)
Na1	Na3	3.484 (7)

$Na_{13}Ag_{2.7}Sn_{24}$		
atoms		**Distance (Å)**
Sn1	Sn1	2.8875 (7)
	Sn2	2.7623 (7)
	Na1	3.271 (2)
	Na3	3.271 (3)
Sn2	Sn3	2.8066 (4)
	Ag1	3.1832 (8)
	Na1	3.447 (2)
	Na2	3.436 (3)
	Na3	3.305 (2)
Sn3	Sn3	2.8832 (4)
	Ag1	3.1478 (5)
	Na1	3.354 (2)
	Na2	3.279 (2)
	Na3	3.353 (3)
Ag1	Ag1	2.9378 (11)
	Na2	3.160 (4)
Na1	Na1	3.279 (3)
	Na3	3.578 (3)
Na2	Na3	3.234 (2)
Na3	Na3	3.557 (4)

Table S-2. Anisotropic displacement parameters for $Na_{29}Ag_{17.8}Sn_{43}$ and $Na_{13}Ag_{2.7}Sn_{24}$

$Na_{29}Ag_{17.8}Sn_{43}$

Atom	U_{11}	U_{22}	U_{33}	U_{12}	U_{13}	U_{23}
Sn1	0.0166(5)	0.0127(6)	0.0150(6)	0.0064(3)	0	0
Sn2	0.0192(5)	0.0163(5)	0.0197(5)	0.0086(4)	0	0
Sn3	0.0231(4)	0.0162(5)	0.0193(6)	0.0081(3)	0.0002(3)	0
Sn4	0.0261(9)	0.0918(13)	0.0442(11)	0.0130(5)	0	0
Sn5/Ag5	0.0211(5)	0.0181(6)	0.0180(6)	0.0090(3)	0.0004(3)	0.0007(3)
Sn6Ag6	0.0457(16)	0.0457(16)	0.0256(17)	0.0228(8)	0	0
Ag7/Na7	0.0395(8)	0.0194(7)	0.0391(9)	0.0097(4)	0.0090(6)	0
Na1	0.018(3)	0.018(3)	0.014(4)	0.009(1)	0	0
Na2	0.016(5)	0.016(5)	0.019(9)	0.008(3)	0	0
Na3	0.027(3)	0.016(5)	0.021(3)	0.013(2)	-0.001(2)	-0.001(1)
Na4	0.040(5)	0.019(3)	0.025(4)	0.020(3)	0	0
Na5	0.039(4)	0.025(4)	0.017(4)	0.013(2)	0	0

$Na_{13}Ag_{2.7}Sn_{24}$

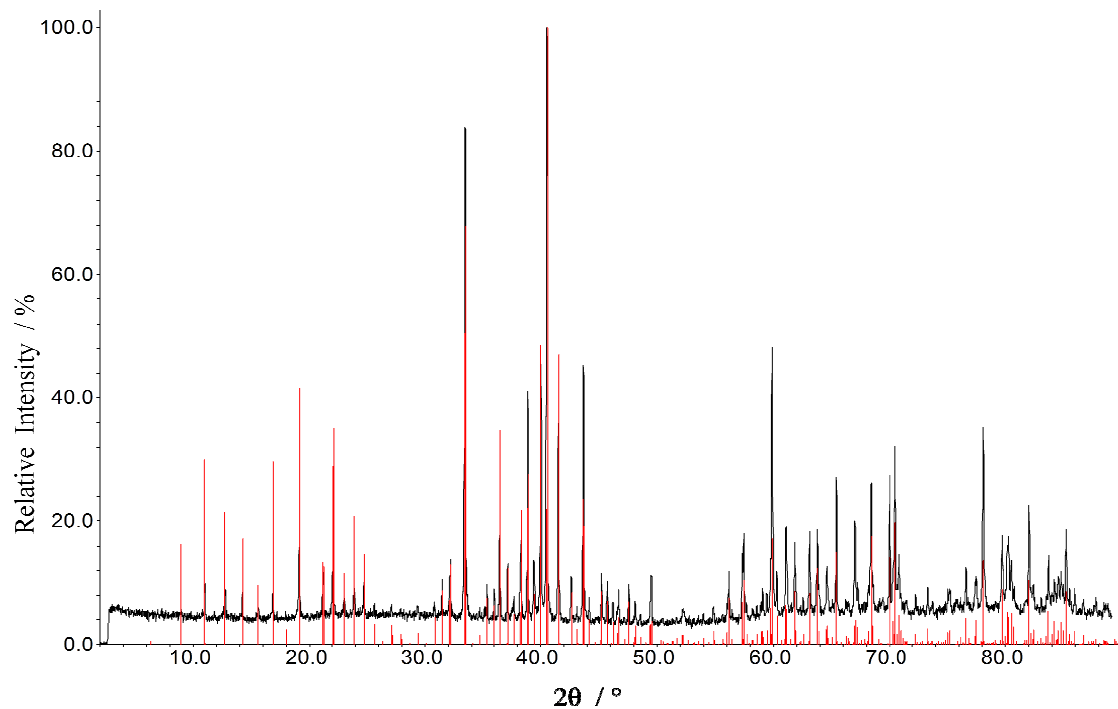| Atom	U_{11}	U_{22}	U_{33}	U_{12}	U_{13}	U_{23}
Sn1	0.0084(3)	0.0088(3)	0.095(3)	-0.0007(2)	0	0
Sn2	0.0140(3)	0.0153(3)	0.0105(2)	-0.0037(2)	0	0
Sn3	0.0136(2)	0.0109(2)	0.0105(2)	0.0015(2)	-0.0001(2)	-0.0017(2)
Ag1	0.0108(5)	0.0102(5)	0.0195(5)	0	0	0
Na1	0.0115(7)	0.0115(7)	0.0115(7)	-0.0007(8)	-0.0007(8)	-0.0007(8)
Na2	0.0116(19)	0.0095(19)	0.0120(19)	0	0	0
Na3	0.0133(14)	0.0097(13)	0.0110(14)	0	-0.0033(11)	0

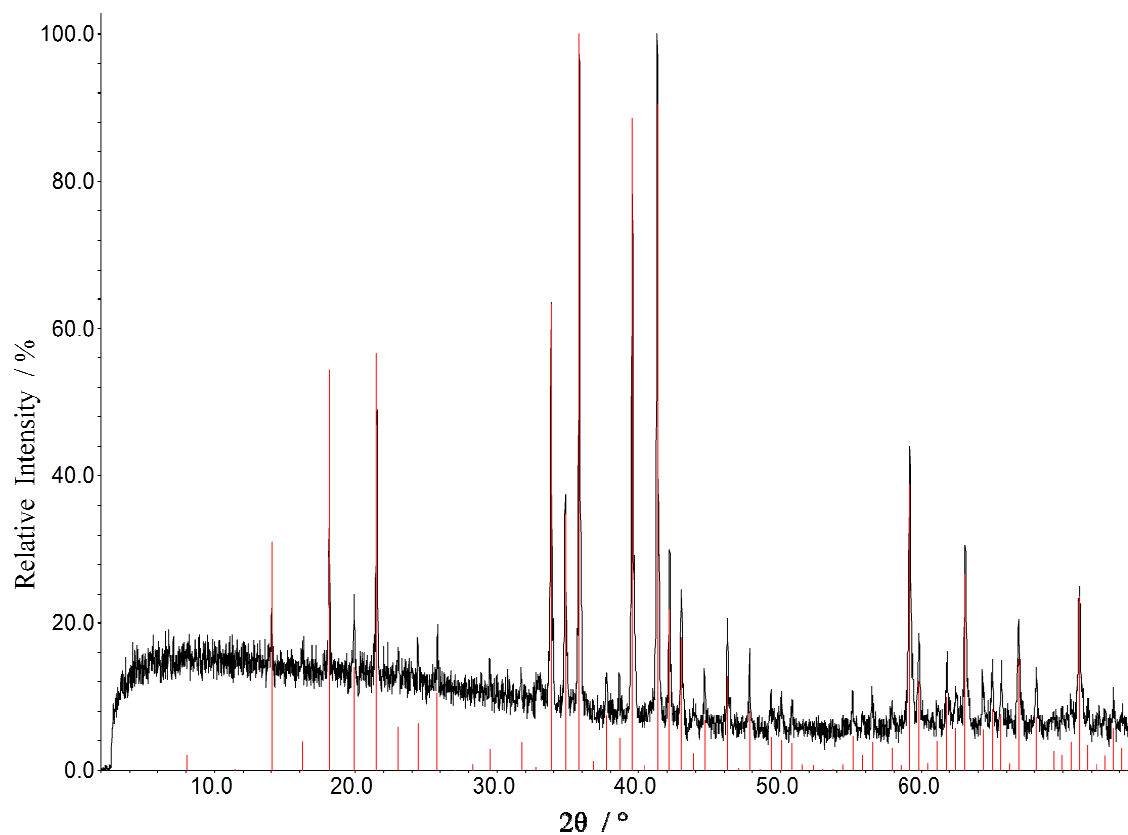**Figure S-1.** Experimental X-ray powder diffractogram (black) with the theoretical pattern of $Na_{29}Ag_{17.8}Sn_{43}$ (red).

Figure S-2. Experimental X-ray powder diffractogram (black) with the theoretical pattern of $Na_{13}Ag_{2.7}Sn_{24}$ (red).
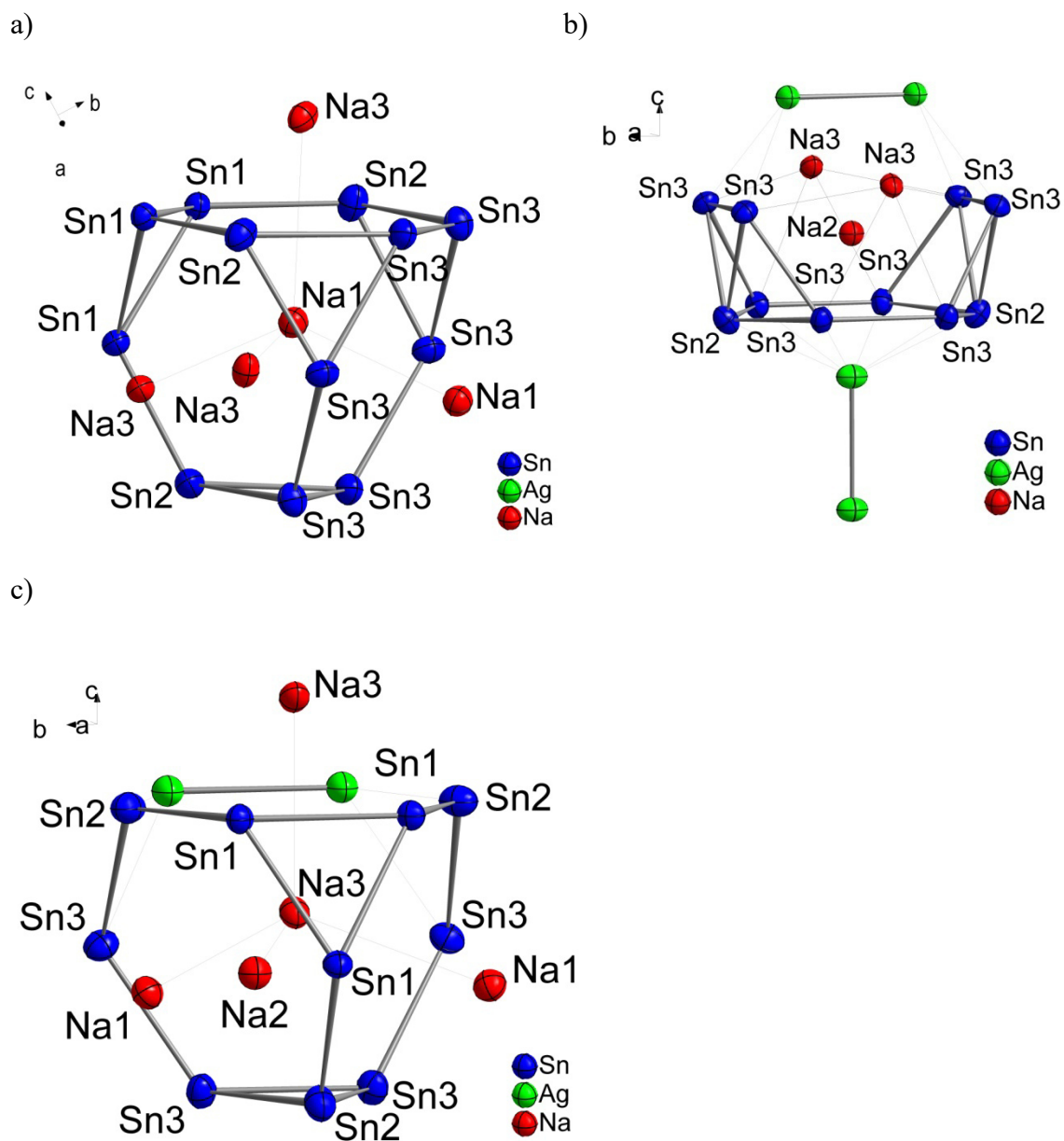
a)

b)

c)

Figure S-3. Coordination sphere of the a) Na1, b) Na2 and c) Na3 position. Na, Ag and Sn are represented as ellipsoids with 90% probability level blue, green and red respectively.
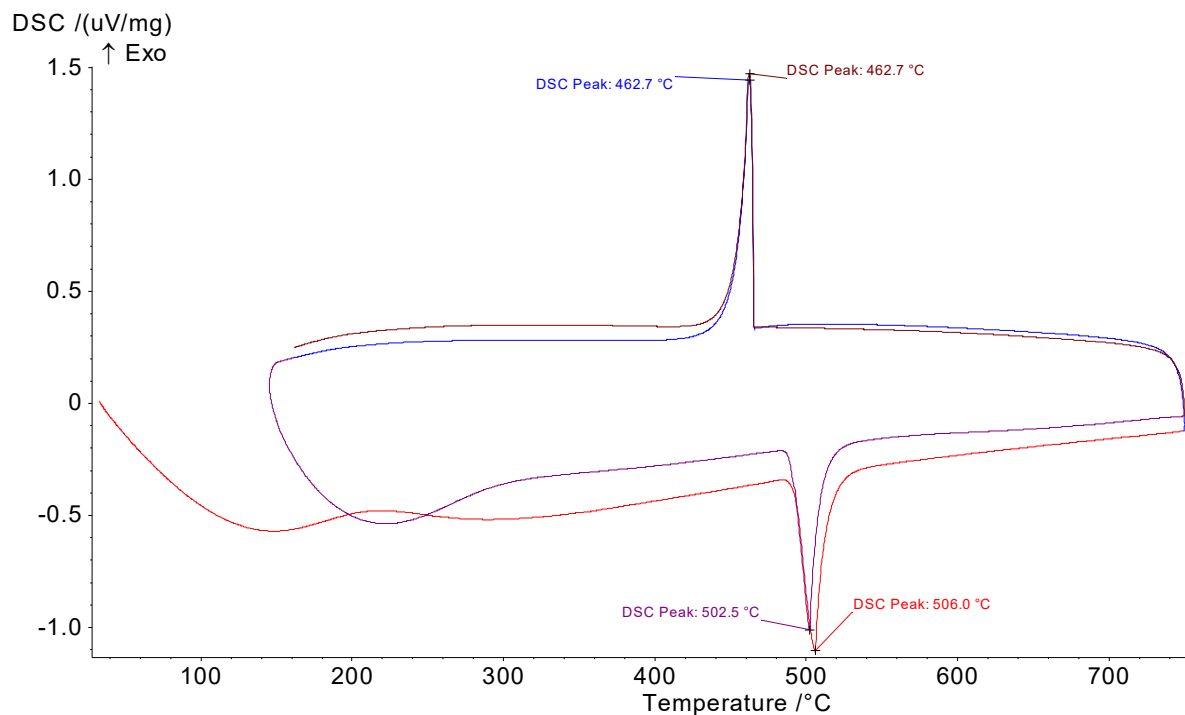
Figure S-4. Thermogram of a phase pure sample of $Na_{29}Ag_{17.8}Sn_{43}$. The heating traces are shown in red and purple, the cooling traces in blue and brown respectively.
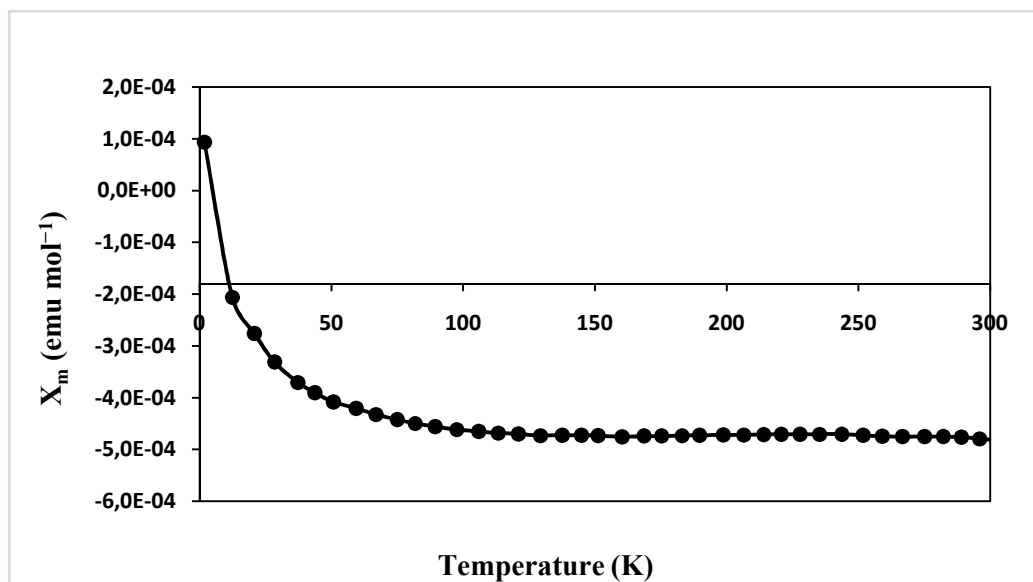

Figure S-5. Molar Susceptibility X_m of $Na_{13}Ag_{2.7}Sn_{24}$ at applied field of 500 Oe over a temperature range from 2 – 300 K. The data were corrected for the mass of the sample holder and the ion-core diamagnetism using Pascal's constants. Non-diamagnetic behavior below 50 K results from small amounts of paramagnetic impurities in the sample.